FINITE ELEMENT ANALYSIS OF SPLAYED STEEL GIRDER BRIDGES

by

Faress Hraib

A Thesis Presented to the Faculty of the
American University of Sharjah
College of Engineering
in Partial Fulfillment
of the Requirements
for the Degree of

Master of Science in
Civil Engineering

Sharjah, United Arab Emirates

June 2015

Approval Signatures

We, the undersigned, approve the Master's Thesis of Faress Hraib.

Thesis Title: Finite Element Analysis of Splayed Steel Girder Bridges

Signature   **Date of Signature**
                                                                  (dd/mm/yyyy)

_____   _____
Dr. Sami Tabsh
Professor, Department of Civil Engineering
Thesis Advisor

_____   _____
Dr. Farid Abed
Associate Professor, Department of Civil Engineering
Thesis Committee Member

_____   _____
Dr. Mohammad AlHamaydeh
Associate Professor, Department of Civil Engineering
Thesis Committee Member

_____   _____
Dr. Mamoun Abdel-Hafez
Associate Professor, Department of Mechanical Engineering
Thesis Committee Member

_____   _____
Dr. Aliosman Akan
Department Head, Department of Civil Engineering

_____   _____
Dr. Mohamed El-Tarhuni
Associate Dean, College of Engineering

_____   _____
Dr. Leland Blank
Dean, College of Engineering

_____   _____
Dr. Khaled Assaleh
Director of Graduate Studies

Acknowledgements

Abstract

A splayed girder bridge is a bridge which consists of a deck slab supported on girders with linearly varying spacing. The simple formulas and approximate design procedures in the AASHTO LRFD Bridge Design Specifications are supposed to be used with regular bridges, where the girders are parallel and the deck slab width is constant. For splayed girder bridges, the specifications suggest a refined method of analysis, which could be expensive and time-consuming. Extending the simple live load girder distribution factors and the deck slab strip method to splayed girder bridges would be very helpful for bridge designers. The objective of this research is to investigate the effect of girder splayedness in slab-on-steel-girder bridges on the dead and live load distribution in the deck slab as well as among the interior and exterior girders. Fifteen composite steel girder bridges are analyzed by the finite element method using the computer software ANSYS. In the computer model, 4-node rectangular shell elements were used for the steel girder flanges and web, 2-node beam elements for the cross-bracing, and 8-node solid elements in the deck slab. Linearly-elastic material behavior is utilized and the model is verified against laboratory and field tests of actual bridges. The effects of the girder splayedness angle, girder spacing, number of girders, deck slab thickness, span length, girder stiffness, and presence of cross-bracing are considered. The study showed that the tributary width concept is reliable for determining the dead load on the splayed girders. Also, the girder distribution factors for flexure in the AASHTO LRFD specifications can be reasonably used for splayed girder bridges if the specific girder spacing at the location of each axle of the truck in the longitudinal direction is considered. On the other hand, the lever rule can provide a good estimate of the live load distribution among splayed girders when subjected to shear. With regard to the live and dead load effect in the deck slab, the equivalent strip method can be a reasonable predictor of the critical positive and negative bending moments in the slab interior regions and in the overhang, provided more than one strip are taken at some discrete locations along the bridge centerline.

Search terms: Bridges, Finite Element Analysis, Flared girders, Live load distribution, Splayed girders.

Table of Contents

List of Figures

List of Tables

Chapter 1: Introduction

1.1 Introduction

A bridge is a structure at least six meters long, built in order to cross over an obstacle of a road, a valley, or a river. Nowadays transportation networks are getting complex in order control the huge volumes of traffic, which often requires the use of irregular bridges to account for different traffic levels and highway separations. Thus, a better understanding of traffic load distribution on the superstructure of these bridges is required. In many cases of complex transportation networks, special types of bridges are needed to account for the gradual change in the number of traffic lanes, which requires widening or narrowing of the bridge width along the span length; this results in a bridge with varying width. An example of such a bridge is at a highway bridge partial separation (on-off ramp) shown in Figure 1 and, where a gradual widening of the bridge before separation is needed to account for more traffic lanes going in or out of the highway.
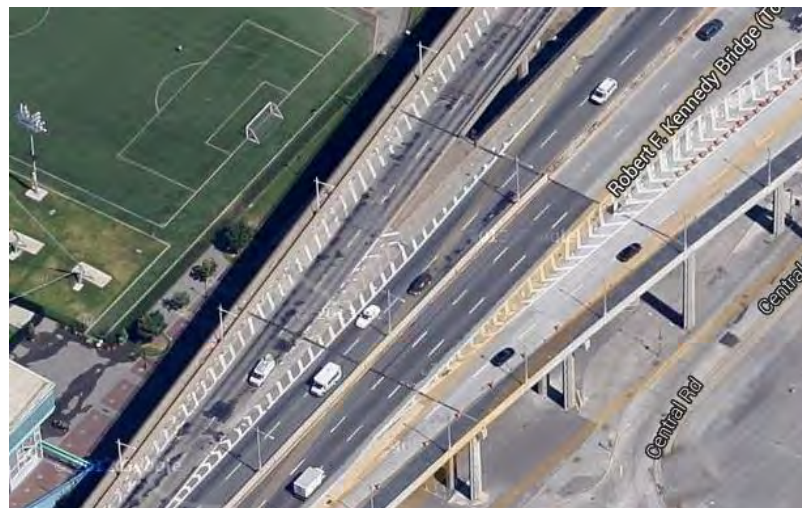
Figure 1 Typical on-off ramp [1]

Another important application of bridges with varying width is a bridge used in toll roads, where at collection stations the bridge width is increased in order to ease the fee collection process as shown in Figure 2. This results in a gradual change in the bridge width before and after the collection stations. One last example is a single point urban interchange (SPUI) which is used to move a large volume of traffic in a limited space efficiently and safely. Figure 3 shows a typical SPUI bridge under construction.

Figure 2: Toll road [1]

Figure 3: Single point urban interchange [2]

To satisfy the varying nature of a bridge's width, splayed girders are used in slab-on-girder bridges, which leads into non-uniform distribution of loads along each girder. This problem is not usually addressed in bridge design specifications and codes. Since steel girder bridges are widespread structures around the world, this type of bridges is addressed in this study.

Splayed, flared, or non-parallel girders are in general a number of girders with varying spacing along the span of the bridge, where the girder spacing is defined by a minimum value S_1 at the narrow end of the bridge and a maximum value S_2 at the wide end of the bridge as shown in Figure 4 for a typical simply-supported splayed girder bridge.
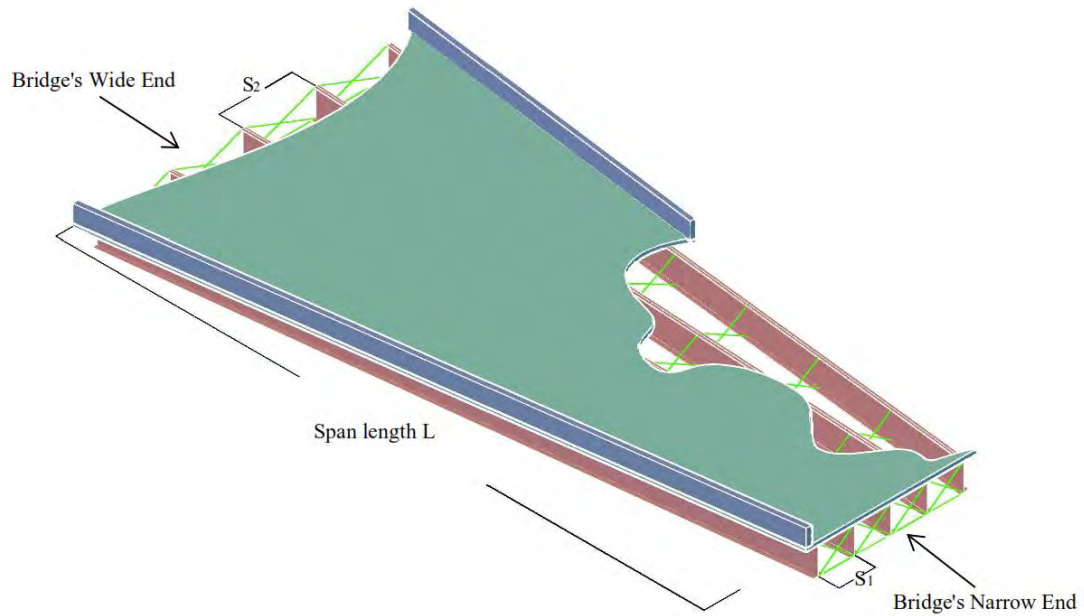
Figure 4: Splayed girder bridge definition

1.2 Problem Statement

Transportation systems are like veins of the city, and they are getting more complicated and massive with the development of cities and progression of economies. Nowadays, more irregular bridges are needed to satisfy the complexity of transportation interchanges, and to give smoother, easier, and safer movability and rideability of traffic. Some transportation systems are now requiring bridges with varying width, which results in non-parallel girders. Such bridges are usually called splayed or flared girder bridges.

Searching the available literature shows almost nonexistent comprehensive treatment of splayed girder bridges. Thus, to accurately analyze a splayed girder bridge, a 3D mathematical model should be developed using a refined method such as the Finite Elements or Grillage Analogy. However, modeling a fully-detailed 3D splayed girder bridge is a very complicated, error-prone, and time consuming process and is not commonly employed for girder-type bridges.

Hence, there is a need to find the effect of girder splayedness on the distribution of dead and live loads. This study quantifies the effect of the gradual change in girder spacing, due to the bridge's width variations, on live load distribution in exterior and interior girders of composite steel girder bridges. In order to generalize the outcomes of this study, different bridge parameters are considered in both flexure and shear, such as girder spacing, slab thickness, span length, and cross-bracing spacing.

16

1.3 Objectives and Scope

The objectives of this study are to:

1. Investigate the effect of splayed girders on dead and live load distribution represented in girder distribution factors for composite steel girder bridges.

2. Study the effect of girder spacing, slab thickness, span length, girder stiffness, and cross-bracing spacing on the girder distribution factors for both flexure and shear in splayed girder bridges.

3. Research the effect of dead and live loads on the structural behavior of the deck slab at different locations along the span of splayed girder bridges.

4. Recommend a simple approximate approach to determine the girder distribution factor for flexure and shear in splayed girder bridges.

5. Propose a practical procedure for predicting the bending moment in the deck slab subjected to loads in splayed girder bridges.

The scope of this study addresses concrete slab-on-steel girder bridges, where composite action is satisfied by using shear studs welded to the top steel flange. Simply supported short and medium length bridges up to 50 m are considered. All of the considered girder bridges are splayed at both sides of the central line of symmetry. In all cases, linearly-variable deck widths with the corresponding girder splayedness ratio are addressed. Other examined variables include the span length (ranging from 30 m to 50 m), girder spacing (ranging from 1500 mm to 5250 mm), deck slab thickness (ranging from 150 mm to 300 mm), girder depth (ranging from 1400 mm to 2000 mm), number of girders (ranging from 3 to 7), and cross-bracing spacing (ranging from 40 to 5 m). The bridge overhang width also varies along the span length; however, its width is always kept equal to one-third of the corresponding girder spacing at any section along the bridge. Different loading scenarios are considered in order to maximize the effect of live load in both flexure and shear, using one, two, and three trucks in separate lanes to account for the live load. All bridges are modeled within the linearly elastic range using the finite element analysis software ANSYS release 14.0 [3] to carry out a parametric study of the variables mentioned above. Modeling with the linear-elastic range is in line with common practice of bridge analysis [4]. The results of the parametric study are organized and discussed in order to understand the effect of all mentioned bridge parameters on the live load distribution in splayed girder bridges.

1.4 Approach

In this study, finite element modeling is used to build a number of splayed girder bridges to study the behavior of this type of bridge. ANSYS software [3] is chosen to perform the finite element analysis because of its proven capabilities in solving and visualizing these types of structures reliably. The finite element model in this study is verified through a series of verification including analysis of analytical and experimental studies available in the literature. 3D solid elements are chosen to model the concrete deck slab in 4 layers, shell elements are used to model the steel girder web and flanges, and beam elements are employed for the diaphragms. All bridges are simply supported, and built and analyzed in the linear-elastic range. Moreover, the simulated live load represented by the AASHTO LRFD design truck is applied through loading patches modeled as shell elements. The truck is moved in both longitudinal and transverse directions to maximize the effect of live load in the considered members in flexure and shear. In the longitudinal direction, a simple approach is proposed to approximately predict the distance of mid axle of the truck away from mid span due to the splayed girders, while for shear effect on girders the truck rear axle is placed at the supported end of the bridge that has the maximum girder spacing. In the transverse direction, one, two, and three trucks are moved and rotated at constant increments starting from the edge of the bridge and ending at its middle, because of the symmetry of all bridges under consideration. The truck(s) keeps changing location in the transverse direction until capturing the maximum effect, whether in flexure or shear. After applying this approach to all bridges considered in the parametric study, the results are analyzed and discussed to derive final conclusions and recommendations.

1.5 Thesis Organization

The thesis is divided into seven chapters. This chapter (Chapter 1) outlines the problem, the reasons behind it, and the main concerns. Also, it summarizes the objectives, scope, and methodology of the study.

Chapter 2 introduces a brief background about the slab-on-girder bridge type and the girder distribution factor notion. Also, past research by scholars is summarized in a literature review on girder bridges and parameters that affect the behavior of such bridges.

Chapter 3 presents the finite element method and the use of finite element modeling in bridge design, and explores different modeling approaches from the literature. In addition, a finite element model is introduced, and proof of its validity through a series of verifications is included.

Chapter 4 explains the research methodology, by clarifying the girder distribution factor (GDF) calculation process, and identifying critical locations of the AASHTO LRFD truck to maximize the effect of live load in both flexure and shear in girders. Moreover, it illustrates live load flexure effect in the deck slab.

Chapter 5 presents a parametric study conducted to obtain the GDF to a number of bridges to determine the influence of different parameters on the behavior of the interior and exterior girders in both flexure and shear. Moreover, an approximate approach to calculate the GDF is presented, and then compared with the finite element results of the splayed girder bridges.

Chapter 6 includes the finite element analysis of the deck slab with consideration of the AASHTO's LRFD equivalent strip method. In this chapter, consideration is given to flexure in the interior regions of the slab, as well as in the overhang area.

Finally, Chapter 7 summarizes all the results and outcomes, and then outlines final conclusions and recommendations. In addition, it gives suggestions for further research needed on this topic, and new ideas that can be explored in future studies.

Chapter 2: Background and Literature Review

2.1 Introduction

This chapter introduces the different types of bridge superstructures, and provides details on the slab-on-girder type. Also, it explores composite steel girder bridges with all their components and properties. An introduction to live load distribution among the bridge girders is presented, summarizing three live load distribution approaches, and focusing on the AASHTO LRFD method in more detail and depth. Finally, a literature review on splayed girder bridges and related aspects is presented and discussed.

2.2 Types of Bridges

Bridges can be divided into two main parts, the first one is the superstructure which is the span that directly receives the live load and then carries it to the substructure as reactions. In contrast, the substructure is the system that supports the superstructure parts and transfers the loads into the ground, as shown in Figure 5. It consists of many structural parts such as abutments, piers, foundation, and bearings.
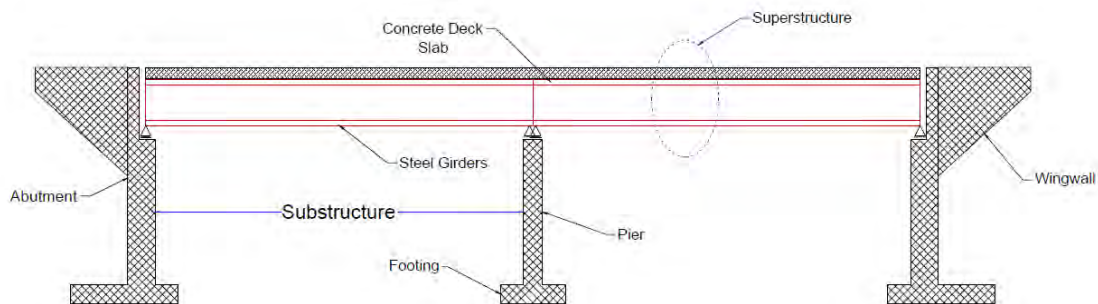
Figure 5: Bridges main two parts

Bridges are categorized in many different ways according to different aspects, such as span length, structural material used, floor system, function, and structural systems. The structural system classification can be considered more important than others for structural engineers. The structural system in this classification can be slab, slab-on-girders, truss, cable-stayed, arch, or suspension. In general, choosing a structural system for a certain bridge project can be judged by different considerations, such as material properties, span length, topography, cost, aesthetics, and others [5].

One of the most commonly-used forms around the world is the slab-on-girder bridge. It can be defined as a concrete deck slab resting on a number of concrete or steel girders acting together in a composite or non-composite way. This study is concerned with cast-in-place concrete deck slab acting compositely with several steel girders, and this composite action can be provided by using shear studs welded to the steel girder's top flange as shown in Figure 6. Therefore, due to this composite action, the steel girders and the concrete deck slab resist bending moment together [6]. The method of construction in this case can be shored or un-shored.
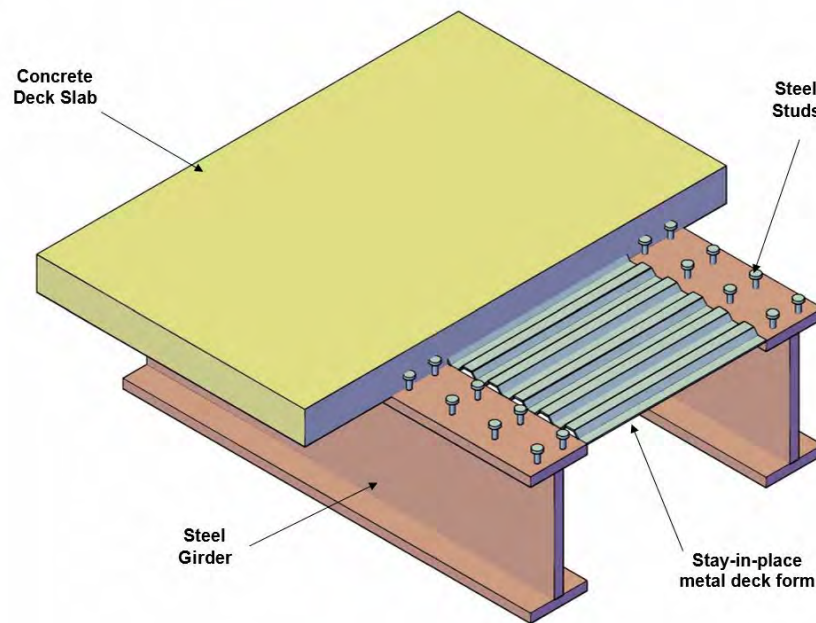
Figure 6: Composite beam action

This system utilizes both the concrete and steel benefits to the maximum. Compared to other types, the slab-on-girder bridge advantages are decreased weight, high stiffness-to-weight ratio, relatively low cost, enhanced ductility, fast construction, and flexibility in accommodating non-prismatic steel plate girders. Some disadvantages are possible corrosion of steel sections and the high costs of maintenance needed to avoid it, danger of plate buckling, temperature conductivity, and susceptibility to fatigue and fracture. Figure 7 shows an example of a composite steel girder bridge.

To ensure lateral stability during construction and give the superstructure more rigidity, cross-bracing or diaphragms are used between the steel girders at different spacing along the span of the bridge. Cross-bracing can also provide more live load distribution among the supporting girders.

21

Figure 7: Example of composite steel girder bridge [7]

2.3 AASHTO LRFD Live Load

The live load in bridge design is primarily the weight of vehicular traffic moving on the bridge, and it is critical because of its high uncertainty compared with dead load, heavy weight, and concentration at few points. In the AASHTO LRFD Bridge Design Specifications (2012), the design live load is specified as HL-93 [4], which consists of a design truck or a design tandem, whichever gives a larger effect, together with a design lane load. Mostly, the design truck governs when the bridge span is greater than 12 m. The design lane is 3600 mm in the transverse direction, and uniform live load can only be distributed on 3000 mm of it, with 9.3 N/mm uniform load. However, concentrated loads at truck or tandem axles specify the design truck or the design tandem. The gross design truck weight is 325 KN divided into three axles at specified spacings in the longitudinal direction as shown in Figure 8, while in the transverse direction each axle end takes half of the total axle load at a spacing of 1800 mm. The design tandem has two axles with a load of 110 KN each, and a spacing of 1200 mm in the longitudinal direction and 1800 mm between wheels in the transverse direction. In order to account for dynamic movement of the truck or the tandem, an impact factor of 0.33 is applied to each axle in the truck or tandem load. The truck wheels can be at least at a distance of 300 mm away from the parapet in the transverse direction when designing the concrete deck slab, while at least 600 mm is required by the AASHTO to design any other structural element, as shown in Figure 9. Also, the distance between the truck wheel and the edge of a design lane should be at least 600 mm [4].
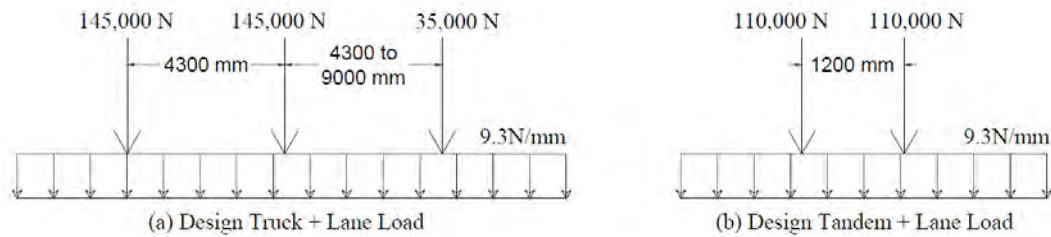
Figure 8: AASHTO LRFD HL-93 live load [4]
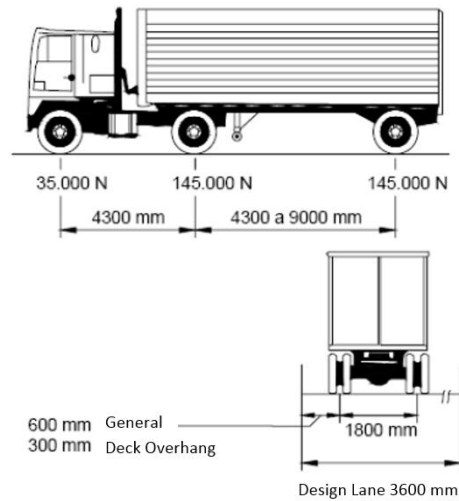
Figure 9: Characteristics of AASHTO LRFD design truck [4]

2.4 Live Load Distribution Methods

In bridges, distribution of the live load can be the most critical step in the design process. The concentrated truck or tandem live load, applied to the deck slab, will be supported by all girders on the bridge, and the load will tend to favor the girders nearest to it. Many factors can affect distribution of the live load such as girder spacing, slab thickness, diaphragm presence, truck position, girder stiffness, and span length. Based on this, many approaches were developed in the past to calculate the distribution of live load to supporting girders. The simplest approach uses equations that can approximate each girder share from the truck load, and this share is represented by the Girder Distribution Factor (GDF). The AASHTO LRFD Bridge Design Specifications [4] present such formulas and allow bridge engineers to use them for designing bridges but under some limitations and constrains. Such GDF expressions are often based on advanced structural analysis methods such as the finite element method. Usually, these formulas yield conservative GDF values, whether in flexure or shear.

Complex analytical methods of analysis for slab-on-girder bridges, such as the finite element method, finite difference procedure, or grillage analogy, are the most

accurate methods for determining the distribution of live load on bridges. Three dimensional finite element models can provide very accurate results if the model is reasonable and detailed. However, it can be time-consuming for the designer, and may be prone to error in modeling because of the sensitivity of the results to the type of element in use, connection types, and meshing styles. Nowadays, this method is becoming more popular because of the progress of computers hardware and technology, which reduces the computational time and has improved the processing capabilities. This is especially true for bridges, since a huge number of elements is needed, besides the fact that the location of the truck in the transverse direction is very critical and cannot be determined without a reasonable number of trails. This method is highly recommended by researchers and the AASHTO's LRFD specifications for the analysis of irregular geometry, critical bridges, highly curved bridges, and bridges with very high skewness.

2.5 AASHTO LRFD Live Load Distribution Method

In AASHTO's Standard Specifications for Highway Bridges (1996), a simple method was used to calculate the live load distribution factor for girder bridges. For flexure, this method is based on simply dividing the girder spacing by a constant to get the live load distribution factor [8]. This results in a conservative live load effect, particularly for bridges with large girder spacing. In 1993, new equations were developed by Zokaie et al. and proposed by the National Cooperative Highway Research Program (NCHRP) Project 12-26 [9]. These expressions used additional parameters to the girder spacing used in the old method to find a more accurate live load distribution factor [10], and as a result they have been included in the AASHTO LRFD Bridge Design Specifications since 1994. The new GDF equations were developed based on computational methods and verified against field work for a wide range of bridges, which makes them applicable to many cases and types of slab-on-girder bridges. Although the new equations are relatively complicated in comparison to the old approach, they yield better accuracy because of the consideration of other parameters not included in the old approach.

In order to design bridge girders, the portion of live load carried by each girder should be determined, where it's represented by the GDF. However, after that a number of steps should be followed to complete the design of the girder. The first one is to

compute the effect of the live load, whether it's shear or flexural, by loading a single lane on a line element. To maximize this effect, the truck location in the longitudinal direction can be determined using the influence lines. After that, shear or moment in a single critical girder is calculated by multiplying the GDF for moment or shear by the corresponding live load effect in a single lane. Equations (1) and (2) describe the previous steps.

$$M_{girder} = (DF)_M \cdot (M_{lane})_{LL} \tag{1}$$

$$V_{girder} = (DF)_V \cdot (V_{lane})_{LL} \tag{2}$$

where M_{girder} and V_{girder} are the girder moment and shear, respectively, and M_{lane} and V_{lane} are the single lane moment and shear, respectively, due to HL-93 loading. Finally, GDF_M and GDF_V are the girder distribution factors for moment and shear, respectively.

The AASHTO LRFD Bridge Design Specifications [4] give the girder distribution factor for flexure in the interior girder in slab-on-girder bridges:

For one live load lane:

$$GDF_M = 0.06 + \left(\frac{S}{4300}\right)^{0.4} \left(\frac{S}{L}\right)^{0.3} \left(\frac{K_g}{Lt_s^3}\right)^{0.1} \tag{3}$$

For two to more lanes:

$$GDF_M = 0.075 + \left(\frac{S}{2900}\right)^{0.6} \left(\frac{S}{L}\right)^{0.2} \left(\frac{K_g}{Lt_s^3}\right)^{0.1} \tag{4}$$

where S is the girder spacing (mm), L is the bridge span length (mm), $K_g = n (I+Ae^2)$ is the girder longitudinal stiffness factor (mm^4), t_s is the deck slab thickness (mm), I is the non-composite girder moment of inertia (mm^4), A is the bare girder cross-sectional area (mm^2), e is the eccentricity between centroid of the girder and the deck slab, and n is the modular ratio between the girder and the deck slab materials.

Similarly, the girder distribution factor for shear in interior girder for the same bridge type is given by:

For one live load lane:

$$GDF_V = 0.2 + \frac{S}{7600} \tag{5}$$

25

For one live load lane or more:

$$GDF_V = 0.2 + \frac{S}{3600} - (\frac{S}{10700})^2 \qquad (6)$$

However, for exterior girders, other expressions are used to calculate GDF as shown below:

$$(GDF)_{Ext} = e*(GDF)_{Int} \qquad (7)$$

where:

$$e = \begin{cases} \text{Flexure:} & e = 0.77 + (d_e/2800) \qquad (8) \\ \text{Shear:} & e = 0.60 + (d_e/3000) \qquad (9) \end{cases}$$

Limitations and restrictions on using these equations are applied, and in some cases other methods, such as the lever rule, should be used to find the girder distribution factor. Also, in case of diaphragms or cross-bracing presence, another check against the rigid body rotation should be applied for exterior girders. In addition, modification factors should be applied when the bridge has a degree of skewness.

For a few special cases, the AASHTO LRFD specifications [4] recommends using the lever rule to compute the GDF instead of using the GDF expressions explained before. For example, it is suggested to use the lever rule to find the GDF for flexure and shear in bridges consisting of deck slab on only three girders, as well as for bridges loaded with one design load lane in the case of shear. The lever rule is a simple method that is based on assuming an internal hinge develops in the deck slab over each interior girder, and then using statics to solve for the reaction of the considered girder as a fraction of the truck load. The computed reaction at the considered girder, representing the GDF, should account for different loading scenarios in the transverse direction and it should be multiplied by the corresponding multiple present factor. Figure 10 shows the lever rule procedure for a bridge section consisting of five girders, in which the GDF is computed for the first interior girder using two-lane loading.
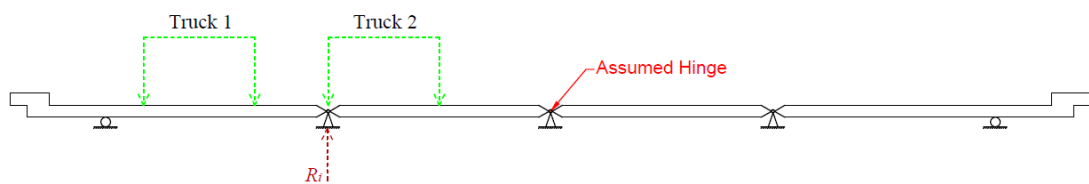
Figure 10: Lever rule procedure

Many researchers are working on developing more accurate and simpler expressions because in many studies it was found that GDF formulas presented by AASHTO LRFD may be too conservative. In particular, it appears that GDFs are more conservative for bridges with large girder spacings and long spans, while they can be somewhat un-conservative for bridges with small girder spacings and short spans [11].

2.6 Deck Slab Analysis in AASHTO

Traditionally in slab-on-girder bridges, the slab is usually designed as a one-way slab rigidly supported by the bridge girders. In this case the main reinforcement steel is perpendicular to traffic flow. This approach was implemented by AASHTO for the first time based on the work of Westergaard in 1930 [12].

The standard AASHTO specifications [8] proposed designing the deck slab for live load moment in 1 m wide strips supported by the girders, based on the following equation:

$$M = \frac{0.8(S + 0.6)P}{9.76} \tag{10}$$

where

S : Effective span length of the slab (m)

P : Weight of the heaviest wheel in the design truck (KN)

Most recently, the AASHTO LRFD specifications [4] recommended using one of three methods to design the concrete deck slab of a bridge for live load. The first one is called the empirical design method based on the internal arching action developed in the deck slab. This approach can be used if some conditions are satisfied; then the reinforcement steel area can be obtained directly in both transverse and longitudinal directions. The second method is called the equivalent strip design, and it is based on the flexural behavior of the deck slab, without considering the internal arching action. This method is based on dividing the concrete deck slab into strips perpendicular to the supporting girders, and subjected to the heavy axle of the truck, then analyzing the strips as a continuous beam on rigid supports at the locations of the girders. The third approach is to use a detailed finite element model to analyze the deck slab behavior. In this study both the equivalent strip procedure and the finite element methods are used to understand the deck slab structural behavior in splayed girder bridges.

The AASTO LRFD specifications introduce three expressions to compute the width of the design strip (SW) at three different critical locations in the deck slab. The first one is at the positive moment regions between the girders, while the second and the third one are at the negative moment regions with one at the overhang, and the other at the interior regions over the girders. Table 1 and Figure 11 summarize the three different expressions of the strip widths for cast-in-place concrete deck slabs.

Table 1: Equivalent strip width equations

Critical moment location	Strip Width (SW) mm
Overhang negative moment	$1140 + 0.833X$
Interior region positive moment	$660 + 0.55S$
Interior region negative moment	$1220 + 0.25S$

Where S is the center-to-center girder spacing (mm) and X is the distance from wheel load to centerline of girder (mm)
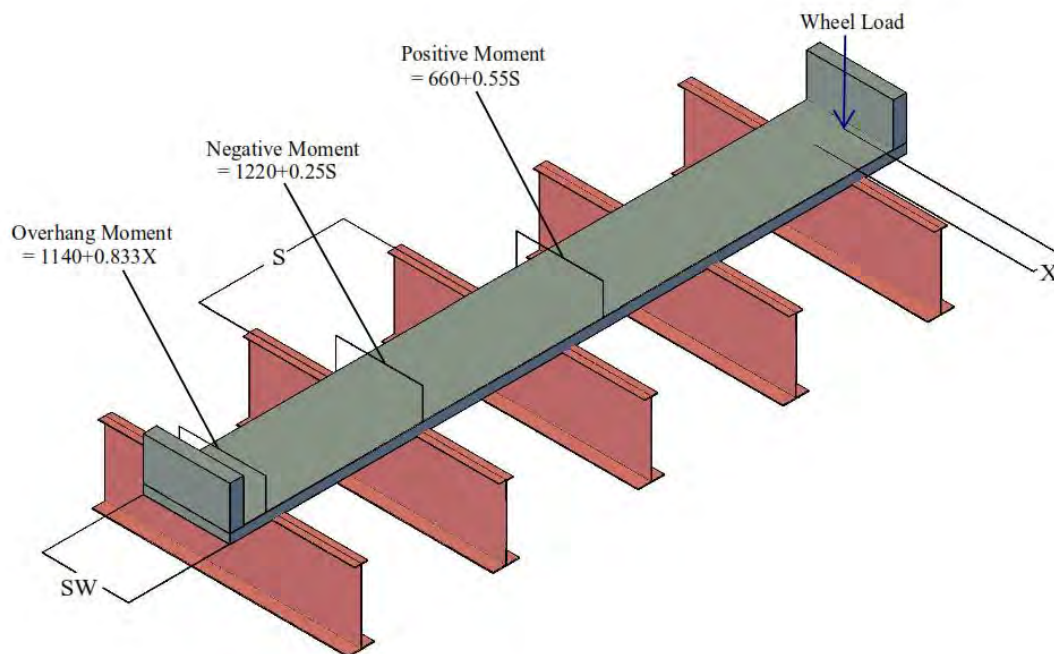
Figure 11: Equivalent strip width expressions

AASHTO stats that the above methods are all applicable for regular slab-on-girder bridges, where all girders are parallel to each other. Note that the use of the strip method to determine critical positive and negative moments in the deck slab requires the use of influence lines. This is because the truck(s) location is not always obvious. Also, multiple presence factor should be used in the calculations.

2.7 Splayed Girder Bridges

A literature search of available research on the subject of splayed girder bridges indicated little published work. Splayed girder bridges are required nowadays more often for many transportation applications. However, the AASHTO LRFD Highway Bridge Design Specifications do not account for the varying girder spacing in the distribution factor formulas. This leads to more conservative designs for splayed girder bridges if the larger girder spacing is used for the whole bridge. Also, this varying girder spacing can have a significant effect on the bridge deck behavior and design.

Buckler et al. [13] studied the effect of girder spacing on bridge deck behavior using the finite element method by modeling three bridges with different girder spacings for each one. As expected, the results gave significant increases in deflections, compressive stresses, and tensile stresses in the deck slab due to the increased girder spacing. For example, an increase in girder spacing by 0.84 m increased the maximum deflection from 0.076 mm to 0.175 mm, which is about 130%. Also, it increased the maximum transverse tensile stresses in the deck slab from 777 KPa to 1074 KPa, which is about 38%. Barr and Amin in 2006 [14] examined the effect of girder spacing on shear distribution factors by modeling more than 200 simply-supported bridges using the finite element method. Their results showed that on average an increase by 0.71 m in girder spacing results in a 7.6% and 27% increase in the distribution factors for shear in the exterior and interior girders, respectively. The study also showed that the formulas used in the AASHTO LRFD Bridge Specification to calculate shear distribution factors for interior girders are slightly un-conservative when compared with the finite element models for small girder spacing of about 1.2 m.

Tabsh and Sahajwani in 1997 [15] investigated the use of an approximate method to calculate the distribution factors for bridges with unequal girder spacing. The method is based on analyzing transverse strips of the deck slab directly under the wheel loads as continuous beams on elastic spring supports referring to the girders, and then placing the resulting reactions on the girders to calculate the girder distribution factor. They examined thirty-one slab-on-steel girder simply-supported and continuous bridges with different unequal girder spacings, and calculated flexural and shear girder distribution factors for each one. They then compared the results with finite element analysis. It was concluded that girder distribution factors calculated using the proposed method for simply supported bridges were on average 5.7% and 3.1% higher than the

corresponding finite element results for flexure and shear, respectively. For continuous bridges, the results showed 13% and 7.6% more conservative estimates for flexure and shear, respectively.

Song et al. in 2003 [16] examined a two-span continuous box-girder bridge with a maximum flare of 6.25% at one of the bridge ends. In the study, the bridge was modeled using the grillage method to find girder distribution factors. The results were then compared with the formulas from AASHTO LRFD specifications when applied to the same bridge, but with constant width equal to the largest in the splayed girder bridge. The authors concluded that distribution factor formulas for box-girder bridges in the AASHTO LRFD specifications can be applied to non-parallel girders, but the values will be more conservative, especially for exterior girders.

As stated earlier, live load distribution factor formulas specified in the AASHTO LRFD specifications [4] might be used only if the bridge geometry met some conditions. Otherwise, the specifications recommend using other applicable refined methods to determine the live load distribution. However, for bridges with splayed girders, the AASHTO LRFD specifications suggest calculating GDFs along the bridge span using a simplified approximate approach. It proposes to use a girder spacing value equal to the average between the two girder spacing values at either side of the considered girder at any section along the girder, which results in a distribution factor value at each point along the span of the bridge [4]. Also, a report by the National Cooperative Highway Research Program NCHRP (Report 592) in 2007 noted that in order to use the lever rule or formulas presented in the AASHTO LRFD specifications for splayed girder bridge design, the largest girder spacing should be conservatively used [17].

Regarding computer software, most of the existing line girder computer programs only allow for constant girder spacing. The AASHTO LRFD specifications suggest to model the splayed girder bridge using parallel girders with the maximum girder spacing in the span, and then run the program and apply the results for the entire span without taking the bridge's splayedness into account, which results in a conservative design [4]. Kansas Department of Transportation (KDOT) proposes the use of AASHTOWare Bridge Design [18] for modeling a splayed girder. Here, an equivalent non-splayed girder bridge with the maximum girder spacing can be modeled in order to represent only the interior girders [19]. Other State Departments of Transportation, like Utah DOT, suggest using a girder spacing at 2/3 of the span on the

wider bridge side to model a non-splayed girder bridge representing the splayed one [20]. Washington State DOT has developed a computer software called PGSuper to design and analyze precast-prestressed girders. In February 2009, a new version 2.1.0 was published with new features, one of them being the capability of modeling bridges with different girder spacings at each end of the bridge [21].

Other concerns regarding the use of splayed girders are cross-frames and diaphragms. Grubb et al. in 2007 [22] advised to keep girders as parallel as possible to avoid varying of cross-frames, complex framing, and changing of overhang width which can result in significant costs and complex framing and reinforcement detailing. Also, Kansas Department of Transportation recommends the use of cast-in-place intermediate diaphragms whenever designing a splayed prestressed girder bridge [19].

Chapter 3: Finite Element Modeling

3.1 Introduction

In this chapter, the finite element method (FEM) is introduced by presenting a brief background about the method development, the general steps of FEM, and the most commonly used elements in composite steel girder bridge analysis. Some of the bridge models used in the literature are explored and compared with each other. Also included in this chapter are details of the finite element model used for analyzing the bridges in this study, with the needed validations to insure the accuracy of the chosen model, elements, and connectivity.

3.2 Background

The early development of the finite element method began in the early 1940s when Hrennikoff in 1941 used one-dimensional elements to solve continuous solids [23]. In 1943, Courant raised the idea of using variational form analysis to obtain the solution of stresses in vibration systems [24]. As a result, a study by Turner et al. [25] outlined the direct stiffness method, which is used to obtain the stiffness matrix for the whole structure, and they derived the stiffness matrices for different types of one- and two-dimensional elements. Although this method started to develop in the early 1940s, the term "finite element" was introduced for the first time by Clough [26] in 1960 when he used triangular and rectangular elements for plane stress analysis. After 1960, more research and development were conducted on the method, where the method was extended to three-dimensional elements, thermal analysis, and large deflections. Later, dynamic analysis was considered, and was associated with other problems such as nonlinear dynamic behavior and material and geometrical nonlinearities.

The finite element method is considered as a numerical method to solve complicated problems in many fields of engineering and physics. It's usually used when an analytical solution is hard to achieve because of the geometrical complexity, material properties, and loading scenarios. Hence, a numerical solution is needed with acceptable accuracy. The concept of this method is based on discretizing the structural system into several smaller parts called "elements" interconnected to each other at particular points called "nodes." Each considers the behavior and properties of the modeled material. These elements are defined by a displacement function with consideration of the stress-strain relationship for each element. The individual elements

32

are then assembled in a global stiffness matrix in order to be solved using matrix analysis to give the behavior of the whole structure with consideration of boundary conditions. Theory of the finite element method is covered in many text books [27] [28] [29].

With the method development, different types of elements with many connections are used to solve complex structures. For better accuracy, the number of elements within the structure gets higher, which means more equations need to be solved. High-speed computers and the developed finite element software take part in modeling accurately complex structures. There are numerous numbers of finite element programs, and each has different capabilities and uses [30], such as Abaqus, ANSYS, NASTRAN, and LS-DYNA.

In this study, ANSYS Finite Element software [3], available in the College of Engineering at AUS, is used to model all the analyzed bridges. This software has powerful capabilities in performing 3D complex structural analysis whether it's static or dynamic, linear or nonlinear, or elastic or inelastic. Such features make it usable in different engineering fields including fluids, mechanics, thermal, and structural.

3.3 Finite Element Modeling of Bridges

Due to the significant time, expense, and complex physical testing needed for a full-scale bridge, some approximate analytical methods were used to determine the behavior of the bridge superstructure. The AASHTO LRFD Bridge Design Specifications [4] approve the use of a method that satisfies compatibility and equilibrium in design and analysis. Examples of these methods can be the grillage analogy method used by Song et al. [16], yield line method, and finite element method [15] [31] [32] [33] [34] [35].

In order to develop an accurate 3D model for any slab-on-girder superstructure using finite element modeling, element types must be chosen carefully and connectivity must be understood. Figure 12 shows the superstructure components and the different types of elements often used in finite element modeling.

Many slab-on-girder bridge models have been developed through the past years in different approaches using different types of finite elements. The simplest finite element model was developed using shell elements for deck slabs, and beam elements for girders, connected to each other by rigid links to account for the eccentricity between c.g of the slab and c.g of the girder [34] [35].

33
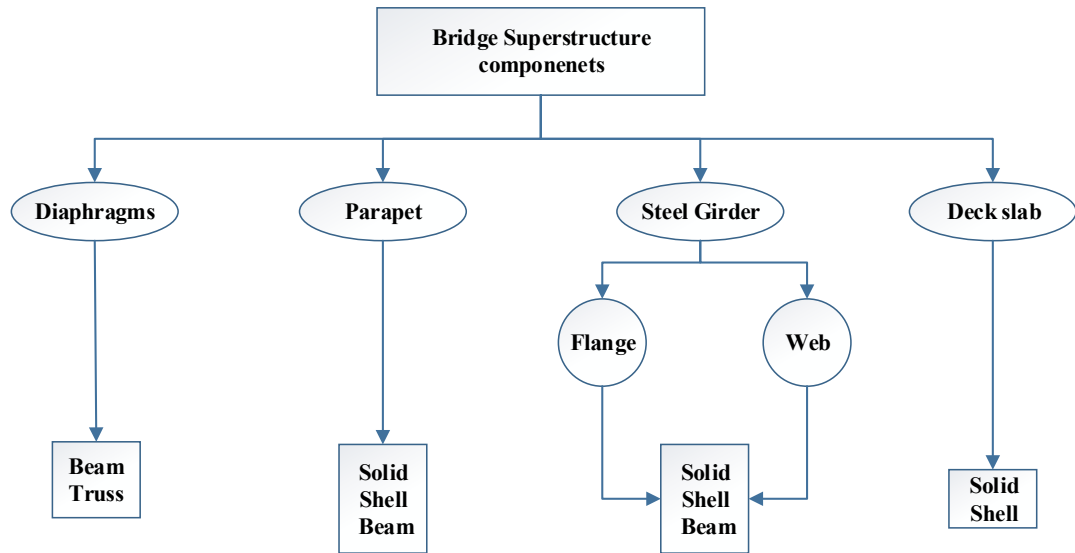
Figure 12: Finite element types used for each superstructure component

A simpler approach was used by Hays et al. [33], but the deck slab and the girders shared nodes at the center of the girder without accounting for eccentricity between the two of them. A model used by Ventura et al. [34] used the same approach as Hays et al. [33], but with increased moment of inertia in beam elements used to model the girders positioned at the top flange in order to account for the composite action between the deck slab and the girders. The problem in Hays et al. [33] and Ventura et al. [34] models is that they cannot accurately define the boundary condition because in both models the boundary conditions are applied at the beam element nodes that represent the entire girder, while it should be applied at the bottom flange of the girder, resulting in great error. Chen's model [35] overcomes this problem by using zero dimensional elements at the girder's bottom flange, and connecting these elements to the center of the beam element using rigid links.

(a) Chen [35]   (b) Ventura et al [34]   (c)Hays et al. [33]
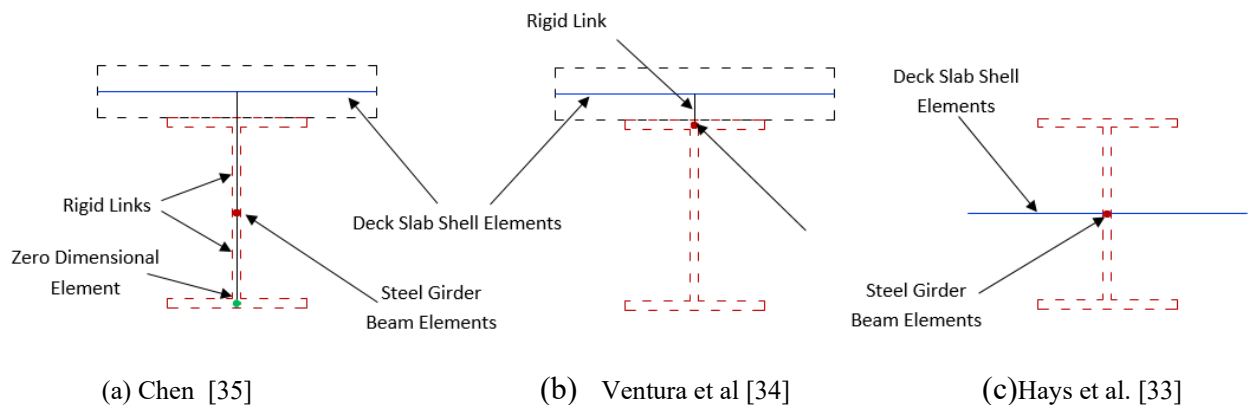
Figure 13: Difference between three finite element modeling approaches

In Tabsh and Sahajwani [15] and Tabsh and Tabtabai [36], four-node rectangular shell elements are used to model the deck slab, where the steel girders were divided into two parts. The top and bottom flanges are modeled as beam elements, while the web is modeled as a shell element. The composite action between the deck slab and steel girder was accomplished using rigid short beams as shown in Figure 14. Bishara et al. used the same approach to model the steel girders, but they used triangular three-node elements to model the deck slab [37]. Machado et al. used the same model used by Tabsh [15] [36] to model the deck slab, but the steel girder top flange, bottom flange, and the web were modeled each as three-dimensional Euler beam elements [38].
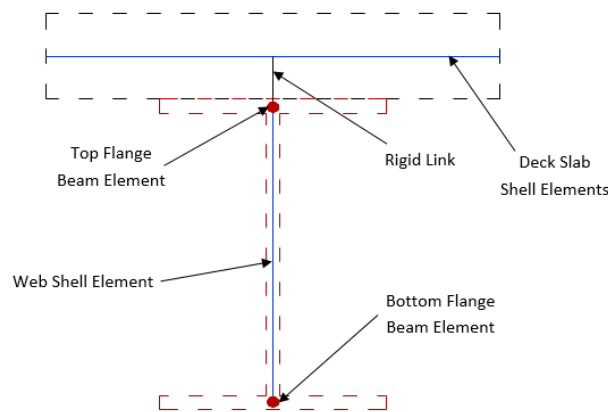
Figure 14: Finite element model by Tabsh [15] [36]

Mabsout et al. [39] used solid elements to model the deck slab and four node shell elements to model the steel girder top flange, bottom flange, and web as shown in Figure 15. Similarly, Wu modeled the deck slab using solid elements, and the steel girder using shell elements, but both with reduced integrations in order to decrease the computation time [40]. Eamon and Nowak developed another model using solid elements to model the deck slab, beam elements to model the girders, and rigid links to account for the composite action between the deck slab and steel girder [41]. The main disadvantage of modeling the deck slab as solid elements is that multiple layers of solid elements are required through the deck slab cross-section to account for the constant strain variation of these elements through thickness. Therefore, a higher computational time is needed to get the flexural behavior of the structure [42]. Multiple layers of solid elements in the deck slab are required if the slab behavior is needed in the study.
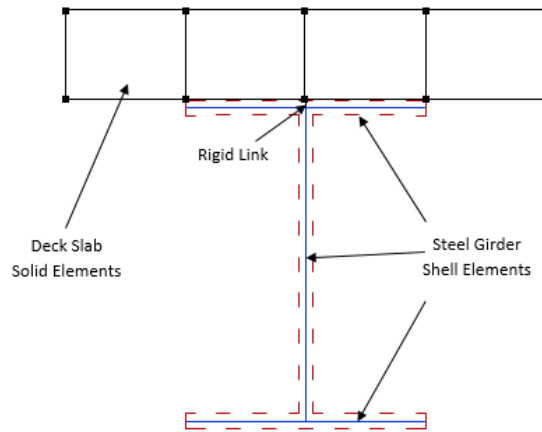
Figure 15: Finite element model by Mabsout et al. [39]

Chung and Sotelino used eight node Mindlin shell elements to model the deck slab in order to account for transverse shear flexibility, and four different approaches to model the steel girders named as G1, G2, G3 and G4 as shown in Table 2.

Table 2: Chung and Sotelino (2005) girder finite element models [42]

Model Name	Girders	
	Flanges	Web
G1	Shell Elements	Shell Elements
G2	Beam Elements	Shell Elements
G3	Shell Elements	Beam Elements
G4	Beam Elements	Beam Elements

As shown in Table 2, G1 was modeled using shell elements for both flanges and web, where G2 used shell elements for web and beam elements for flanges. On the other hand, G3 was modeled using shell elements for flanges and beam elements for the web, and G4 flanges and web were modeled as beam elements. All models were modeled and evaluated using the commercial software ABAQUS, and it was concluded that models G3 and G4, as simple they are, gave accurate results regardless of the mesh refinement. Models G1 and G2 required a considerable mesh in order to give accurate results, which results in higher computational costs. However, models G1 and G2 give more accurate results for the local behavior of the system.

Using ANSYS software, the girders are going to be modeled in this study with four-node shell elements for both flanges and the web. In ANSYS SHELL181 [3] the elements are suitable, where it's effective in analyzing thin elements to elements with average thickness, and it's a four-node element where each node has six DOF (3

36

translational and 3 rotational). The material for all girders is steel which has a 200 GPa modulus of elasticity and 0.3 Poisson ratio.

The concrete deck slab is going to be modeled in ANSYS with eight-node solid elements. Many researchers in the literature used shell elements for modeling the deck slab which results in a big eccentricity between the top flange and the center of the deck slab represented by the shell element, and in this case rigid links are used to connect the elements as shown in Figure 14 in the model for Tabsh and Sahjwani [15]. The problem in using rigid links is the concentration of the stresses at the end points of the rigid links within the deck slab. Using solid elements to model the deck slab will decrease this eccentricity, but if the flange shell element is away from the deck slab to account for the flange thickness, as in Mabsout et al. [39], the concentration of stresses within the deck slab will still affect the behavior of the structure. In this study in order to reduce this effect the top flange shell element will be exactly at the bottom layer of the deck slab, and the lost thickness of the top flange within the deck slab is going to be added to the girders web, to maintain the section properties. Moreover, the ANSYS SOLID185 [3] element is used in the deck slab modeling, where it's defined by eight nodes with each using three translational DOF. This element has large strain capabilities, plasticity, and large deflections. The deck slab material is concrete with a 25 GPa modulus of elasticity (corresponding to 30 MPa compressive strength), and 0.2 Poisson ratio. Past studies have shown that the stiffness of the concrete in the deck slab has little effect on the load distribution in the bridge members.

Diaphragms in the form of cross-bracing are modeled using two-node beam elements. ANSYS BEAM188 [3] elements are suitable for such structures, where they have 6 DOF (3 translational and 3 rotational) and can be used to analyze slender members. The diaphragm material is steel which has a 200 GPa modulus of elasticity, and 0.3 Poisson ratio.

All bridges listed in this study are simply-supported. Therefore, any girder has fixed translations in all directions except for the one along the span length, where the girder is free to move in this direction at only one end. This simulates a pin support at one end and a roller at the opposite one for each girder, which can precisely model the boundary conditions of the bridge. Live load is represented by moving HL-93 trucks, each one with 6 wheels. In order to accurately locate the trucks on the bridge, loading patches are used to transfer the loads to the deck slab, where each loading patch is 300x300 mm and 1 mm thick. ANSYS SHELL181 [3] is used to model the loading

patches (tier patches), and the material assigned to it is steel with the same properties as the one used for the girders. The loading patch is loaded by only one concentrated load at the center of the patch. The purpose of using these elements is to load the bridge at the exact desired location, without loading the deck slab directly which gives more freedom in meshing the deck slab. The loading patches, expressing the trucks, are moved around the deck slab in the longitudinal and transversely directions to maximize their effect in flexure and shear, resulting in the maximum girder distribution factor (GDF) in a specific girder. Figure 16 and Table 3 summarize the finite elements used in this study to model composite steel bridge superstructures.
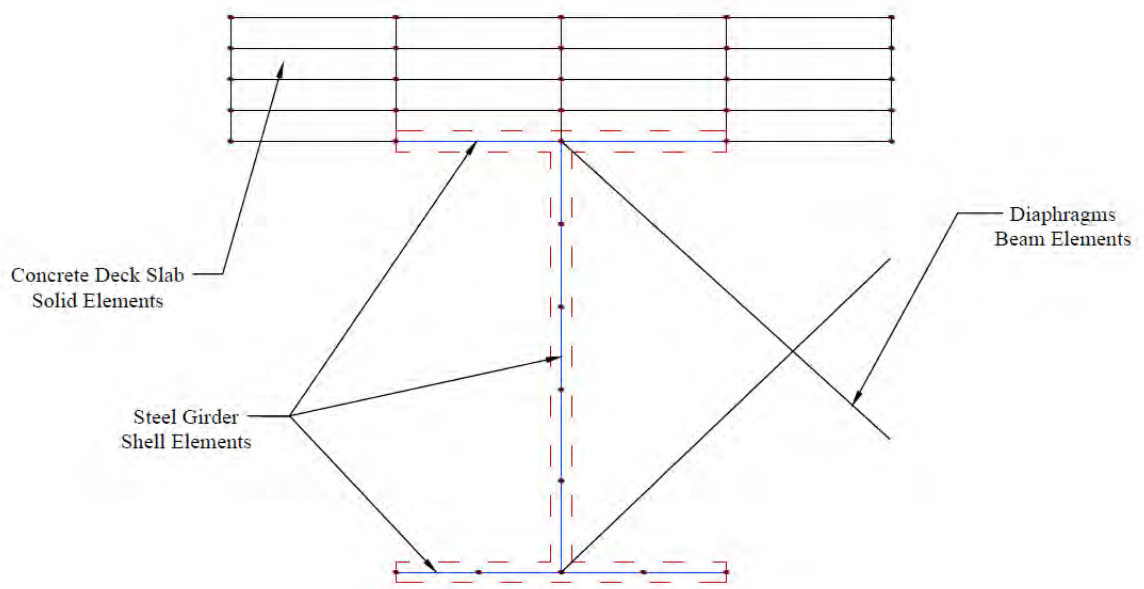
Figure 16: Types of finite elements used in the proposed model

Table 3: Finite elements used in the study
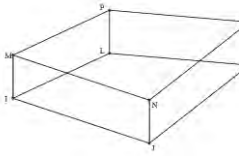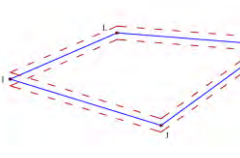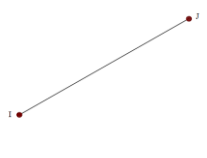
Bridge Element	Deck Slab	Girder (web and flanges)	Loading Patch	Diaphragms
ANSYS Element				
	Solid 145	Shell 181		Beam 188
Number of Nodes	8 (I,J,K,L,M,N,O,P)	4 (I,J,K,L)		2 (I,J)
DOF	3 (3 translational)	6 (3 translational and 3 rotational)		6 (3 translational and 3 rotational)

Figure 17 shows a full bridge superstructure modeled using ANSYS using the finite elements described before. The bridge consists of 5 parallel girders simply supported with a span length of 40 m, the girder spacing is 3.375 m, and the diaphragm

spacing is 5 m. This bridge will be used later in this chapter as part of the model verifications.
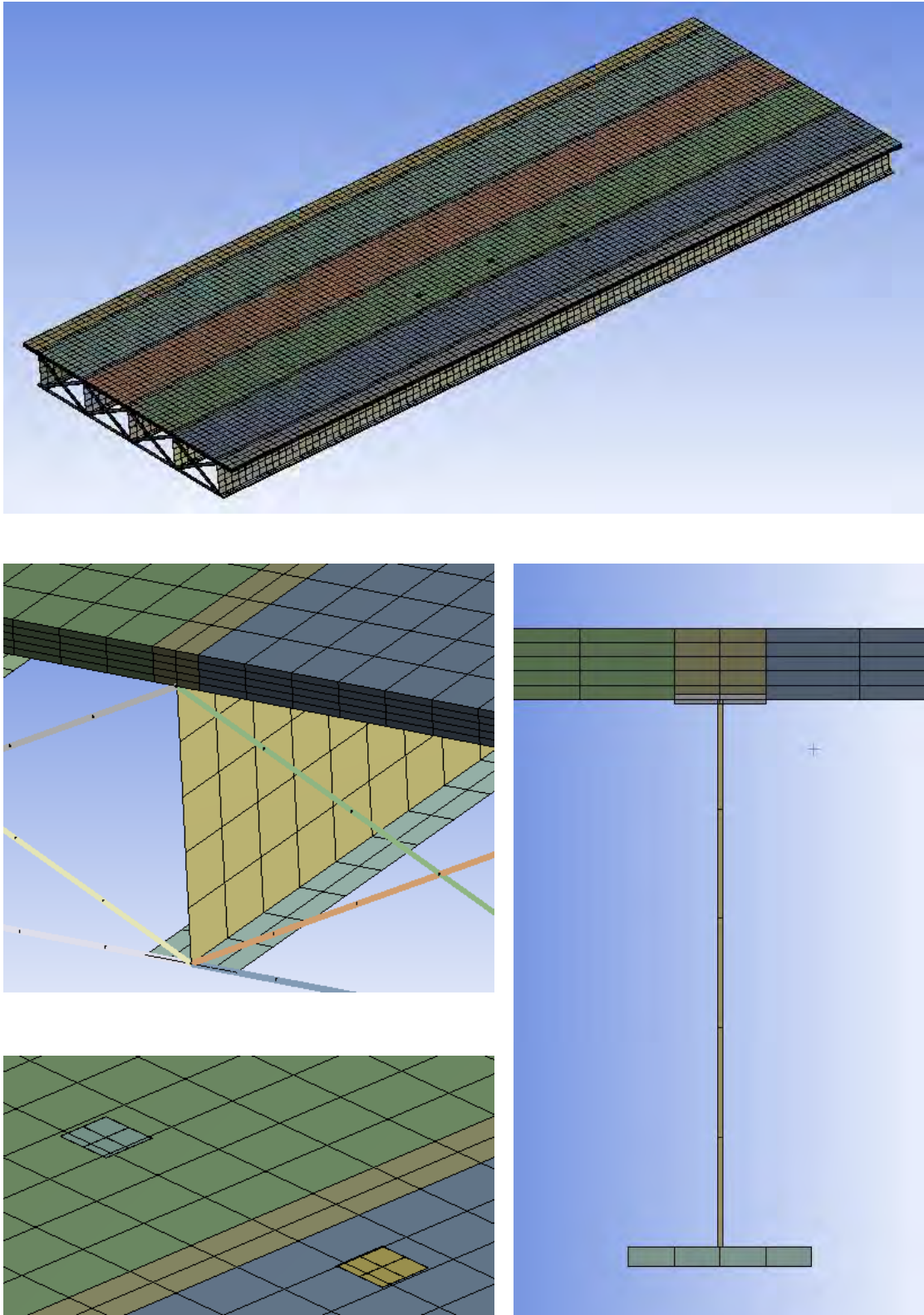
Figure 17: FE model for a 40 m simply-supported bridge with 5 parallel girders

3.4 Model Verification

In this section, the previously suggested finite element model is verified in different ways to ensure that the model and the chosen elements are reasonably accurate. Although the finite elements in use were verified by scholars in different studies as shown back in Section 3.3, it is better to double-check the model. Four different types of verification approaches are listed: a single composite girder with varying deck width, a full-scale bridge model stress comparison, a full-scale experimental bridge, and two constructed bridges tested and analyzed in the literature.

A simply-supported composite girder is modeled using ANSYS, and the results are compared with the analytical approach. This verification has two goals: the first one is to make sure that the finite elements types and connectivity give a good accuracy, and the second one is to ensure that the use of thin loading patches described before in Section 3.3 will not affect the outcomes. In this approach two outcomes are tested: the maximum deflection, and the maximum stress of the girder. The composite girder modeled by ANSYS has a varying deck slab width of 4500 mm at one end and 2250 mm at the opposite end. The modulus of elasticity is 25000 MPa and 200000 MPa for concrete and steel, respectively. The girder is loaded with 100 KN at the middle of the span, and the rest of dimensions and details are described in Figure 18. In the analytical approach, an average width of 3375 mm is taken as the deck slab width for the entire span, and the girder dimensions and other properties are the same as shown in Figure 19. The maximum stress was calculated for the analytical solution using equation (11) listed below:

$$\sigma_{max} = \frac{M.c}{I_c} \tag{11}$$

where:

I_c :   Composite girder moment of inertia (mm^4)

M :   Moment due to point load at mid span (N.mm)

c :   Distance from neutral axis (mm)

The finite element mesh size used to model this single girder by ANSYS is the same used for all the modeled bridges in this study. The girder is going to be modeled twice for this particular verification. The first model is loaded with a 100 KN point load at the mid span of the girder directly on the deck slab solid elements, where on the second model a shell element loading patch placed at the mid span of the girder is used,

and then this loading patch is loaded with a point load of 100 KN. For both models, the maximum deflection and the maximum stress in the longitudinal direction values from the finite element solution are compared with each other, and then the stresses are compared with the analytical solution.
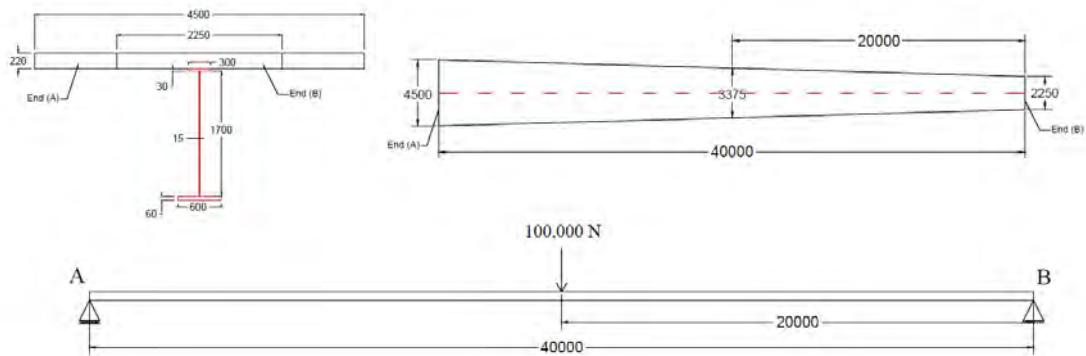
Figure 18: Simply supported girder with varying width
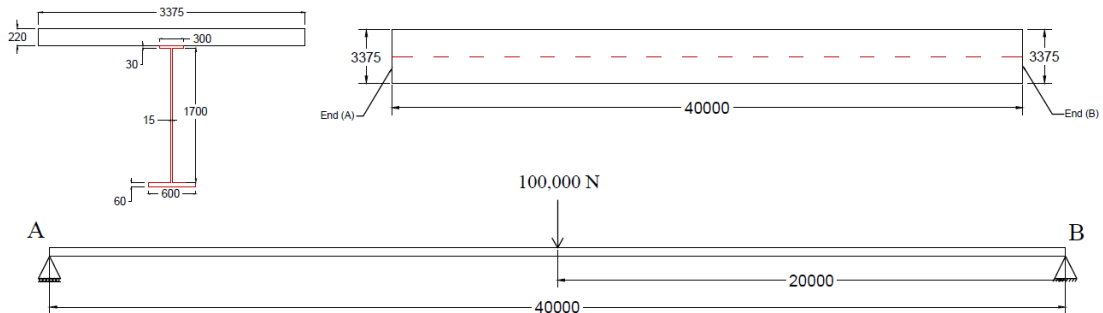
Figure 19: Simply supported girder with average width

The maximum stress and the maximum deflection from the first model (the deck slab is directly loaded) are 12.866 MPa and 7.094 mm, respectively. By using a loading patch to transfer the load to the deck slab, the values from the second model are 12.864 MPa and 7.093 mm, respectively. This means there is only a 0.016% difference in the stress, and a 0.014% difference in the deflection value, which indicates that using a loading patch will not affect the results of the model because the difference is negligible. This comparison is summarized in Table 4.

Table 4: First verification results summary

Measured outcome	With no loading patch	With loading patch	Percentage difference
Maximum stress (MPa)	12.866	12.864	0.016%
Maximum deflection (mm)	7.094	7.093	0.014%

41

After calculation, the value of the maximum stress from the analytical approach is equal to 12.98 MPa. This means there was only a 0.9% difference in stress between the analytical approach and the finite element results from ANSYS.

The second verification is based on modeling a bridge and comparing its stress results with the analytical solution of a beam line (one girder). The modeled simply-supported bridge consists of five parallel steel girders with the same size used for the first verification, spaced at 3.375 m, and connected to a concrete deck slab that is 220 mm thick, with a span of 40 m and an overhang width of 1.125 m. The modulus of elasticity is 25000 MPa and 200000 MPa for concrete and steel, respectively, with the Poisson ratio of 0.2 and 0.3, respectively. The bridge is loaded using AASHTO LRFD design Truck HL-93 at the mid span of the bridge, but at different locations in the transverse direction. Figure 20 shows all dimensions and truck loading positions and magnitudes.
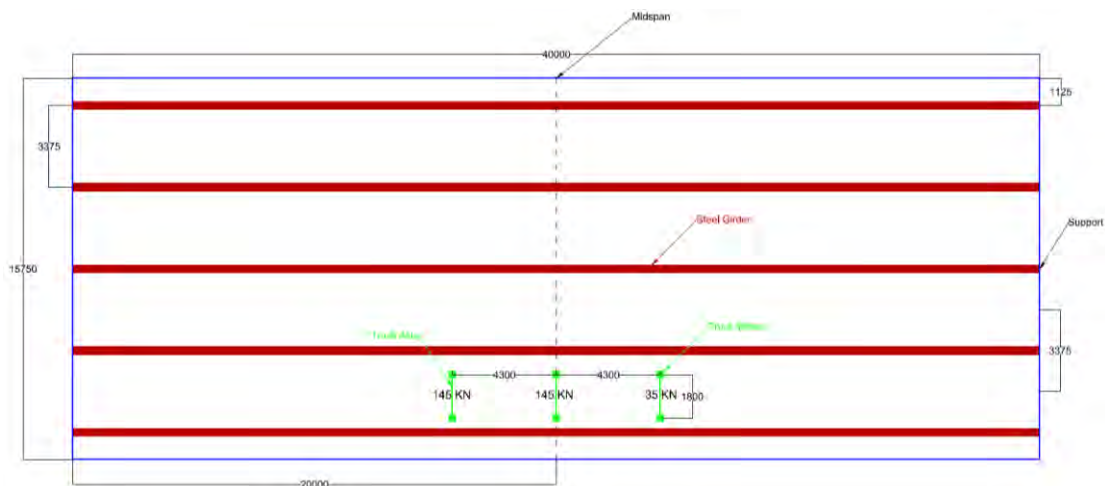
Figure 20: Simply-supported 40m span bridge with 5 parallel girder

In order to compare this bridge with the beam line method, a single composite girder with a deck slab width equal to the bridge deck slab total width divided by the number of girders (15750/5=3150 mm) is loaded with the HL-93 truck at the mid span. Then the longitudinal stress at the girder's bottom flange is compared with the sum of stresses due to loading the whole bridge with the same truck load at the mid span of the bridge. The girders' dimensions and loads are shown in Figure 21.

Figure 21: Single beam girder dimensions and loading for analytical solution

42

The flexural stress in the longitudinal direction at the bottom flange of the girder at mid span in the single beam theory is 36.790 MPa. On the other hand, the sum of flexural stresses in the longitudinal direction due to the HL-93 load at different locations in the transverse direction are shown in Table 5.

Table 5: Summation of girder stresses in the second model verification

Distance from parapet	G1 (MPa)	G2 (MPa)	G3 (MPa)	G4 (MPa)	G5 (MPa)	Sum (MPa)
600	23.489	12.082	3.639	-0.034	-2.317	36.859
1200	20.339	13.434	4.504	0.482	-1.948	36.811
1800	17.294	14.574	5.455	1.024	-1.568	36.779
2400	14.475	15.338	6.534	1.604	-1.174	36.777
3000	11.939	15.581	7.758	2.223	-0.762	36.749

It can be noted that the maximum difference in flexural stress does not exceed 0.19% between the beam line method and the finite element model of the whole bridge, which means that sum of the distributed stresses among the girders is almost the same stress value for the beam line method.

The third verification is to compare the finite element model with an experimental test of a full-scale bridge constructed and tested in a laboratory by Fang et al. [43]. The bridge chosen for this approach is a simply-supported bridge consisting of three parallel composite steel girders with a span of 14.93 m. The concrete deck slab is 190.5 mm thick connected to three W36x150 steel girders using shear studs, the girder spacing is 2134 mm center to center, and the overhang width is 991 mm. Diaphragms were placed at both ends of the bridge, and one at the mid span of the bridge. All dimensions are shown in the bridge layout in Figure 22.

The bridge is loaded with four point loads. Each is 89 KN in magnitude placed at 4420 mm from the support in the longitudinal direction, and 914 mm from the symmetry line in the transverse direction as shown in Figure 22. The modulus of elasticity has a value of 28,720 MPa, and 199,950 MPa for the concrete deck slab and the steel girders, respectively. Also, the Poisson ratio is 0.2 and 0.3, respectively.
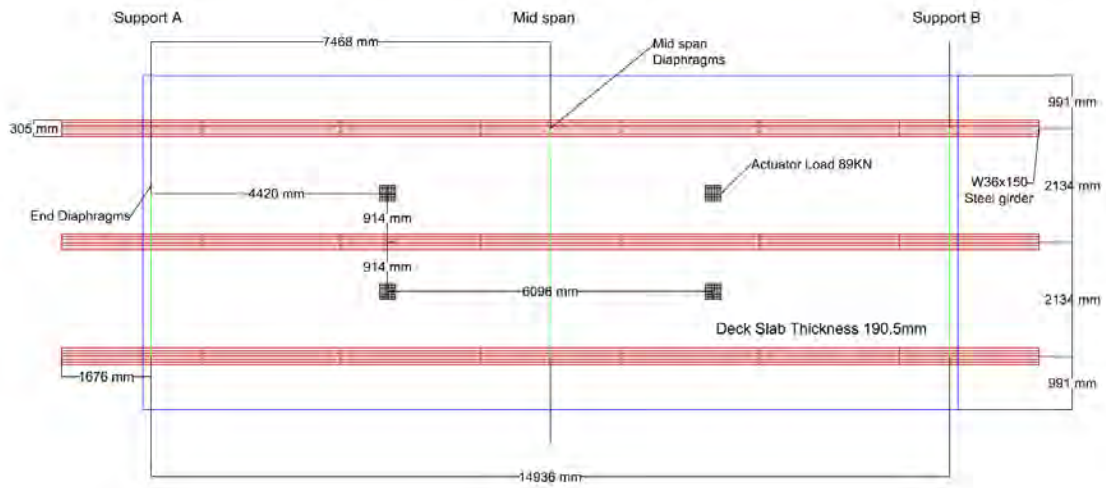
Figure 22: Full scale experimental bridge plan layout, Fang et al. [43]

This bridge is modeled by ANSYS using the same elements and meshing approach described before and used for the first verification. The behavior of the bridge is examined and compared with the test results. Figure 23 shows the behavior of the bridge described through the deflected shape and the deflection contour.
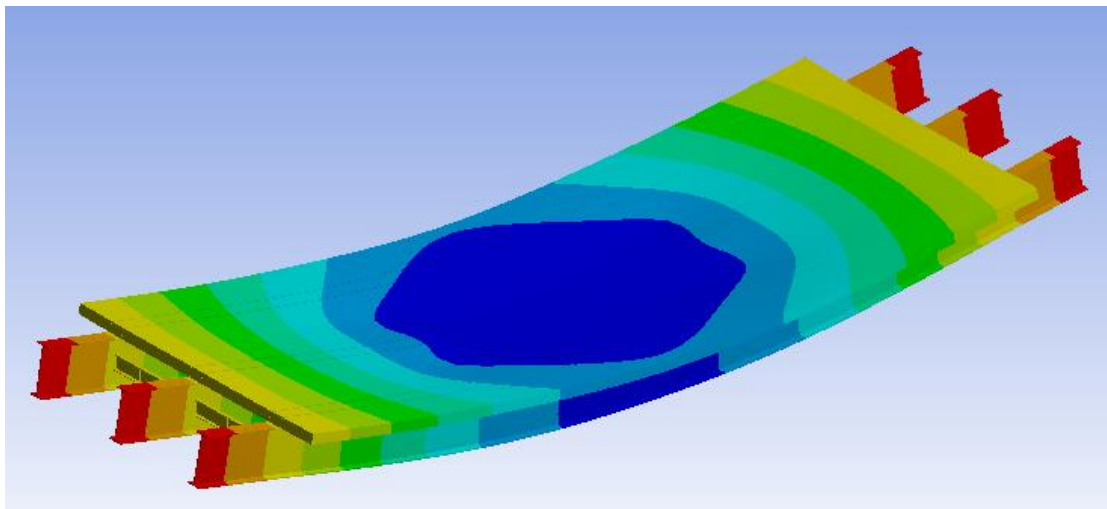
Figure 23: Deflected shape and deflection contour from ANSYS, Fang [43].

A comparison between the deflection values from the experimental test and the ones from the finite element model by ANSYS is summarized in Table 6, where the difference is in the accepted limits. It can be concluded that the model can adequately represent this full scale experimental bridge.

Table 6: Second verification results summary

Examined aspect	Lab test result Fang et al.	Finite Element results	Difference	Difference Percentage
Deflection at the **exterior girder**, at a point through the load in the transverse direction (mm)	2.413	2.860	0.447	19.8%
Deflection at the **interior girder**, at a point through the load in the transverse direction (mm)	3.302	3.350	0.048	1.45%
Deflection at the loading point (mm)	3.556	3.393	0.163	4.58%

The fourth verification consists of comparing a field-tested bridge analyzed in the literature with the finite element findings of the same bridge modeled by ANSYS. The considered bridge, shown in Figure 24, was tested by Schönwetter in the late 1990s [44], and it is called the Big Creek Relief Bridge in Texas. The tested unit of the bridge is a symmetric 4-span continuous unit, and the span lengths are 7925 mm, 10363 mm, 10363 mm, and 7925 mm.

Figure 24: Big Creek Relief bridge [44]

The bridge cross-section is presented in Figure 25, and consists of 5 steel girders spaced at 1980 mm, and a concrete deck slab of 152 mm. The modulus of elasticity is 200,000 MPa for the steel girders, while it is 19,515 MPa for the concrete deck slab.

The bridge was loaded using one truck placed longitudinally at the third span of the bridge as shown in Figure 26. In the transverse direction, the truck is positioned at 5 different locations each to maximize the flexure effect in the girder under consideration. The stresses were recorded using strain gauges located at the bottom flange of the girders at the longitudinal location shown in Figure 26.
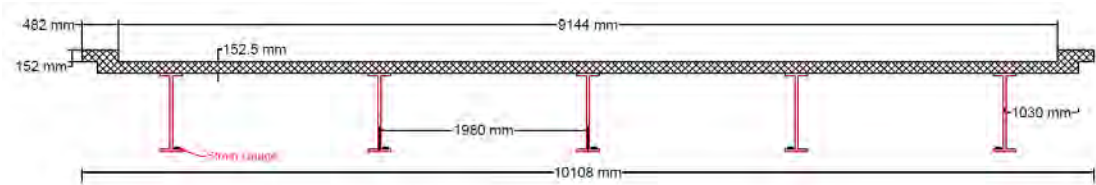
Figure 25: Big Creek Relief bridge cross-section [44]
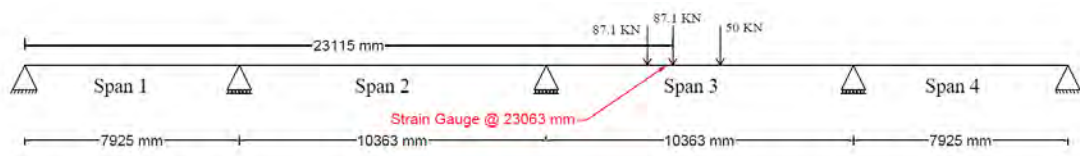
Figure 26: Big Creek Relief bridge truck loading position and magnitude [44]

This bridge is modeled by ANSYS using the same elements and meshing properties, and is then loaded at the same location with the same magnitude. However due to the symmetry of the bridge in the transverse direction, only three stress values for the exterior, first interior, and intermediate girder were recorded and compared with the field test results. Table 7 compares the FE stress results with the field test results at the same locations, and it can be concluded that the FE results are reasonable and close to the field test results, especially for exterior and intermediate girders.

Table 7: Creek Relief Bridge verification results [44]

Method	Girders stress (MPa)						
	Exterior			interior			
	G1	G5	Critical	G2	G3	G4	Critical
Field Test	5.5	4.9	5.5	4.0	5.2	4.5	5.2
FE	5.73	5.73	5.73	5.41	5.44	5.41	5.44
Percentage difference			4.18%				4.62%

It is interesting to note that although the bridge geometry and loading are both symmetrical, the experimental testing showed different stress values in the exterior girders (G1 and G5) and interior girders (G2, G3 and G4). Therefore, the maximum critical stress values in both interior and exterior girders are compared with the FE findings by ANSYS.

Based on the previous literature review, and the four model verification approaches, it can be concluded that the proposed finite element model compared to the theoretical calculations gives very small errors, and compared to the experimental test the results are within the accepted limits. It should be noted that the literature predicts that stresses by finite element analysis will be higher than the ones recorded in the field. This is because field conditions involve un-intended fixity at the supports. Thus, the considered finite element model by ANSYS is reliable, and it can be used to carry out the modeling process of all bridges under study.

Chapter 4: Methodology

4.1 Introduction

This chapter addresses the methodology followed in this research, where it explains and discusses the splayed girder bridge parameters under consideration. Also, it presents the truck loading approach and positioning in splayed girder bridges in order to maximize live load effect in interior and exterior girders as well as its effect on deck slab stresses, whether in the longitudinal or the transverse direction. Moreover, the girder distribution factor calculation process through finite element method results is presented. This chapter discusses in depth only one splayed girder bridge that is taken as a reference to the other bridges examined through the parametric study. Whenever possible, comparisons with the AASHTO formula for live load distribution are included.

4.2 Bridges and Parameters Considered

A splayed girder bridge with particular dimensions and material properties is chosen as a reference bridge. The considered parameters are the girder spacings (S_1 and S_2), slab thickness (t_s), diaphragms spacing (D), girder stiffness in terms of the girders' web depths (d), number of girders (n), and span length (L). In the parametric study, one parameter is increased and decreased beyond the reference value, while all other five parameters are kept unchanged. As the girders in this study are splayed, and the spacing at the beginning of the bridge differs from the one at the end, and the girder spacing parameter is changed four times using two different aspects. The first one is (S_2-S_1)/L which represents the degree of splayedness of the bridge, and by varying this parameter twice, once up and once down, the girder spacing as a result is changed at one end and kept constant at the other. The second aspect is the S_1/S_2 ratio, where the degree of splayedness ((S_2-S_1)/L) is kept constant by changing the girder spacing of the end that was kept constant through the first aspect, which also generates two different bridges. The overhang cantilever width (OH) is taken as a percentage of the interior girder spacing equal to 0.33 in all bridges which is a common practice. Therefore, a total of fifteen bridges are modeled by ANSYS to carry out the parametric study. The steel girder used in all considered bridges consists of a 30 x 300 mm top flange, 60 x 600 mm bottom flange, and a web with a thickness of 15 mm and varying girder depth (d)

as shown in Figure 27. The chosen cross-bracing consists of two or three equal angle sections of 150x15 mm. Three equal-angle sections are used at the ends of the girders, while between the ends of the bridge only two sections are used, as shown in Figure 28. The concrete parapet cross-section is 300 mm wide with 1000 mm height. Figure 29 shows the parameters under consideration through a standard splayed girder bridge arrangement, and the bridge's characteristics with the affected parameter are shown in Table 8.
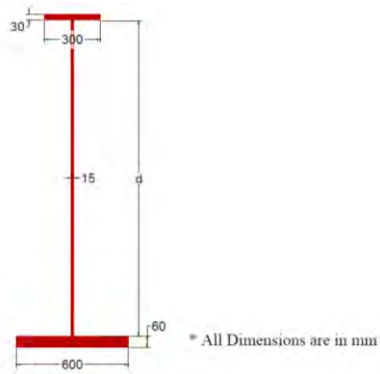
Figure 27: Steel girder dimensions
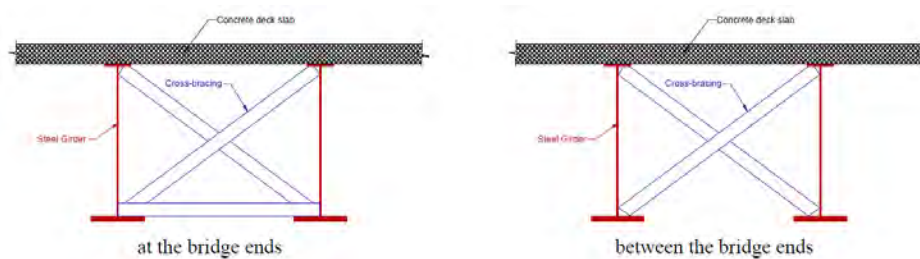
Figure 28: different cross-bracing types
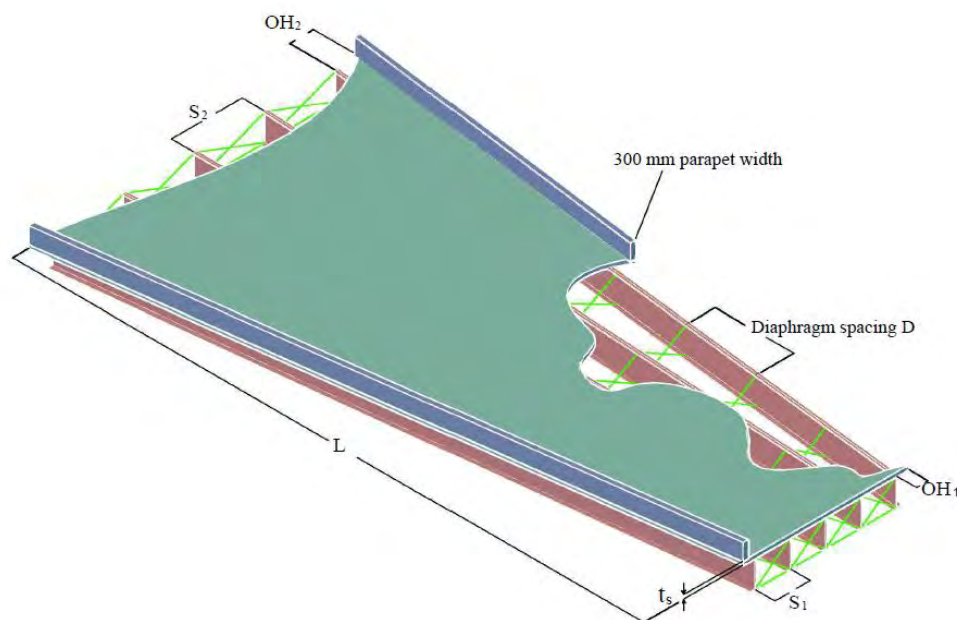
Figure 29: Standard splayed girder bridge arrangement

Table 8: Bridge parameters considered in the study

Parameter	Girder Spacing				Slab Thickness t_s (mm)	Diaphragm Spacing D (m)	No. of girders n	Girder Depth d (mm)	Span Length L (mm)
	$(S_2-S_1)/L$		S_1/S_2						
	S_1 (mm)	S_2 (mm)	S_1 (mm)	S_2 (mm)					
Reference	2250	4500	2250	4500	220	40	5	1700	40000
Lower value	3000	4500	3000	5250	150	5	3	1400	30000
Upper value	1500	4500	1500	3750	300	10	7	2000	50000

The fifteen considered bridges shown in Table 9 are modeled using the finite element software ANSYS [3] to find the girder distribution factor and load effect in the deck slab. The truck position is changed in each model to maximize the live load effect in the transverse and longitudinal directions for moment and shear. Also the truck rotational angle within the bridge plan is examined to maximize this effect, as shown in the sections to follow.

Table 9: Considered bridges 1 to 15

Bridge No	S_1 (mm)	S_2 (mm)	L (mm)	t_s (mm)	D (m)	n	d (mm)	OH_1 (mm)	OH_2 (mm)
1	2250	4500	40000	220	40	5	1700	750	1500
2	3000	4500	40000	220	40	5	1700	1000	1500
3	1500	4500	40000	220	40	5	1700	500	1500
4	1500	3750	40000	220	40	5	1700	500	1250
5	3000	5250	40000	220	40	5	1700	1000	1750
6	2250	4500	40000	150	40	5	1700	750	1500
7	2250	4500	40000	300	40	5	1700	750	1500
8	2250	4500	40000	220	5	5	1700	750	1500
9	2250	4500	40000	220	10	5	1700	750	1500
10	2250	4500	40000	220	40	3	1700	750	1500
11	2250	4500	40000	220	40	7	1700	750	1500
12	2250	4500	40000	220	40	5	1400	750	1500
13	2250	4500	40000	220	40	5	2000	750	1500
14	2250	4500	30000	220	40	5	1700	750	1500
15	2250	4500	50000	220	40	5	1700	750	1500

4.3 GDF and Truck Critical Position

This study considers the behavior of composite steel splayed girder bridges. Therefore, to understand the live load effect in such bridges, one or more trucks are placed on the bridges' superstructure in different lanes. The girder distribution factor is calculated for flexure and shear to analyze, and deck slab stresses are determined. The truck position in the longitudinal and transverse direction is very critical to maximize the effect of live load in the bridge elements. This chapter will explain the approach used to maximize these effects, and the logic behind it.

4.3.1   Live load effect in girders.

Traditionally in the US, the live load effect in girders is considered by the use of a girder distribution factor (GDF) for flexure or shear. Such a factor depends on the most critical truck position. In this section, the truck position issue is addressed and explained.

4.3.1.1 Truck longitudinal positioning.

As per the AASHTO LRFD specifications [4], no more than one truck is allowed to be placed in each lane. In order to maximize the moment in a simply-supported bridge with parallel girders, the truck is generally placed at the mid span of the bridge, and by using an HL-93 truck the middle axle is placed at the mid span of the bridge. This moment is not necessarily the largest moment, but since the dead load moment occurs at the mid span, it is a common practice to consider the combined effect at the mid span. However, in a splayed girder bridge this is not the case, because the varying width of the bridge deck slab causes the maximum moment in the girders to be shifted away from the mid span toward the region with larger girder spacing.

This shift is approximated in this study using a simple approach, based on the longitudinal location of the dead load maximum moment position. Thus, in a splayed girder simply-supported bridge, a single composite girder is isolated and analyzed to find the maximum moment position due to the trapezoidal uniform dead load. As the approach is empirical, there is no need to consider the weight of the parapet, diaphragms, stay-in-place metal deck form, or wearing surface. The truck is then placed longitudinally at this position to maximize the live load effect. Figure 30 shows a single composite girder isolated from the reference bridge (B1) loaded by its own self-weight, with the resulting shear and bending moment diaphragms. The shift from mid span for

the reference bridge is 835 mm which represents the location of zero shear or maximum moment from mid span.
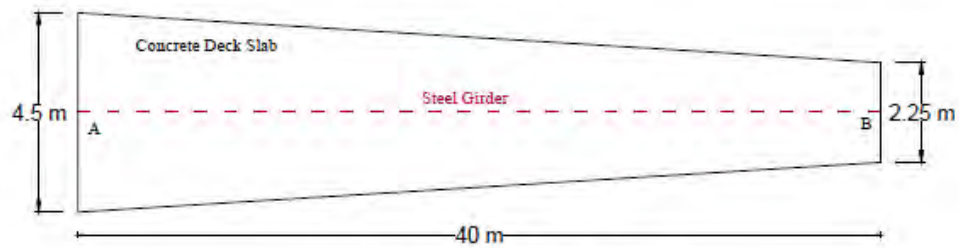
(a) Isolated girder plan view
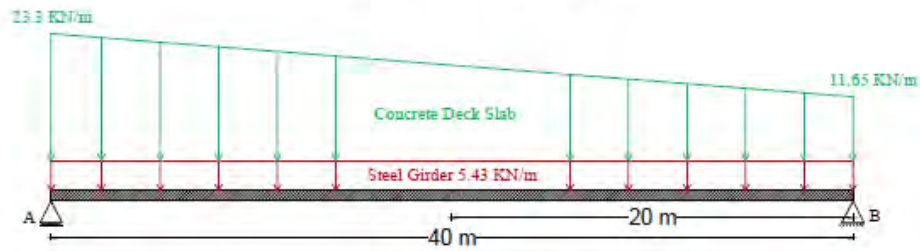
(b) Self weight loading
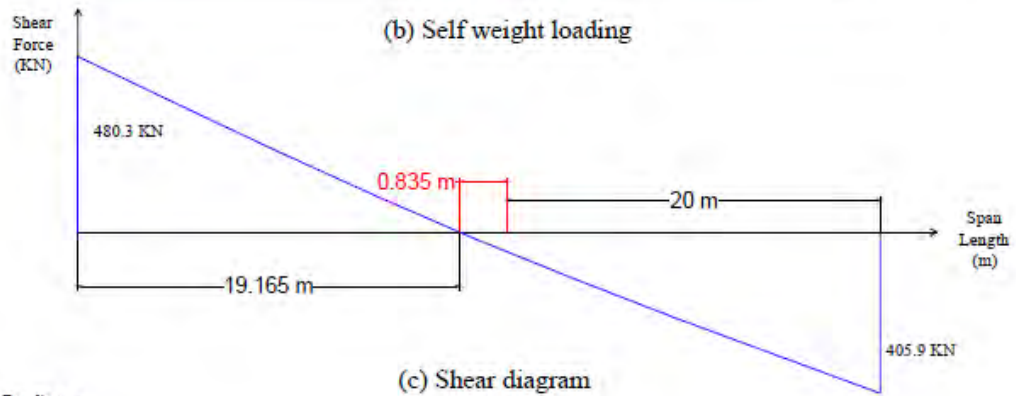
(c) Shear diagram
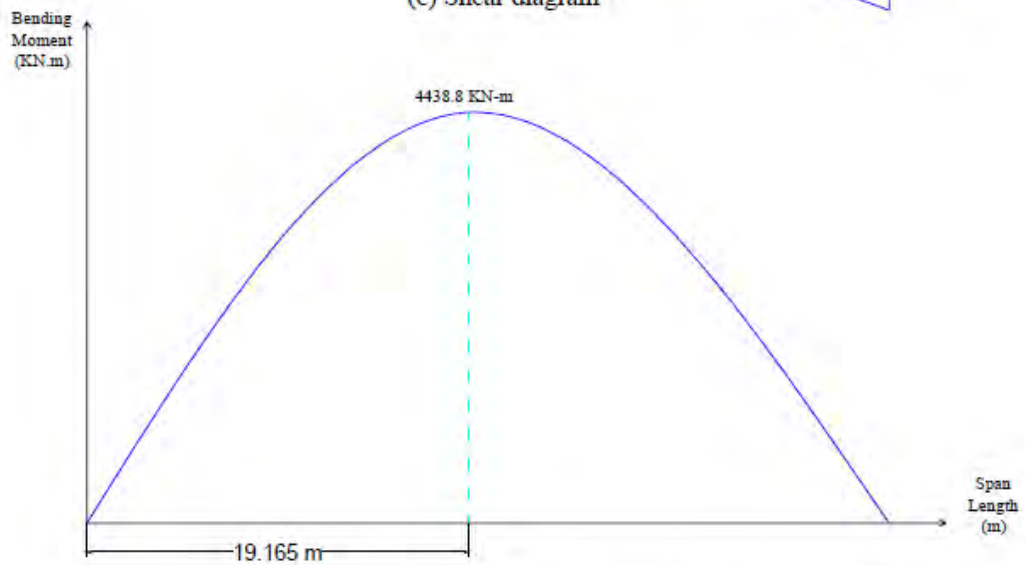
(d) Bending moment diagram

Figure 30: Isolated girder self-weight moment and shear diagram

The truck is placed at 19165 mm from the left support to maximize the live load moment, as shown in Figure 31. By trial and error in the 3D finite element model, it was verified that this approach is a good approximation for the longitudinal position of the truck for maximum stress in the interior girders. Thus, this approach is used for all bridges modeled in this study, and Table 10 shows truck positioning in the longitudinal direction for bridges 1 to 15 represented by the distance between the middle axle of the truck and the mid span.

Table 10: Truck longitudinal position for studied bridges

Bridge	Mid span shift	Distance from support	Bridge	Mid span shift	Distance from support	Bridge	Mid span shift	Distance from support
B1	835	20835	B6	750	2075	B11	835	20835
B2	515	20515	B7	892	20892	B12	848	20848
B3	1208	21208	B8	835	20835	B13	822	20822
B4	1000	21000	B9	835	20835	B14	626	15626
B5	715	20715	B10	835	20835	B15	1043	26043

In order to maximize the shear effect in a splayed girder bridge, the AASHTO LRFD HL-93 truck rear axle, which is the heaviest, is placed just off the support at the end of the bridge with maximum width and largest girder spacing, as illustrated in Figure 32.
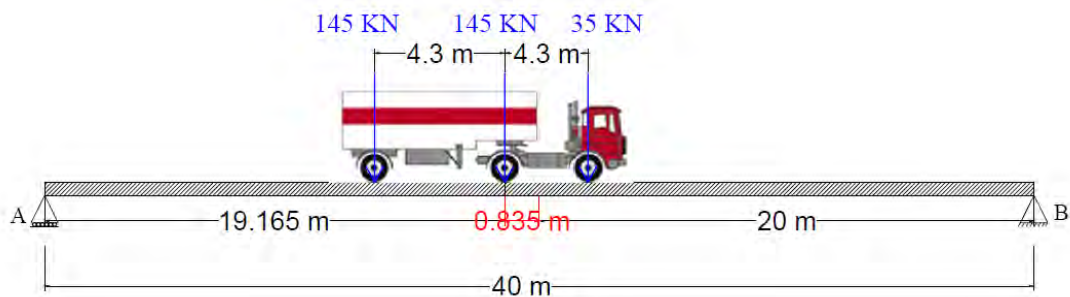
Figure 31: Reference bridge maximum moment longitudinal position
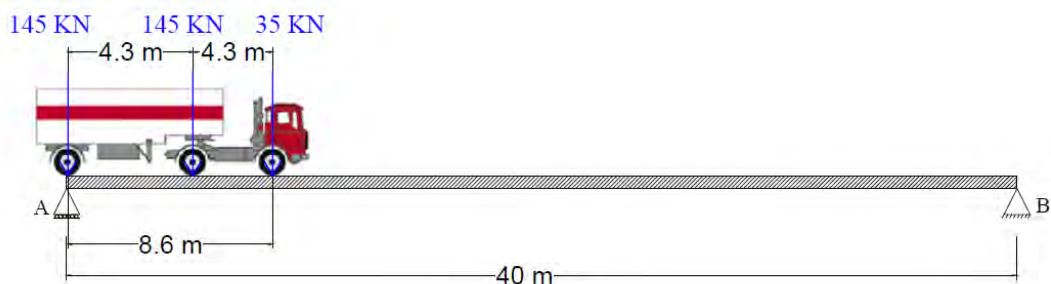
Figure 32: Reference bridge maximum shear longitudinal position

53

4.3.1.2 Truck transverse positioning.

The bridge is loaded by single or multiple lanes in the direction perpendicular to the traffic flow, referred to as the transverse direction, as shown in Figure 33 , to maximize the live load effect in an exterior or interior girder in both flexure and shear. To account for the lower probability of simultaneous presence of multiple trucks over a bridge, AASHTO LRFD employs a multiple presence factor [4]. Table 11 gives the value of the multiple presence factor for various numbers of loaded lanes.

Table 11: Multiple presence factor by AASHTO LRFD

Number of laded lanes	Multiple Presence Factor m
1	1.2
2	1
3	0.85
>3	0.65
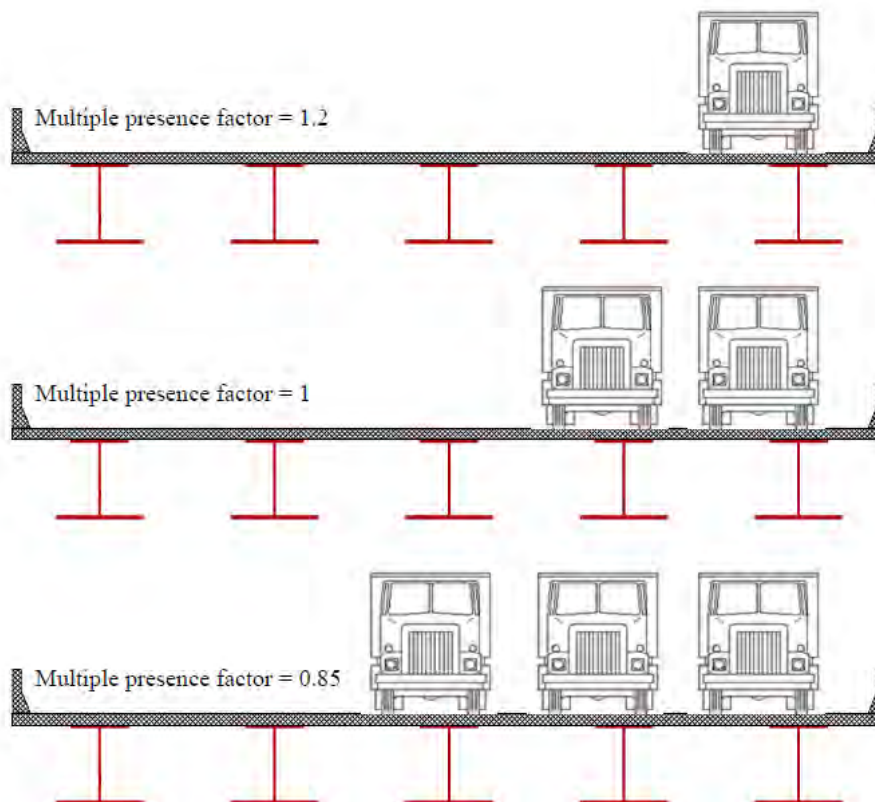
Figure 33: Trucks loading in transverse direction

In order to find the maximum live load effect on the exterior or interior girders, a truck or more with an appropriate multiple presence factor should be placed on the bridge at the chosen longitudinal location. Then, different locations should be tested in

the transverse direction for maximum effect on the girder. Usually the truck is first placed at a minimum distance from the edge of the bridge (near the parapet), then is moved in small increments until the considered girder archives the greatest live load effect. The AASHTO LRFD suggests that a minimum distance of 300 mm between the wheels of the truck and the parapet should be maintained when considering the concrete deck slab, while 600 mm is required as a minimum when addressing any other structural element. Also, AASHTO LRFD requires a minimum distance of 600 mm between the truck wheels and the design lane edge, as shown in Figure 34.
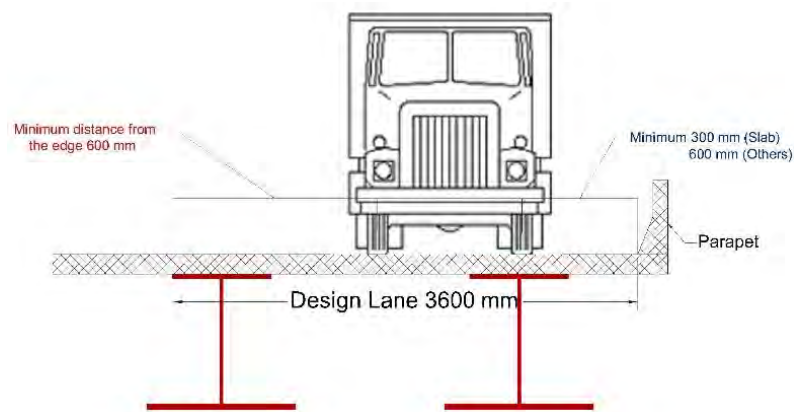
Figure 34: Truck transverse position limits by AASHTO LRFD

In this study, the splayedness of the girders has an effect on truck positioning in the transverse direction where beside the position of the truck, the truck direction angle affects the loading results. By giving the truck the correct angle in the right position, the live load effect can be maximized. Finite element analysis showed that the truck angle affects both interior and exterior girders, but it has a higher effect on the exterior girder.

The overhang width is very critical to loading on the exterior girder. By loading the bridge with a truck perpendicular to the transverse direction, with a minimum wheel distance of 600 mm from the parapet as recommended by the AASHTO LRFD, only the wheel at the front or rear axle of the truck will maintain this minimum distance while the other two axles will have a greater distance from the parapet, thus resulting in a lower effect in flexure on the exterior girder as shown in Figure 35.

By rotating the truck till it becomes parallel to the parapet with a constant wheel distance of 600 mm from the parapet, the flexural effect of the truck on the exterior girder will be maximized because all of the truck wheels will contribute more to the girder. Figure 36 shows the truck transverse positioning after rotating the axles. In this

case, in order to maintain the longitudinal required position of the truck, the center of the mid axle should be at the longitudinal position shift from the bridge midspan.
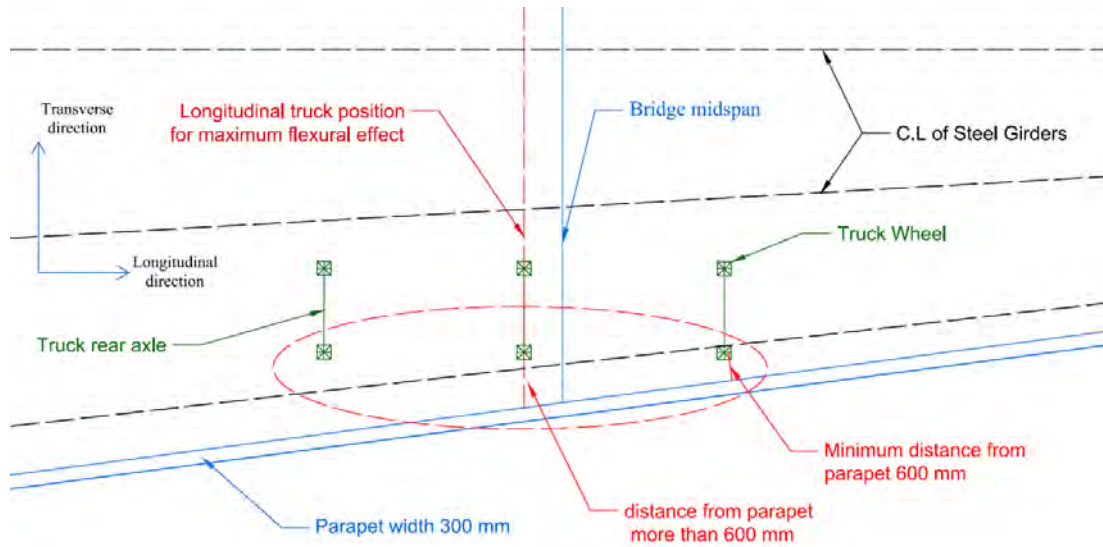
Figure 35: Truck transverse position with no rotation for flexure
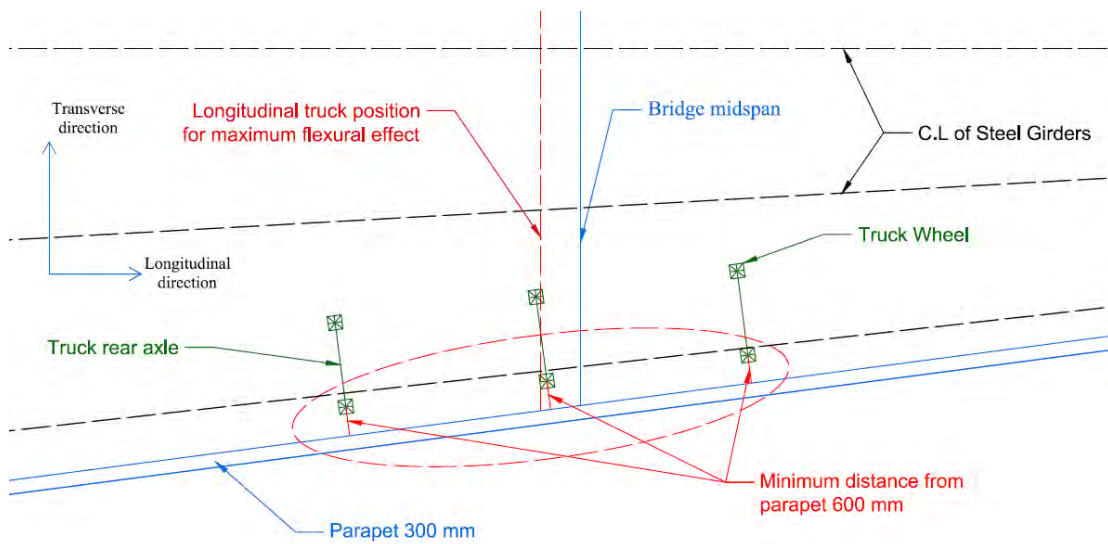
Figure 36: Truck transverse positioning with rotation for flexure

The flexural effect of live load in the critical interior girder also can be maximized by giving the truck an angle at each step of movement in the transverse direction until achieving the maximum effect in the interior girder under consideration. The approach followed in this study is to divide the splayedness angle (θ) by the number of steps that the truck needs to reach the middle of the bridge in the transverse direction starting from the edge of the bridge. This procedure allows the truck axles to be approximately perpendicular to the girder under consideration which maximizes the flexure effect in the girder, as shown in Figure 37, where the truck axles are almost

perpendicular to the first interior girder. When the center of the truck axle reaches the symmetry line of the bridge, the truck should be straight and the axles are perpendicular to the intermediate girder as shown in Figure 38, which maximizes the flexural effect on the girder.
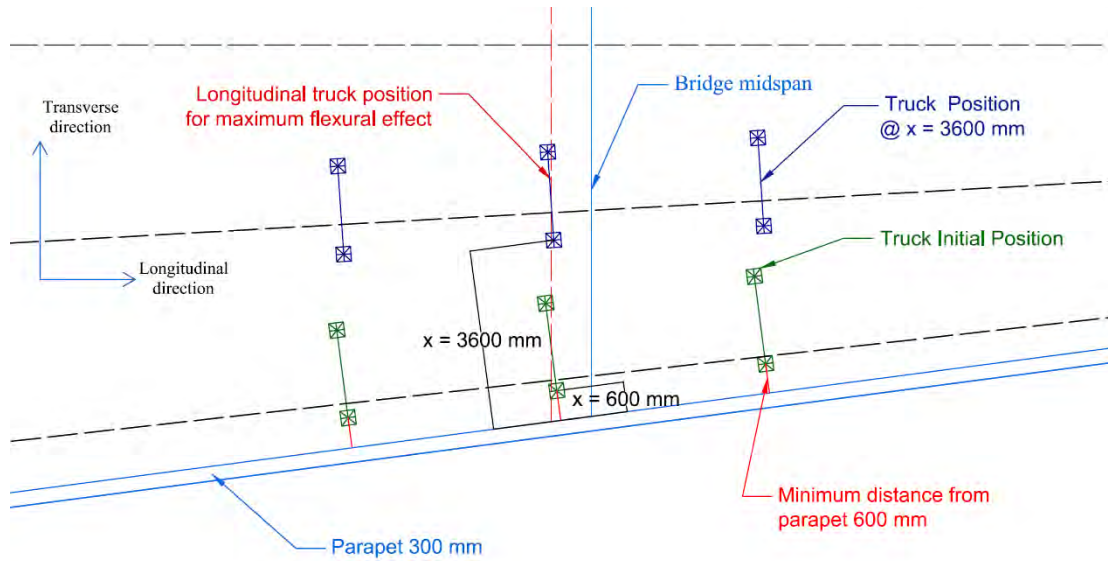
Figure 37: Truck transverse positioning procedure for flexure
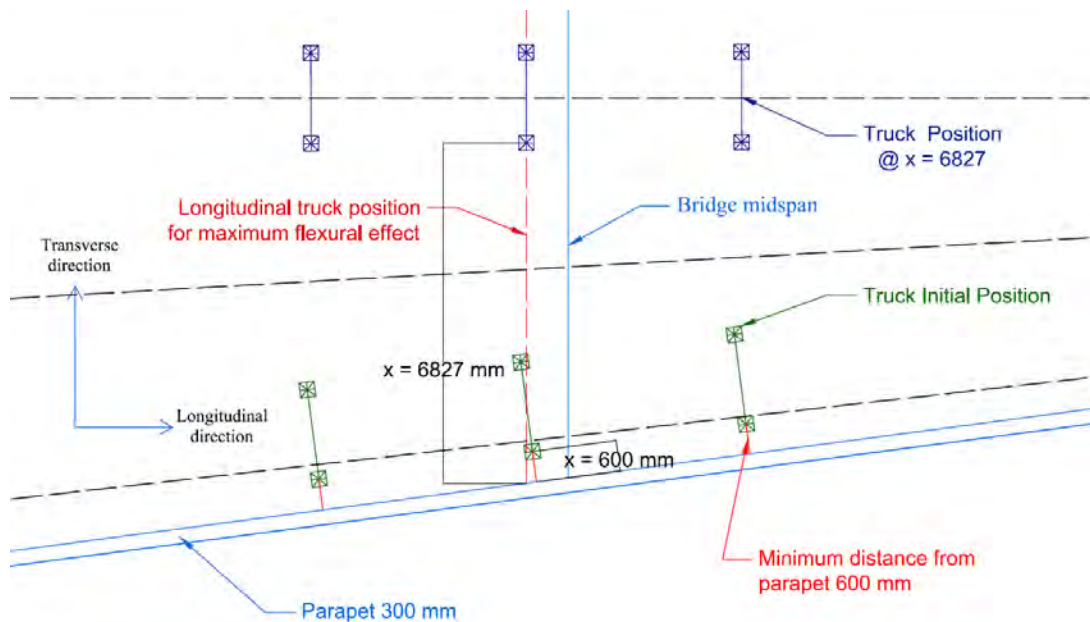
Figure 38: Truck position at the middle of the bridge in the transverse direction

As illustrated in Figure 37, the initial position of the truck is parallel to the parapet and it has an angle equal to the splayedness angle of the bridge θ. By reaching x = 3600 mm at step number 5 (if the step increment is 600 mm), it can be noticed that the truck is almost above the first interior girder, and due to rotating the truck at each step the truck is almost parallel to this girder which will maximize the flexural effect of

live load in the girder. Moreover, in Figure 38 the truck reaches the middle of the bridge at x = 6827 mm and after step number 11, and also due to the rotation at each step the truck is parallel to the middle girder directly under it. For the reference bridge (B1), loading the bridge with one rotated truck results in a maximum stress of 22.418 MPa and 15.613 MPa in the exterior and the first interior girders, respectively. By loading the bridge with one straight, the maximum stress in the exterior and the first interior girders is 20.034 MPa and 15.586 MPa, respectively. This indicates that using the rotation procedure maximizes the flexural effect in the girders, especially in the exterior ones. This procedure is used for the case of whether the bridge is loaded with one truck or multiple trucks.

To maximize the shear effect due to truck loading, the truck is placed just off support at the end of the bridge in the longitudinal direction. However, just like in flexure, the truck should be moved in the transverse direction starting from 600 mm away from the parapet till reaching the maximum effect in the girder under consideration. The analysis showed that rotating the truck to maximize the shear effect was not critical in interior girders, where keeping the truck perpendicular to the support end produces the maximum shear effect for interior girders. On the other hand, rotating the truck to be parallel to the parapet produces the maximum shear effect for the exterior girder. Figure 39 and Figure 40 show the truck positioning in the transverse direction to maximize the shear effect in the interior and exterior and interior girders in the reference bridge, respectively.
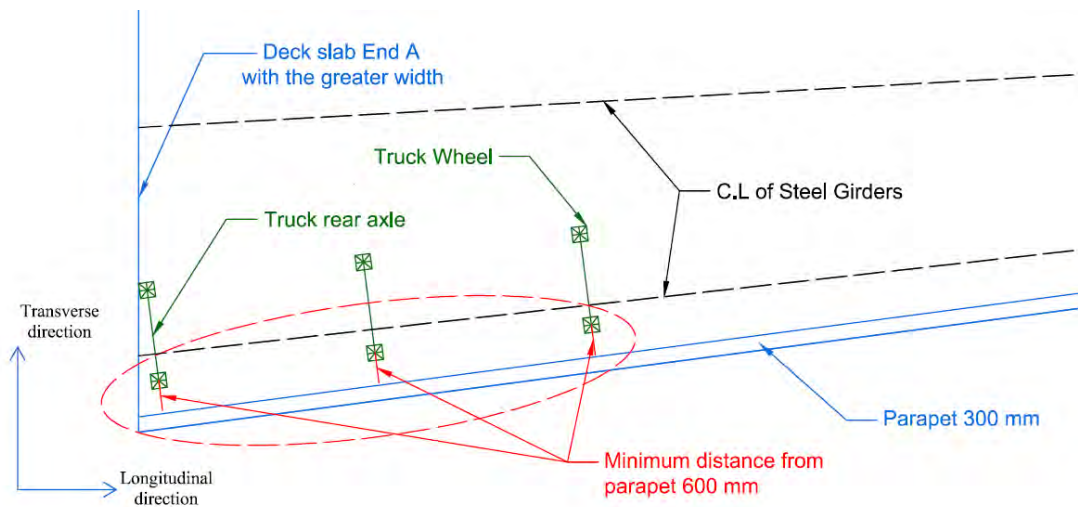
Figure 39: Truck transverse position for maximum shear effect in exterior girder
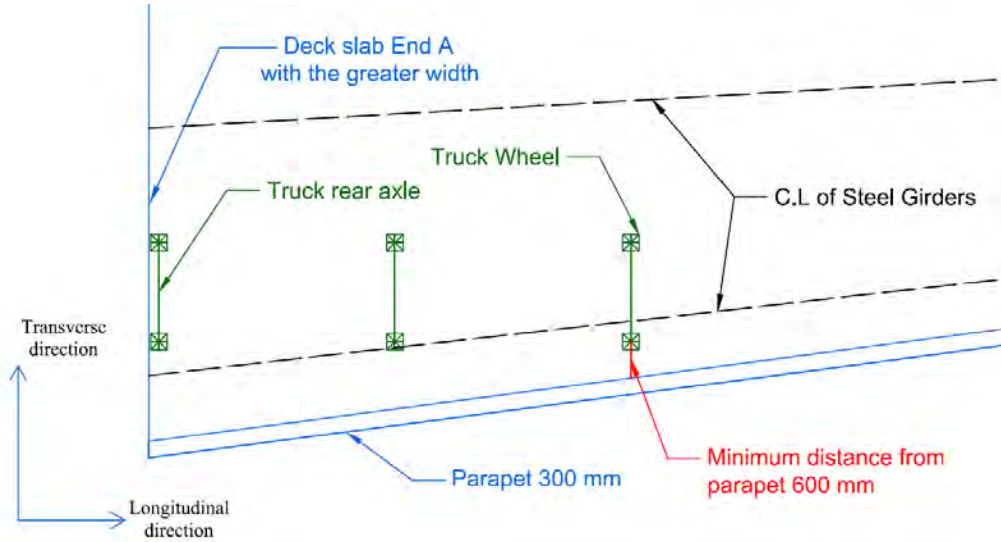
Figure 40: Truck transverse position for maximum shear effect in interior girder

4.3.1.3 Calculation of girder distribution factor.

At each step of truck positioning in the transverse direction for the case of flexure near the midspan, longitudinal stresses at the bottom flange of all girders are recorded along a straight line through the girders representing the truck's chosen longitudinal position. Then the GDF for flexure is calculated for each girder as a ratio of its stress to the summation of stresses in all girders at the particular cross-section. On the other hand, the GDF for shear is computed using the ratio of the support reaction of the girder under consideration to the summation of the reactions of all girders at the loaded end of the bridge. Equations (12) and (13) are used in this study to calculate the GDF for flexure and shear in both interior and exterior girders using the finite element results with consideration of the truck multiple presence factor. These equations are developed from the concept of girder distribution factor, where under linear elastic condition the moment in the girder and the stress at the same longitudinal location are proportional to each other [15]. Therefore, as the finite element method outcomes are stresses and strains, it's easier to work with stresses instead of moments to calculate GDF. Some researchers also use strains instead of stresses to find GDF. For example, Ghosn et al. [45] used the ratio of the strain at the considered girder to the summation of strains in all of the girders, at the same cross-section, to compute GDF. In this study, FE stresses are used to calculate GDF for flexure.

$$GDF_j = \frac{Nm\sigma_j}{\sum_{i=1}^{n}\sigma_i} \qquad (12)$$

59

$$GDF_j = \frac{NmR_j}{\sum\limits_{i=1}^{n} R_i}$$

(13)

where:

  N :   Number of loaded lanes

  m :   Multiple presence factor

  σ_j :   Stress at the bottom flange of girder j

  σ_i :   Stress at the bottom flange of girder i, where i = 1 to n

  R_j :   Support reaction at grider j

  R_i :   Support reaction at girder i, where i = 1 to n

  n :   Number of girders

All stresses obtained from ANSYS at the bottom flange of the girders, where there are five nodes, are weighted average stresses, and the support reactions are taken exactly at the supported nodes.

4.3.2 Live load effect in deck slab.

In order to study the deck slab behavior due to live load, three different bridges are considered (B1, B4, and B5) in this study. The three bridges are loaded with one, two, or three HL-93 trucks at different locations in the longitudinal direction to study the effect of different girder spacings due to bridge splayedness. Multiple truck presence factors are considered in the final computation of the stresses or moments in the deck slab. Multiple truck presence factors are considered in the final computations of the stresses or moments in the deck slab. Also, at each location, the truck(s)' position in transverse directions is changed in order to maximize the negative and positive moments in the concrete deck slab.

Due to the bridge splayedness, the girder spacing varies along the span of the bridge. Hence, in this study three locations along the longitudinal axis of the bridge are chosen to study the positive moment in the deck slab due to live load. The concrete deck slab of a splayed girder bridge is sub-divided into three regions, where each is one-third of the bridge's total length. The first one has the maximum girder spacing, the second has the average, and the last one has the minimum girder spacing. Each region is loaded with the HL-93 truck, where the middle axle of the truck is placed at the mid-length of the region in the longitudinal direction (Sections 1, 2 and 3) as shown in Figure 41. One or two loading lanes are applied at the longitudinal locations, and by

moving the truck(s) transversely, the transverse truck location leading to the maximum positive moment is obtained. By studying flexural stresses at these three positions, we can understand the structural behavior of slabs supported on splayed girders.
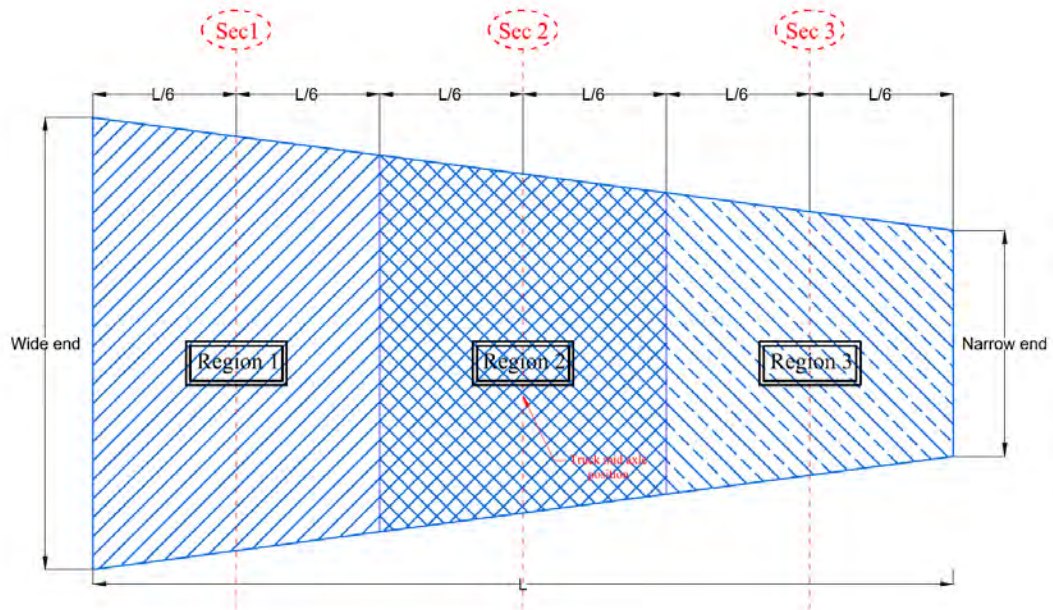
Figure 41: Deck slab regions and sections for positive moment case

For negative moment over interior girders, the same three regions are considered. However, for the first and the third regions, the truck's rear axle is placed 1 m away from the support (Sections 1 and 3) to predict the negative moment at the maximum and minimum girder spacing regions. For the second region, the truck's mid axle is placed exactly at the middle of the region in the longitudinal direction (Section 2) as shown in Figure 42.
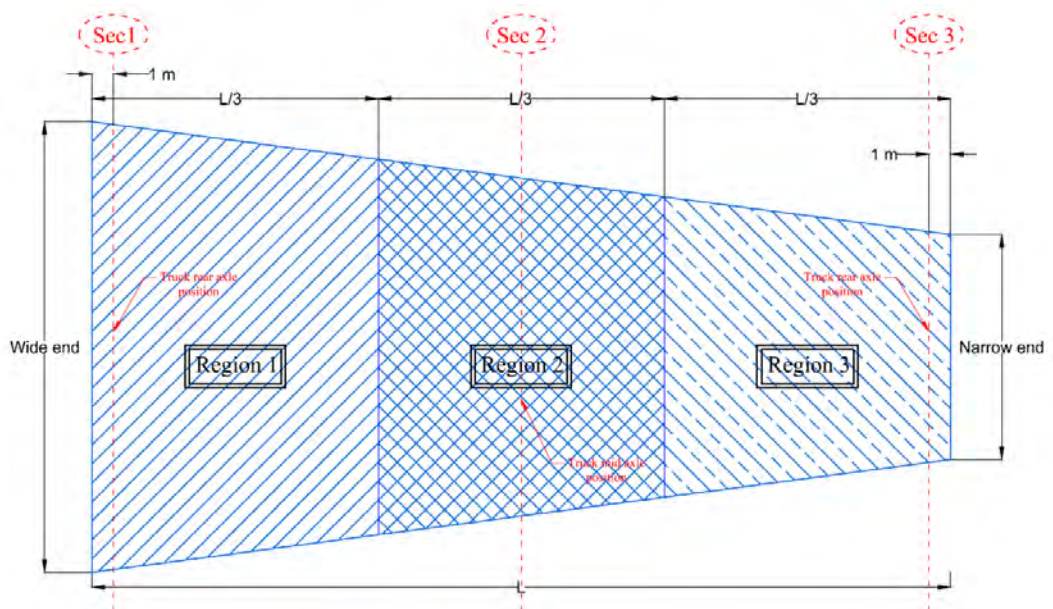
Figure 42: Deck slab regions and sections for negative interior moment case

One or two loading lanes are applied once at each location, and the live load maximum negative moment is then obtained by moving the truck(s) in the transverse direction in small increments.

Finally, for negative moment in the overhang, the bridge is subjected to a single truck parallel to the parapet at the same locations chosen for the positive moment, and the truck wheel is placed at 300 mm from the parapet in the transverse direction to maximize the live load negative moment in the overhang. Table 12 summarizes the girder spacing at each section under consideration for positive or negative moment in bridges B1, B4, and B5.

Table 12: Girder spacing and overhang for considered sections in deck slab

Bridge No.	Considered moment	Girder spacing or Overhang distance (mm)		
		Sec 1	Sec 2	Sec 3
1	Positive	4125	3375	2625
	Negative	4444	3375	2306
	Overhang	1375	1125	875
4	Positive	3375	2625	1875
	Negative	3694	2625	1556
	Overhang	1125	875	625
5	Positive	4875	4125	3375
	Negative	5194	4125	3056
	Overhang	1625	1375	1125

4.4 Live Load Effect in Reference Bridge

In this section, the reference bridge GDFs are calculated from the finite element model for both flexure and shear, and the results are plotted and discussed. Also, the deck slab behavior is discussed in depth for the reference bridge. The composite steel girder considered for the reference bridge is shown in Figure 43 with all details of the girder chosen and the material properties, and it should be noted that the reference bridge has cross-bracing only at the supports.
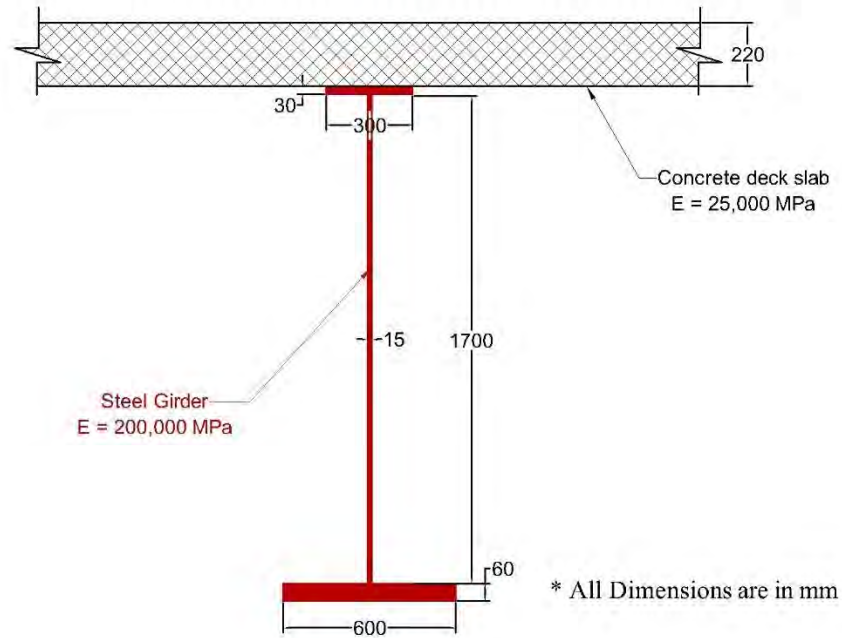
Figure 43: Composite steel girder details and properties

4.4.1 Flexure GDF.

Table 13 shows the longitudinal flexural stresses in the girders due to live load at each corresponding transverse position for one truck load, and Table 14 shows the corresponding GDF for flexure for all five girders at each truck position as well. The calculated GDF due to one truck load is plotted in Figure 44 against the truck distance from the parapet (x). For two-truck loading, both flexure stresses and associated GDF at each transverse position are summarized in Table 15 and Table 16, respectively. The GDF values for two-truck loading are presented in Figure 45 against the trucks' distance from the parapet (x). The same procedure is repeated for three-truck loading and the results are presented in Table 17 for stresses, Table 18 for GDF, and Figure 46 as a plot of the GDF versus the side truck distance from the parapet. The maximum GDF values in all loading cases are summarized at the end of each table. It should be noted that G1 represents the exterior girder and G2 represents the first interior girder, and so on for the rest of the girders.

It is obvious from the results that for the exterior girder, loading the bridge with two trucks governs, while for the interior girder three trucks results in the greatest GDF. Also, it can be concluded that the first interior girder G2 gives the greatest GDF value among all other interior girders. All calculated GDF values include the multiple presence factor. From the results, the obtained GDF values for flexure in the exterior and most critical interior girder are 0.871 and 0.808, respectively.

Table 13: Flexure stresses for reference bridge due to one-lane loading

Dist. (x)	Flexure Stresses at the bottom flange of the girder (MPa)				
(mm)	G1	G2	G3	G4	G5
600	22.418	11.171	3.221	-0.135	-2.073
1200	20.582	13.199	4.298	0.343	-1.901
1800	17.522	14.399	5.259	0.859	-1.562
2400	14.658	15.290	6.333	1.410	-1.211
3000	12.102	15.613	7.569	2.018	-0.841
3600	9.846	15.474	8.917	2.692	-0.447
4200	7.871	14.898	10.323	3.442	-0.024
4800	6.287	13.730	11.724	4.337	0.454
5400	4.937	12.293	12.967	5.354	0.983
6000	3.811	10.689	13.920	6.534	1.577
6600	2.892	9.098	14.310	7.934	2.265
6827	2.562	8.495	14.354	8.495	2.561

Table 14: Flexure GDF for reference bridge due to one-lane loading

Dist. (x)	Flexure GDF				
(mm)	G1	G2	G3	G4	G5
600	0.77748	0.38740	0.11170	-0.00469	-0.07190
1200	0.67629	0.43368	0.14121	0.01128	-0.06246
1800	0.57642	0.47369	0.17302	0.02826	-0.05139
2400	0.48216	0.50296	0.20831	0.04640	-0.03984
3000	0.39830	0.51385	0.24910	0.06642	-0.02767
3600	0.32387	0.50899	0.29330	0.08855	-0.01471
4200	0.25871	0.48965	0.33930	0.11312	-0.00078
4800	0.20653	0.45099	0.38510	0.14246	0.01491
5400	0.16215	0.40377	0.42591	0.17587	0.03229
6000	0.12517	0.35113	0.45726	0.21464	0.05180
6600	0.09508	0.29913	0.47047	0.26084	0.07448
6827	0.08430	0.27956	0.47234	0.27953	0.08428
GDF max	**0.77748**	**0.51385**	**0.47234**		

Table 15: Flexure stresses for reference bridge due to two-lane loading

Dist. (x)	Flexure Stresses at the bottom flange of the girder (MPa)				
(mm)	G1	G2	G3	G4	G5
600	31.830	26.699	13.605	3.224	-2.298
1200	28.699	28.076	14.485	3.713	-1.966
1800	23.978	28.182	16.869	5.117	-1.148
2400	19.699	27.682	19.223	6.691	-0.268
3000	15.949	26.430	21.464	8.476	0.694
3600	12.745	24.660	23.245	10.574	1.782
4200	9.972	22.522	24.596	12.878	3.022
4800	7.685	20.012	25.487	15.376	4.467
5327	5.934	17.661	25.754	17.661	5.934

Table 16: Flexure GDF for reference bridge due to two-lane loading

Dist. (x)	Flexure GDF				
(mm)	G1	G2	G3	G4	G5
600	0.87134	0.73088	0.37243	0.08825	-0.06289
1200	0.78619	0.76913	0.39682	0.10171	-0.05385
1800	0.65694	0.77213	0.46218	0.14020	-0.03145
2400	0.53950	0.75813	0.52645	0.18325	-0.00733
3000	0.43687	0.72397	0.58796	0.23218	0.01902
3600	0.34915	0.67555	0.63680	0.28968	0.04881
4200	0.27325	0.61713	0.67395	0.35287	0.08281
4800	0.21048	0.54808	0.69802	0.42109	0.12233
5327	0.16271	0.48424	0.70612	0.48424	0.16270
GDF max	**0.87134**	**0.77213**	**0.70612**		

Table 17: Flexure stresses for reference bridge due to three-lane loading

Dist. (x)	Flexure Stresses at the bottom flange of the girder (MPa)				
(mm)	G1	G2	G3	G4	G5
600	33.426	33.350	27.290	13.944	1.487
1200	30.014	34.701	28.317	14.591	1.925
1800	24.581	33.556	29.780	17.666	3.916
2400	19.729	31.890	30.914	20.764	6.244
3000	15.498	29.593	31.693	23.721	8.964

Table 18: Flexure GDF for reference bridge due to three-lane loading

Dist. (x) (mm)	Flexure GDF				
	G1	G2	G3	G4	G5
600	0.77844	0.77667	0.63554	0.32472	0.03463
1200	0.69865	0.80776	0.65914	0.33964	0.04480
1800	0.57244	0.78145	0.69351	0.41140	0.09120
2400	0.45928	0.74236	0.71965	0.48336	0.14536
3000	0.36101	0.68935	0.73827	0.55256	0.20882
GDF max	**0.77844**	**0.80776**	**0.73827**		
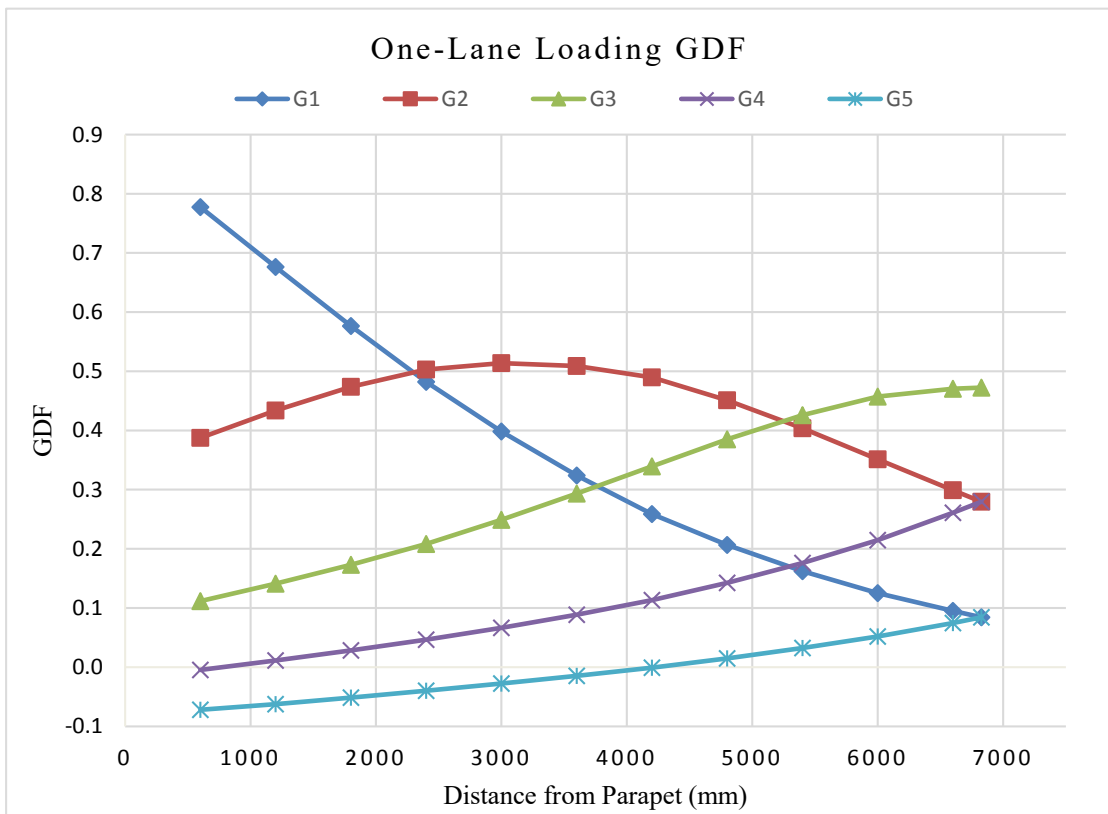
Figure 44: Flexure GDF vs. distance from parapet for 1-lane loading
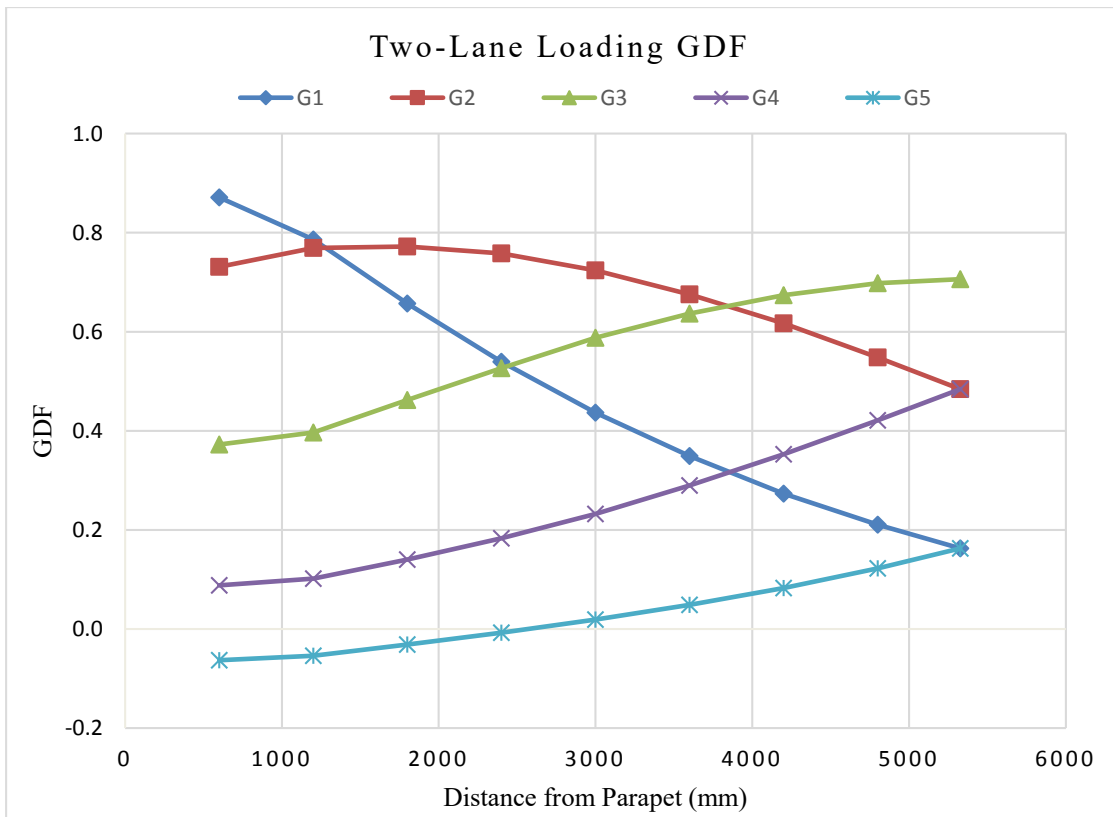
Figure 45: Flexure GDF vs. distance from parapet for 2-lane loading
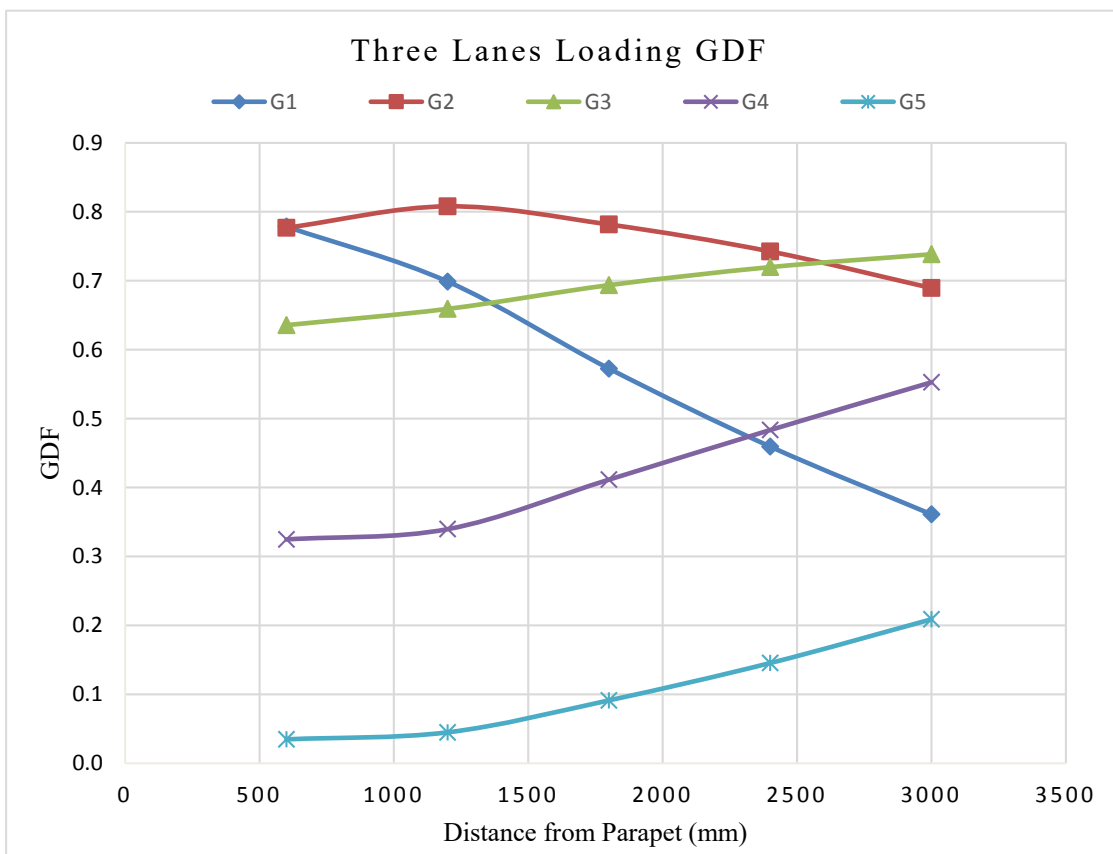
Figure 46: Flexure GDF vs. distance from parapet for 3-lane loading

Figure 47 shows the deflected shape with the FEM mesh of the reference bridge (B1) due to two-truck loading for flexure, and Figure 48 shows the longitudinal stresses in the steel girders' bottom flange in the reference bridge (B1) due to two-truck loading at the longitudinal critical location for flexure.
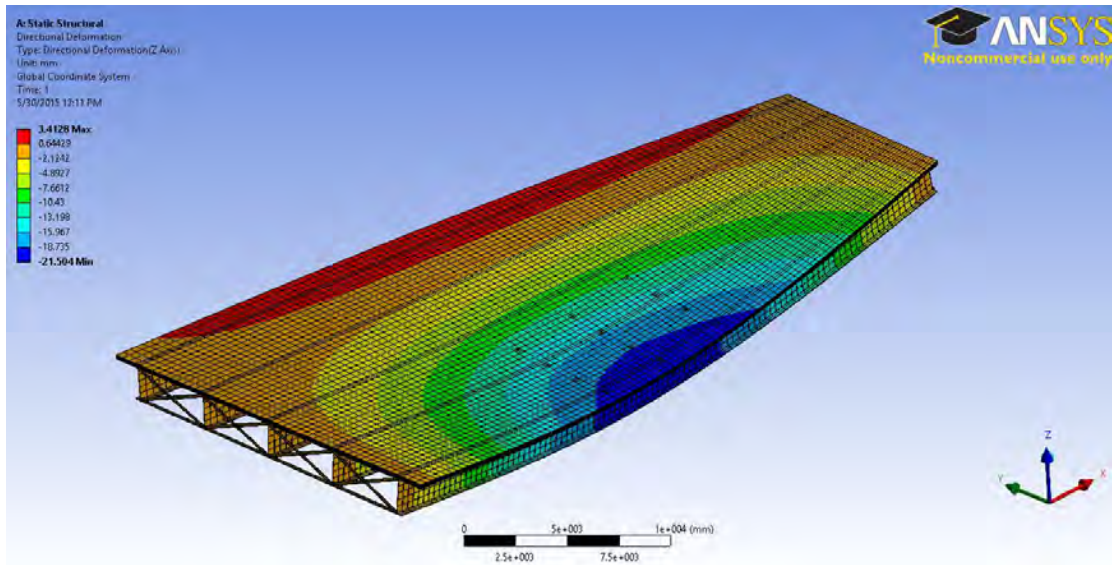
Figure 47: Deflected shape and FEM mesh of reference bridge – flexure
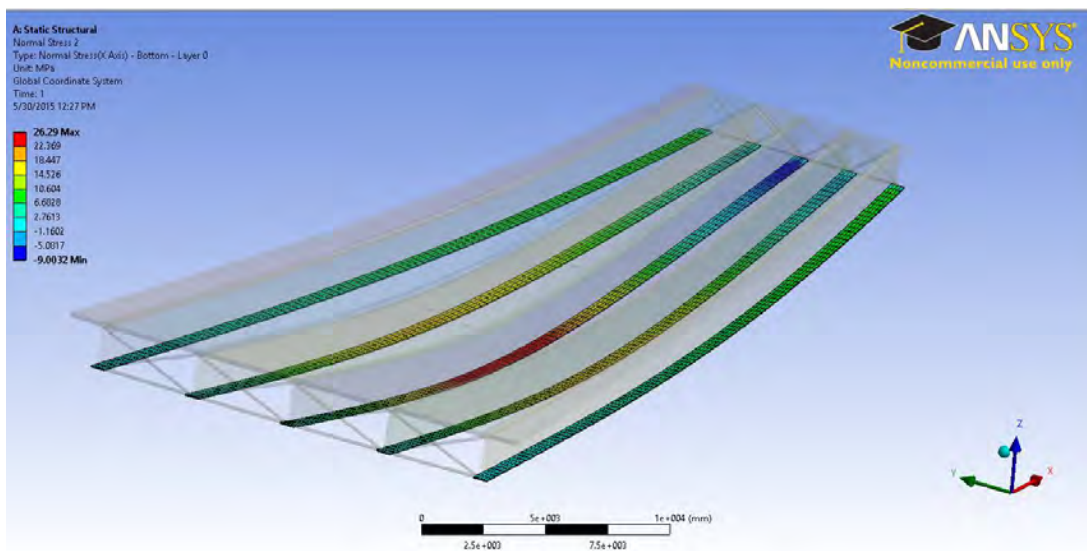
Figure 48: Bottom flange longitudinal stresses in reference bridge

All bridges considered in this study are symmetric around the center line of the bridge. Therefore, in order to ensure that the results of this study are applicable to different splayedness orientations, two bridges similar to the reference bridge are modeled but with different splayedness orientation. For the first bridge (B1-a), the girder that is perpendicular to the supports is the exterior girder. In the second bridge

(B1-b), the first interior girder is the one perpendicular to the supports. Both of these bridges are shown in Figure 49.
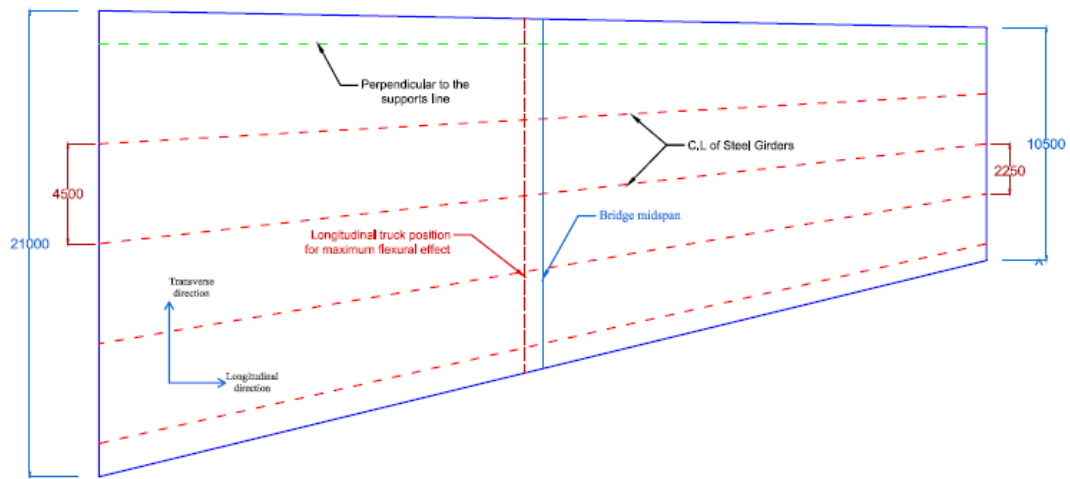
(a) - Perpendicular Exterior girder
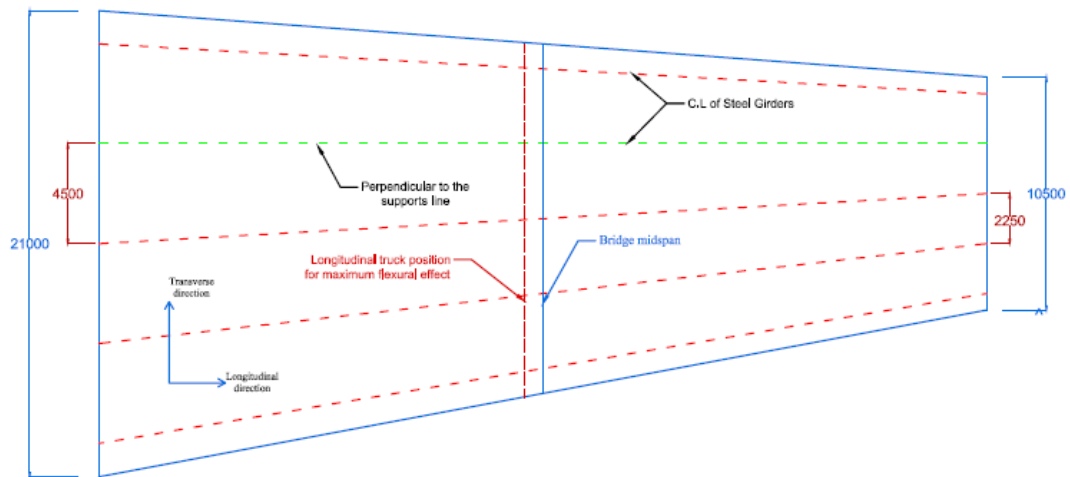
(b) - Perpendicular first interior girder

Figure 49: Different splayedness orientations

Finite element models are built for each of the considered new splayed bridges, B1-a, and B1-b, and the same loading procedure followed in the reference bridge is applied for these two bridges, considering the same longitudinal truck(s) position. Due to lack of symmetry in these two bridges, the maximum GDF values in flexure may not be the same in both exterior girders and first interior girders. Table 19 summarizes the GDF values for both bridges and compares them with the reference bridge. Figure 50 shows the deflected shape with the longitudinal stress contour for bridge (B1-a), while Figure 51 illustrates the same for bridge (B1-b).

Table 19: GDF for bridges with different splayedness orientation

Bridge	GDF*			
	G1	G2	G5	G4
B1	<u>0.871</u>	<u>0.808</u>	<u>0.871</u>	<u>0.808</u>
B1-a	0.844	0.799	0.880	0.810
B1-b	0.859	0.808	0.870	0.805

* G1, and G5 are the exterior girders. G2, and G4 are the first interior girders.

The most critical GDF values whether in the exterior or in the first interior girders negligibly changed in the three considered bridges. The critical GDF in the exterior and interior girders were observed in bridge B1-a, equal respectively to 0.880 and 0.81. However, the percentage difference between these values and the ones in the reference bridge is less than 1%. Based on the above, it can be concluded that lack of symmetry of the girder splaydness is not an important factor in the analysis of splayed girder bridges. Hence, this issue will not be considered further in the study.
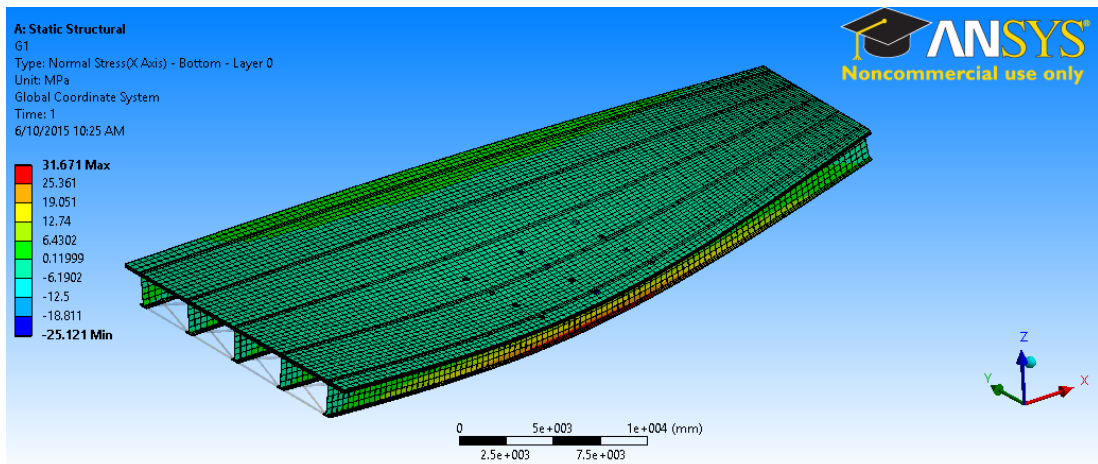
Figure 50: Longitudinal stresses in B1-a
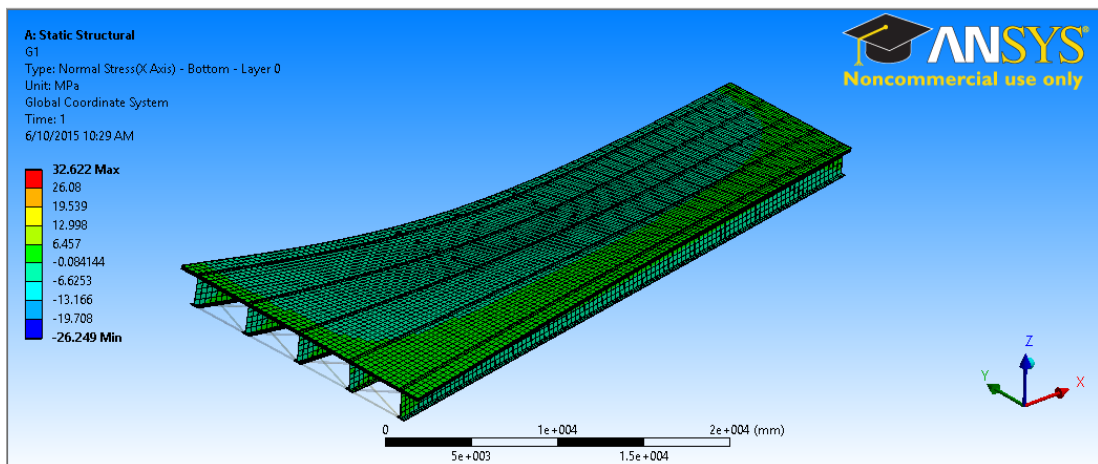
Figure 51: Longitudinal stresses in B1-b

70

4.4.2 Shear GDF.

In shear, the required truck rotation presented back in section 4.3.1.2 results in two cases to be considered. The first one is when the truck is parallel to the parapet, which results in the maximum shear GDF for the exterior girder. The second one is when the truck is perpendicular to the supporting end line of the bridge, which results in a maximum shear GDF for the interior girders. The reaction values at the girder supports and the shear GDF values are presented in the tables below for both cases combined. Also, shear GDF values versus the truck side distance from the parapet are plotted for each case separately. In case 1, the truck starts parallel to the parapet and rotates with each transverse step, and in case 2 the truck is perpendicular to the supporting end line with no rotation of the truck at all steps transversely. Table 20 shows the reactions of all girders due to one-lane loading, and Table 21 presents the corresponding shear GDF. The shear GDF against the truck distance from the parapet is presented in Figure 52 and Figure 55. For two-lane loading, Table 22 and Table 23 present girder reactions and the corresponding shear GDF, respectively. The GDF for two-loading lanes are illustrated in Figure 53 and Figure 56. Similarly, Table 24 and Table 25 show the support reactions and corresponding GDF due to three-lane loading, and Figure 54 and Figure 57 present these GDFs against the trucks' outside distance from the parapet. The critical shear GDF values are summarized in each table.

Table 20: Girders' reaction for reference bridge due to 1-lane loading

Dist. (x)	Reaction at the girders' support (N)				
(mm)	G1	G2	G3	G4	G5
600 (*)	260940.0	49268.0	-4792.2	-884.0	-2315.7
600	2.09E+05	1.07E+05	-5123.6	867.7 2	-2449.1
1200	1.68E+05	1.49E+05	-3875.3	1658.4	-2678.2
1800	1.29E+05	1.85E+05	-679.37	1750.9	-2941.2
2400	9.28E+04	2.13E+05	5935.8	1196.1	-3026.3
3000	6.18E+04	2.31E+05	15662	116.66	-2458
3600	36710	2.37E+05	33116	-1940.8	-1987
4200	18055	2.31E+05	58336	-2769	-1615.5
4800	5289.1	2.15E+05	86718	-2638.5	-1026.5

Table 21: Shear GDF for reference bridge due to 1-lane loading

Dist. (x)	Shear GDF				
(mm)	G1	G2	G3	G4	G5
600 (**)	1.03611	0.19563	-0.01903	-0.00351	-0.00919
600	0.810526	0.415517	-0.0199	0.00337	-0.00951
1200	0.646327	0.572496	-0.0149	0.006377	-0.0103
1800	0.494775	0.712415	-0.00261	0.006734	-0.01131
2400	0.359261	0.824844	0.022981	0.004631	-0.01172
3000	0.242002	0.905867	0.061294	0.000457	-0.00962
3600	0.14521	0.939334	0.130993	-0.00768	-0.00786
4200	0.071496	0.91486	0.231006	-0.01097	-0.0064
4800	0.02091	0.850755	0.342824	-0.01043	-0.00406
GDF max	**1.03611**	**0.939334**			

Table 22: Girders' reaction for reference bridge due to 2-lane loading

Dist. (x)	Reaction at the girders support (N)				
(mm)	G1	G2	G3	G4	G5
600 (*)	297470.0	284050.0	25310.0	-1795.0	-4700.4
600	2.27E+05	3.38E+05	52991	-4031.7	-4254.5
1200	1.86E+05	3.79E+05	54279	-3361.6	-4466.7
1800	1.34E+05	3.98E+05	85781	-3818.2	-4027.8
2400	9.02E+04	3.99E+05	1.26E+05	-3108.1	-3.79E+03
3000	7.90E+04	3.49E+05	1.70E+05	14709	-6078.5

Table 23: Shear GDF for reference bridge due to 2-lane loading

Dist. (x)	Shear GDF				
(mm)	G1	G2	G3	G4	G5
600 (**)	0.99101	0.94631	0.08432	-0.00598	-0.01566
600	0.744053	1.109099	0.174068	-0.01324	-0.01398
1200	0.607913	1.240245	0.177431	-0.01099	-0.0146
1800	0.438092	1.306407	0.281224	-0.01252	-0.0132
2400	0.296584	1.312892	0.413179	-0.01021	-0.01244
3000	0.260401	1.149723	0.56143	0.048483	-0.02004
GDF max	**0.99101**	**1.312892**			

Table 24: Girders' reaction for reference bridge due to 3-lane loading

Dist. (x)	Reaction at the girders support (N)				
(mm)	G1	G2	G3	G4	G5
600 (*)	284740.0	372950.0	232190.0	12363.0	-7444.2
600	2.20E+05	3.92E+05	2.81E+05	24023	-8170
1200	1.79E+05	4.34E+05	2.83E+05	24301	-8393.1
1800	1.28E+05	4.29E+05	3.16E+05	46498	-10580
2400	8.54E+04	4.13E+05	3.45E+05	75066	-12930

Table 25: Shear GDF for reference bridge due to 3-lane loading

Dist. (x)	Shear GDF				
(mm)	G1	G2	G3	G4	G5
600 (**)	0.81145	1.06283	0.66170	0.03523	-0.02121
600	0.616942	1.099307	0.789294	0.067367	-0.02291
1200	0.501847	1.213174	0.790494	0.067956	-0.02347
1800	0.360313	1.201631	0.887335	0.13039	-0.02967
2400	0.240545	1.163968	0.970541	0.211351	-0.0364
GDF max	**0.81145**	**1.201631**			

* represents the girders' reaction at the position that maximizes the GDF for the exterior girder due to the truck alignment with the parapet.

** represents the shear GDF for all girders at the position that maximizes the GDF for the exterior girder due to the truck alignment with the parapet.
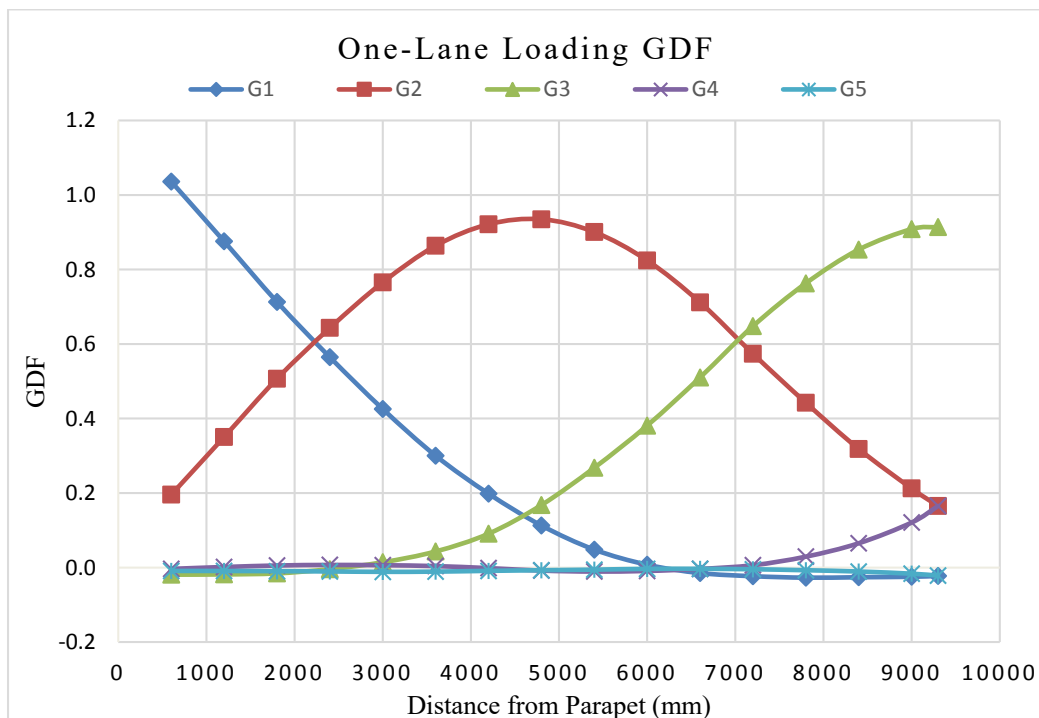
Figure 52: Shear GDF vs. distance from parapet for 1-lane loading – Case 1
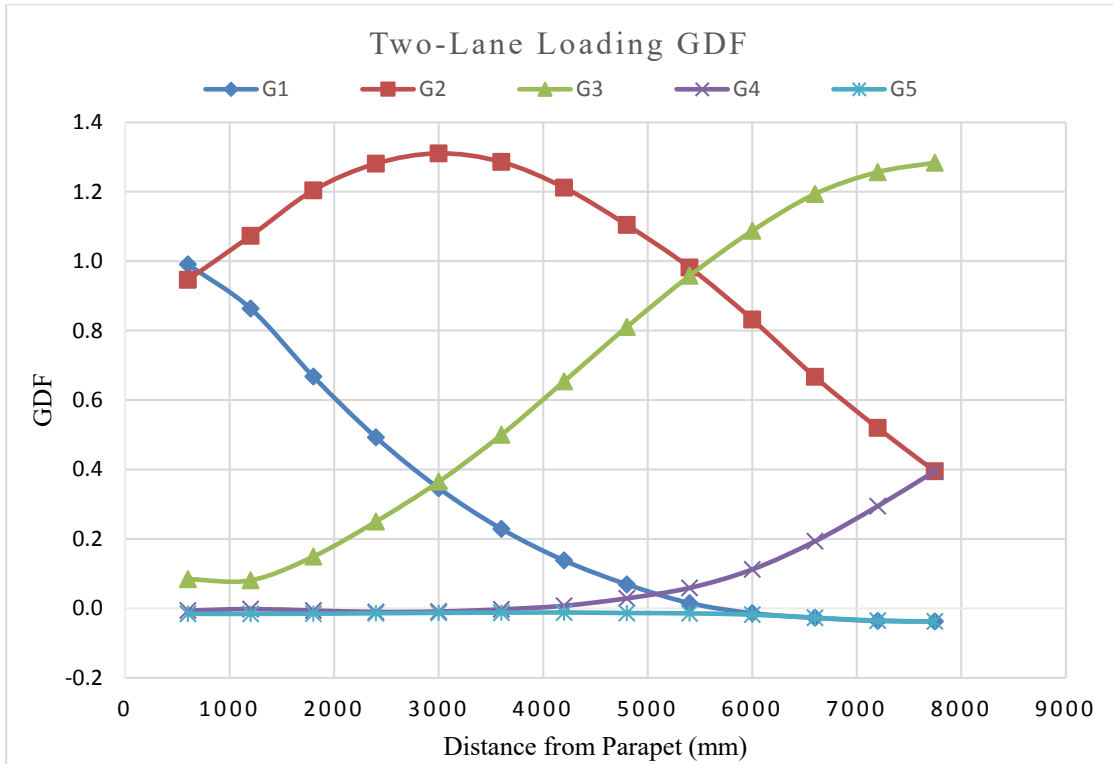
Figure 53: Shear GDF vs. distance from parapet for 2-lane loading – Case 1
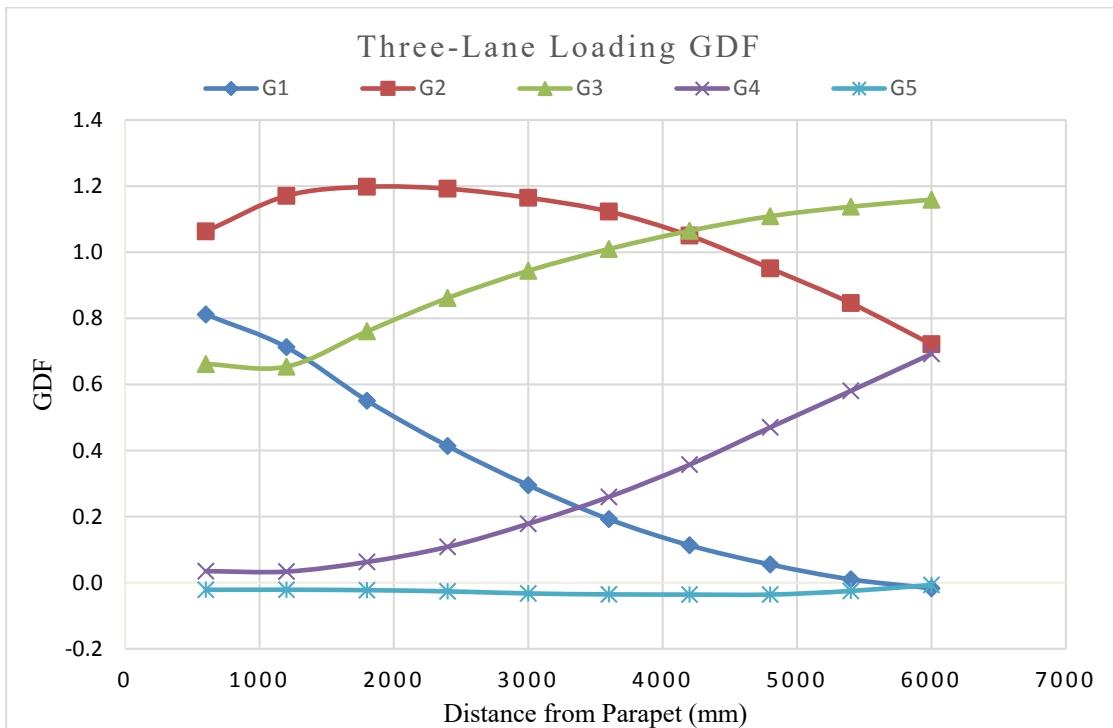
Figure 54: Shear GDF vs. Distance from parapet for 3-lane loading – Case 1

74
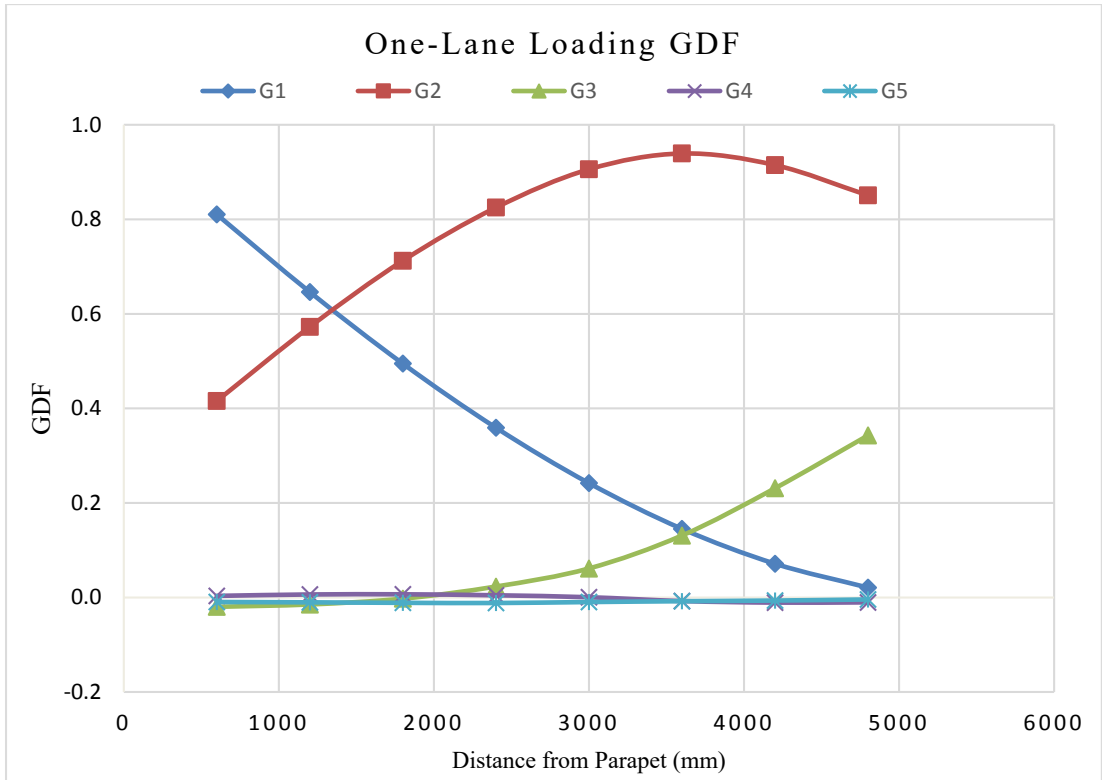
Figure 55: Shear GDF vs. distance from parapet for 1-lane loading - Case 2
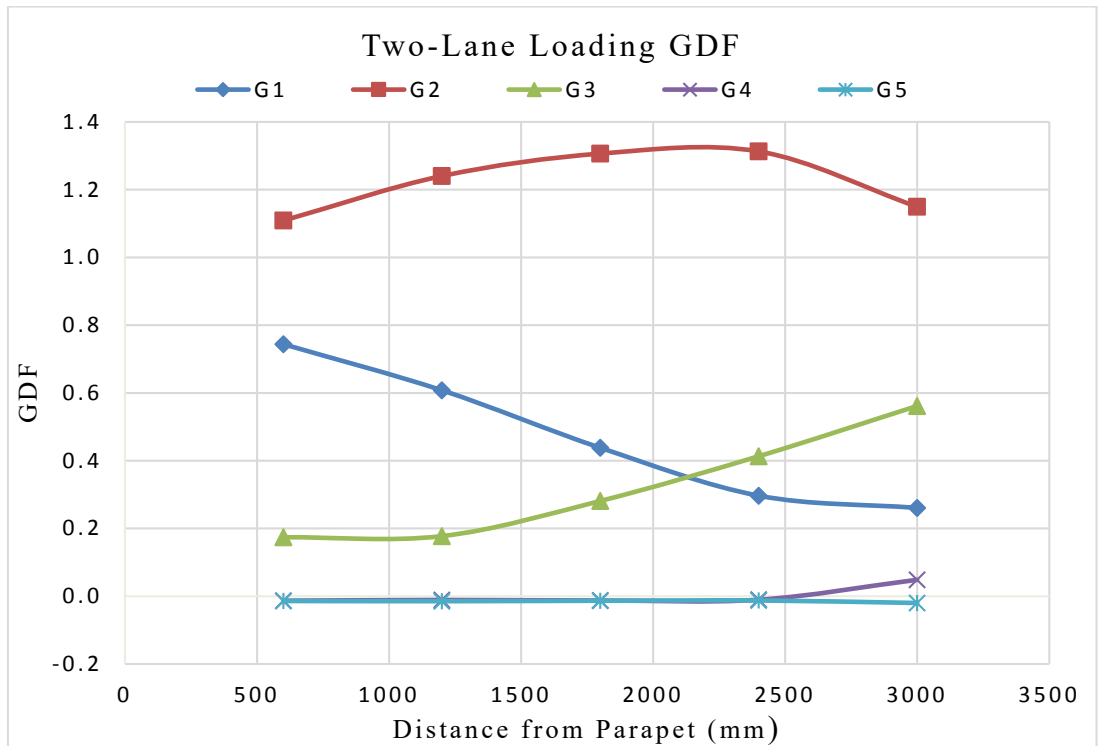
Figure 56: Shear GDF vs. distance from parapet for 2-lane loading - Case 2
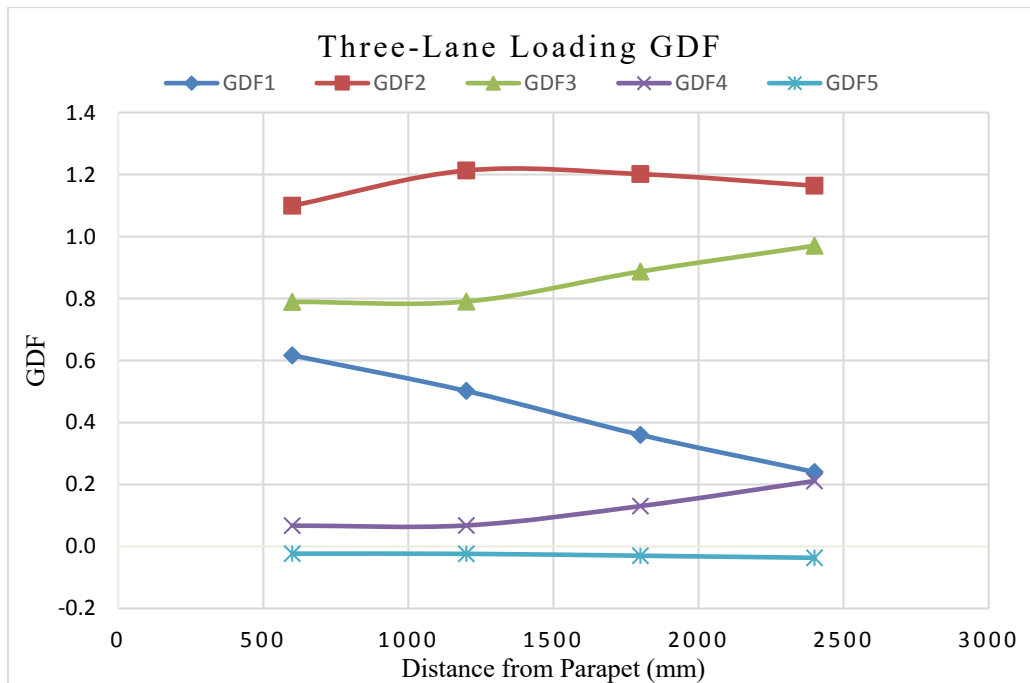
Figure 57: Shear GDF vs. distance from parapet for 3-lane loading - Case 2

The results show that the maximum shear GDF for the exterior girder is governed by one-lane loading, while for the interior girder it is due to two-lane loading. The shear finding is not in agreement with the flexure where three-lane loading governs the GDF of the interior girders. Similar to the flexure case, shear GDF in first interior girder governs over the interior girders. Compared to the flexure GDF, the shear GDF is larger in magnitude. The critical GDF for shear in the exterior girder is 1.036 and for the interior girder it is 1.313.
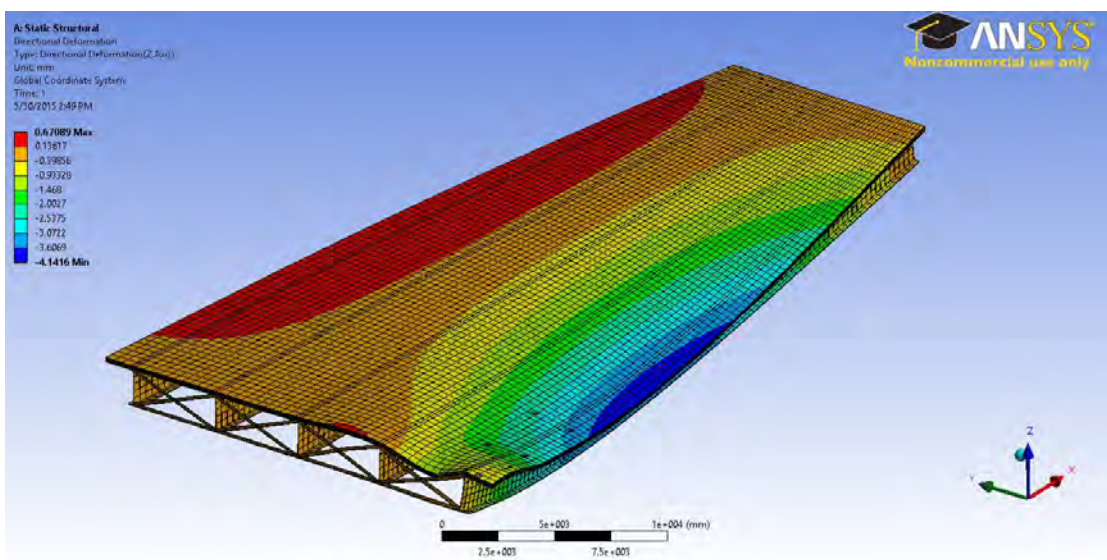
Figure 58: Deflected shape and FEM mesh of Reference Bridge – shear

Figure 58 shows the deflected shape with the FEM mesh of the reference bridge (B1) due to one-truck loading parallel to the parapet, and Figure 59 shows the shear stresses in the steel girders' web in the reference bridge (B1) due to two-truck loading at the longitudinal critical location for shear.
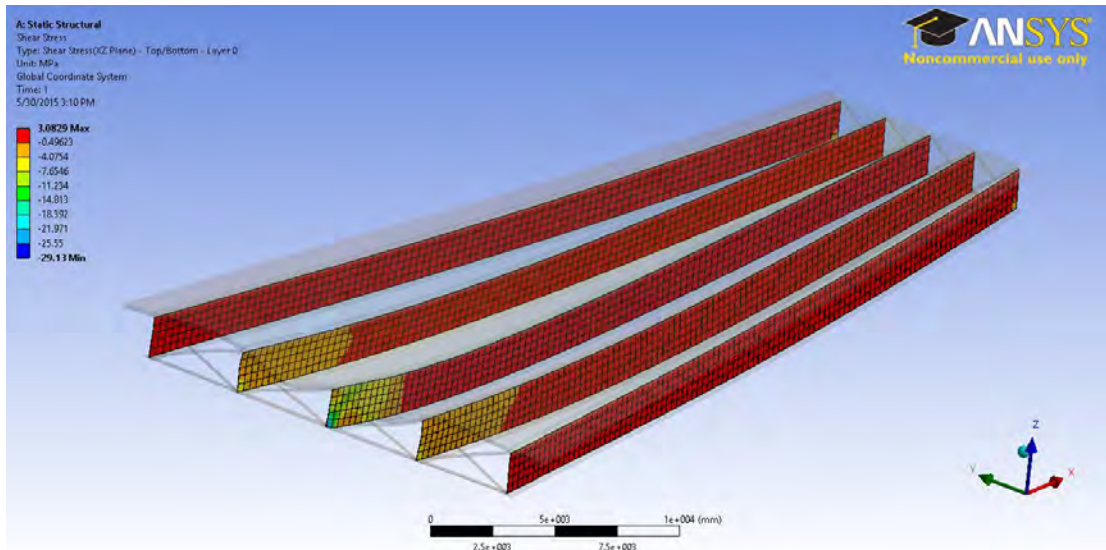
Figure 59: shear stresses in the web of the girders in Reference Bridge

4.4.3   Equivalent AASHTO GDF.

In this section, a proposed approximate procedure to calculate the GDF for flexure and shear in both interior and exterior girders is explained and applied to the reference splayed girder bridge. This procedure is based on the AASHTO LRFD formulas used to calculate the GDF for flexure and shear in parallel girder bridges, presented back in Section 2.5. The objective of this procedure is to find out if such a simple method can be reasonably applied to splayed girder bridges, without the use of FEA.

The general concept of this method is to compute the GDF for interior or exterior girder with consideration of the actual girder spacing at each truck axle position using the AASHTO LRFD formulas. Each of the three GDF values is then multiplied by the corresponding axle load, and the result is applied to a single composite girder at the position that maximizes the live load effect whether for flexure or shear. The same single composite girder is loaded again with only the truck live load, without multiplying it by the GDF. Then, the load effect is recorded in both loading scenarios. Finally, the equivalent GDF is the ratio of the maximum live load effect due to multiplying the load by GDF to the live load effect due to the single truck without any factors.

As the girder spacing changes along the span of splayed girder bridges, this method seems to be a good approximation because it accounts for the girder spacing at each loading axle, especially that the trucks' rear axle has the greatest weight with the greater girder spacing; thus, affecting the GDF results the most. The method will be explained in more detail and depth in the sub-sections to follow for both flexure and shear.

4.4.3.1 Flexure.

The procedure of calculating the equivalent GDF for flexure is presented in Figure 60.

Girder Spacing at truck wheels positions

Smax = 4500 mm

Girder Spacing at midspan

Girder Spacing

Smin = 2250 mm

E 4300 4300 D

A C B

L/2

Truck longitudinal position

Shift from midspan

L

AASHTO LRFD GDF formulas

Exterior Girders

$(GDF)_{Ext} = e*(GDF)_{Int}$

$e = 0.77 + (d_e/2800)$

Interior Girders

One lane $GDF = 0.06 + \left(\dfrac{S}{4300}\right)^{0.4}\left(\dfrac{S}{L}\right)^{0.3}\left(\dfrac{K_g}{Lt_s^3}\right)^{0.1}$

Two lanes or more $GDF = 0.075 + \left(\dfrac{S}{2900}\right)^{0.6}\left(\dfrac{S}{L}\right)^{0.2}\left(\dfrac{K_g}{Lt_s^3}\right)^{0.1}$

Find GDFs at truck wheels positions
(C, D, and E)

GDF $_C$ GDF $_D$ GDF $_E$

145 KN x GDF $_E$ 145 KN x GDF $_C$ 35 KN x GDF $_D$

A B

L/2

L

Girder spacing at C

N.A

y.b

Find Mg @ the truck longitudinal position then find the stress at the bottom flange

$\sigma_g = \dfrac{M_g \cdot y_b}{I_c}$

145 KN   145 KN   35 KN

Without multiplying by GDF

A B

Truck longitudinal position

L/2

L

Find Mtruck @ the truck longitudinal position then find the stress at the bottom flange

$\sigma = \dfrac{M_{truck} \cdot y_b}{I_c}$

Equivalent GDF

$GDF_{Equ} = \dfrac{\sigma_g}{\sigma}$

Figure 60: Procedure for calculating the equivalent AASHTO GDF for flexure

To calculate the equivalent AASHTO GDF for flexure, first the girder spacing at each truck axle position should be found, then by applying the AASHTO LRFD formulas, the GDF at each axle position is calculated based on the actual girder spacing. Based on the beam theory, a simply-supported composite girder is loaded with a truck at the critical longitudinal position for maximum moment, and each axle load is multiplied by the corresponding GDF computed in the previous step. Note that multiple presence factors are not used here since they are embedded within the AASHTO GDF. The girder is analyzed then, and the critical bending moment (M_g) at the middle axle position is computed. The stress at the bottom flange of the girder is calculated using Equation (14) below.

$$\sigma_g = \frac{M_g \cdot y_b}{I_c} \qquad (14)$$

The next step is to load the same composite girder by the same truck at the same position but without multiplying the load by any GDF. The bending moment (M_{truck}) at the same longitudinal position is then computed, and finally the stress at the bottom flange of the girder is found using Equation (15) below.

$$\sigma = \frac{M_{truck} \cdot y_b}{I_c} \qquad (15)$$

The last step is to divide the stress value from the girder by the stress value for the girder loaded with no factors, as shown in Equation (16).

$$GDF_{Equ} = \frac{\sigma_g}{\sigma} \qquad (16)$$

Note that if we were to design a splayed girder bridge using the concept of equivalent AASHTO GDF, then the computed (M_g) would be enough, without continuing further with Equations (14), (15), and (16).

To test the concept of the computed equivalent GDF, the GDF value from the finite element model by ANSYS is compared with the equivalent GDF for all bridges in this study. Starting with the reference bridge, the GDF values for flexure in both interior and exterior girders are compared and summarized in Figure 61.
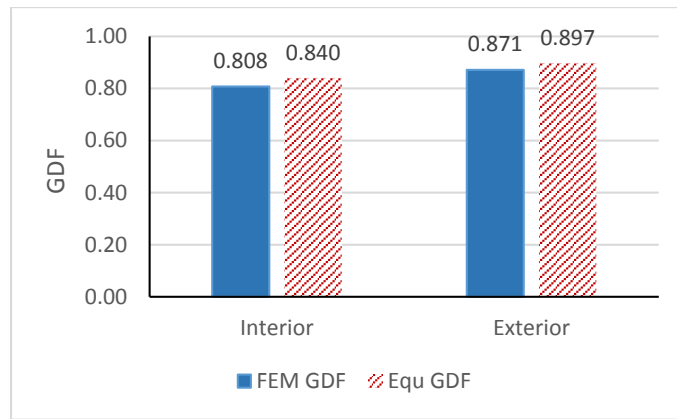
Figure 61: FEM GDF vs. Equ GDF in the reference bridge

The results show that for both interior and exterior girders in the reference bridge, the equivalent GDF values are slightly greater than the ones from the FEM, which means that the suggested approach is reasonable and somewhat safe. However, before fully accepting the approximate approach, we need to consider different bridge parameters. This is done in a later chapter.

4.4.3.2 Shear.

The procedure of calculating the equivalent GDF for shear is presented in Figure 62, where the steps followed are similar to the ones for flexure. It starts with finding the girders' spacing at each truck axle position, then we use the AASHTO LRFD formulas to find the GDF for shear at each girder spacing found in the previous step for the girders. Note that multiple presence factors are not used here since they are embedded within the AASHTO GDF. However in shear, using the lever rule is common and effective in finding the shear GDF for some special cases. Therefore, the lever rule is also considered to find the shear GDF for interior and exterior girders in the considered bridge. The next step is to load a single simply-supported composite girder, at the longitudinal position to maximize shear at the support, with the truck axle loads each multiplied by the corresponding GDF values based on the girder spacing related to the truck axles' longitudinal positions. The girder is then analyzed and the maximum reaction at the supported end (V_g) is computed where it represents the maximum shear in the girder. The next step is to load the same girder at the same longitudinal position with the same truck load but without multiplying the loads by any factor. The girder is then analyzed for the full truck load and the reaction at the supported end (V_{truck}) is computed to represent the maximum shear in the girder. Finally, using Equation (17)

the equivalent GDF for shear is computed once using the lever rule results and once using the AASHTO LRFD formula results.

$$GDF_{Equ} = \frac{V_g}{V_{truck}} \qquad (17)$$
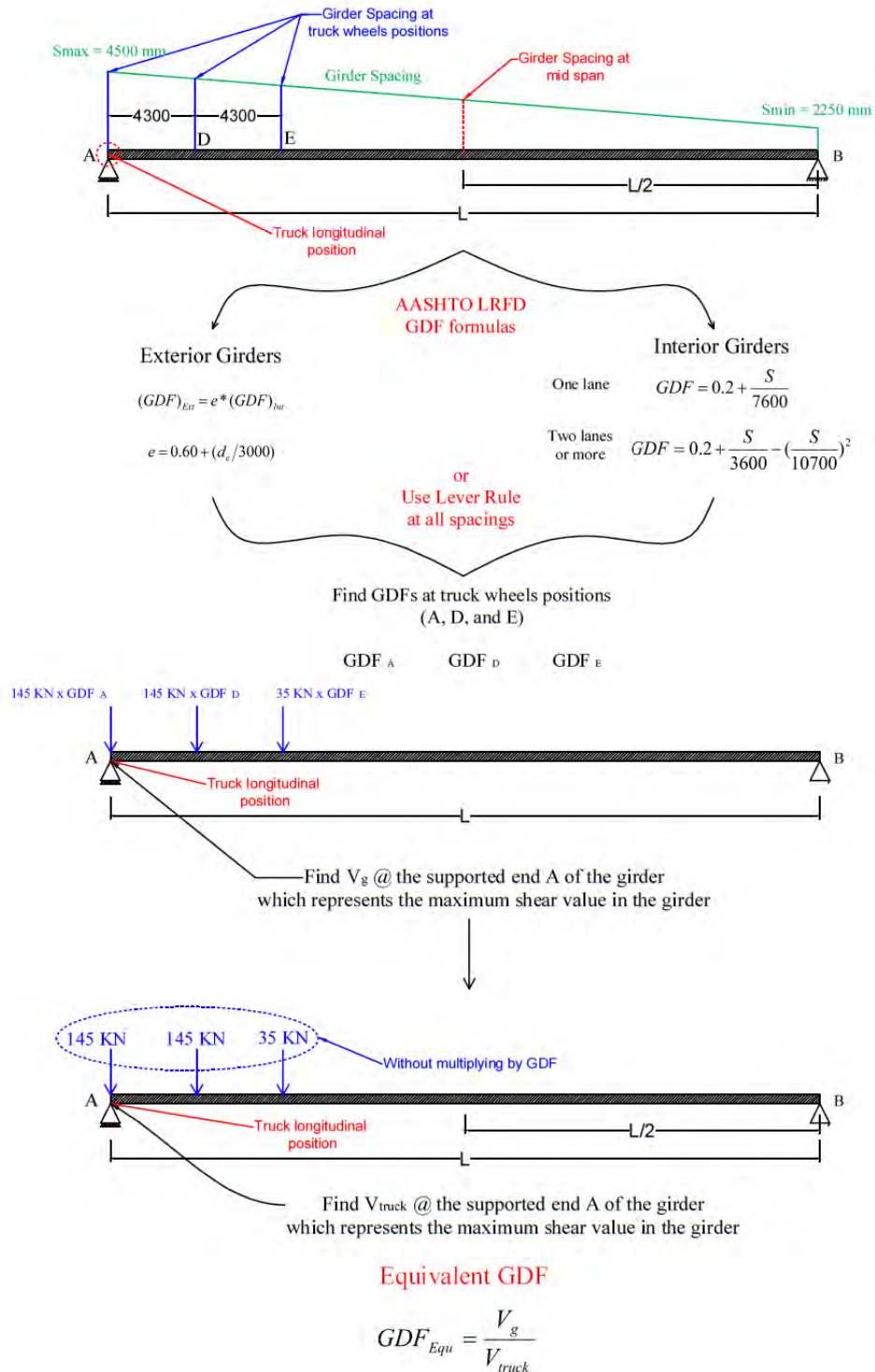
Figure 62: Procedure for calculating the equivalent AASHTO GDF for shear

The equivalent GDF values for shear, whether they are based on AASHTO LRFD formulas or the lever rule, are then compared with the shear GDF values from the finite element models by ANSYS. For the reference bridge, the GDF for shear in both interior and exterior girder are compared and summarized in Figure 63.
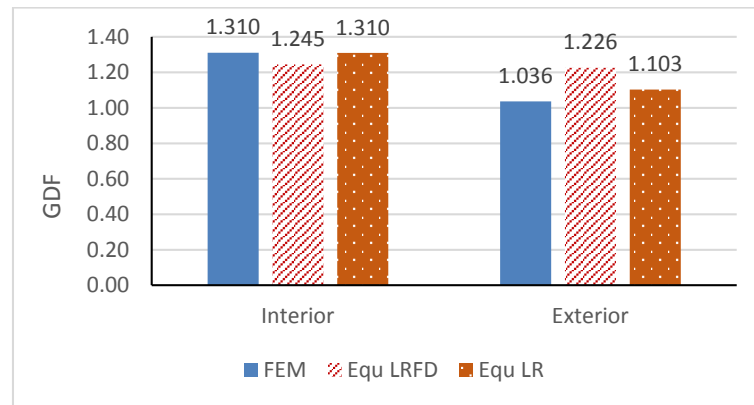
Figure 63: FEM vs. Equ LRFD and Lever rule GDF in the reference bridge

For the reference bridge the GDF value computed from the finite element results in the interior girder being greater than the equivalent AASHTO GDF value computed using the AASHTO LRFD formulas by 5%, while using the lever rule the two values are equal. On the other hand, in the exterior girder the equivalent AASHTO GDF value computed using the AASHTO LRFD formulas is greater than the one from the finite element results by 18.3%. When the same is compared with the equivalent GDF based on the lever rule, the difference is only 6.5%, which is more reasonable. Thus, the equivalent GDF for shear in the reference bridge that is based on the lever rule gives much better results than the one based on the AASHTO LRFD formulas in both interior and exterior girders.

4.4.4 Deck slab.

In order to understand the deck slab behavior in splayed girder bridges, finite element models for all of the considered bridges (B1, B4, and B5) are developed using ANSYS. The bridges are then loaded at each section described in Table 12 using one or two design lanes, and the stresses are recorded after multiplying them by the corresponding multiple presence factor. Here, using five layers of solid elements across the slab thickness to model the deck slab permits more accurate results. In most cases, the largest plan mesh size is about 500 mm x 400 mm. For positive moment stresses at

the bottom layer, nodes of the deck slab are recorded, while for negative moments stresses at the top layer nodes of the deck slab are recorded.

It should be noted that the size of loading patches representing the truck wheel imprints on the bridge deck are not as significant when studying the bridge girders as they are when studying the concrete deck slab behavior. The standard AASHTO LFD specifications [8] suggest that the tire contact area must be a rectangle with an area of 0.01P and length-to-width ratio of 1/2.5, in which the area is in square inches, P is wheel load in pounds, and the length of the wheel imprint is in the direction of traffic. The tire contact area dimensions in mm units represented by the loading patches are illustrated in Figure 64 with the truck load and dimensions.
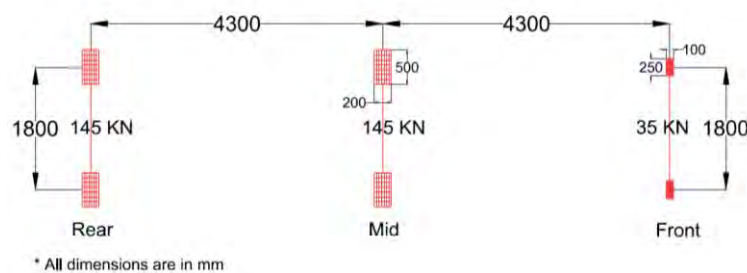
Figure 64: Truck loading patch in deck slab

The same deck slab sections with the corresponding girder spacing described in Table 12 are then analyzed analytically using the AASHTO LRFD strip method. For interior positive and negative moments, a continuous beam representing each deck slab strip under consideration is analyzed. One and two loading lanes are applied at different transverse positions to maximize the live load effect, and the maximum moments are recorded. It should be noted that in the analytical approach the continuous beam is loaded with the heaviest HL-93 truck axle. On the other hand, the overhang is analyzed as a cantilever, and the maximum moment is recorded when the truck wheel is at the minimum distance of 300 mm from the parapet. The stress values are then computed based on a deck slab cross-section with a width equal to the equivalent strip width (SW) for the moment under consideration.

For the case of positive moments in the reference bridge, the finite element analysis resulted in a maximum stress in the bottom layer of the slab equal to 2.242 MPa caused by one truck loading at the wide spacing end of bridge (Section 1) as shown in Figure 65. By using two trucks, a maximum stress value of 2.396 MPa is obtained. However, the stress value resulting from a one-lane loading should be multiplied by a multiple presence factor equal to 1.2, while for the two-lane loading it is multiplied by

1. Therefore, the maximum stress value resulting from one-lane loading governs and it is equal to 2.690 MPa. It should be noted that the maximum stress value is obtained after trying different truck positions in the transverse direction at the same longitudinal location. The deflected shape of the deck slab due to this loading is illustrated in Figure 66 , where it shows the transverse stress contours in the whole deck slab with the finite element mesh. It can be observed that the maximum stresses in the deck slab are developed under the mid and rear axle because they take the largest portion of the truck's load.
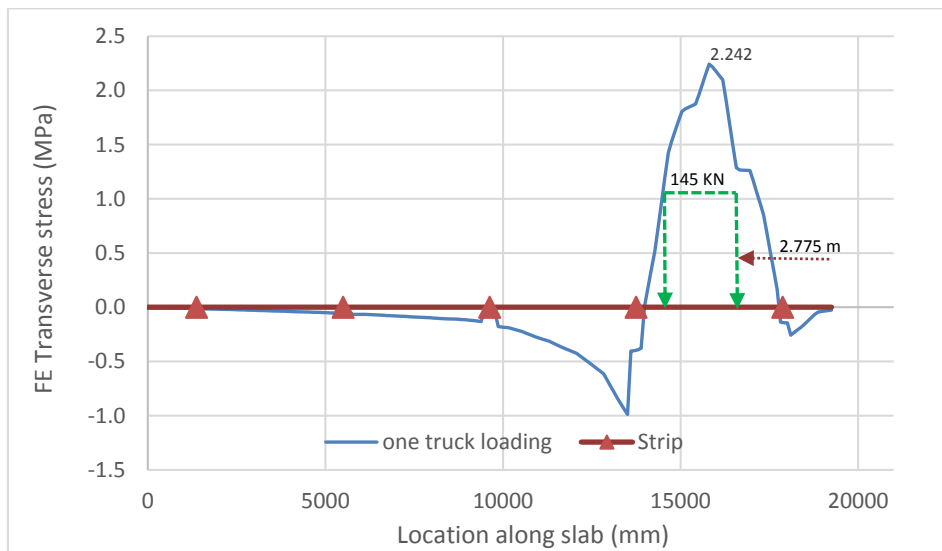
Figure 65: Max stress in deck slab in B1 for positive moment at sec 1
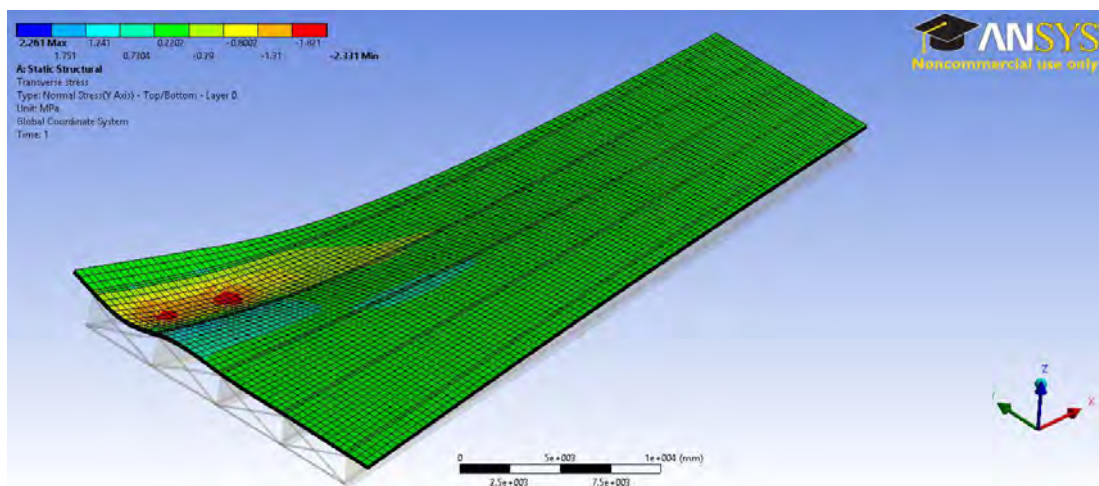
Figure 66: Stress contours in deck slab for positive moment at sec 1

The strip is then analyzed as a continuous beam over rigid supports loaded with a single truck at different locations along the strip in order to maximize the positive moment in the slab. After trying different locations, the maximum positive moment of

73.37 KN-m is obtained. However, this moment value should also be multiplied by a multiple presence factor of 1.2, which results in a maximum positive moment equal to 88.04 KN-m. This moment value can then be converted to a stress using elastic analysis for the equivalent strip section as follows:

$$\sigma = \frac{M.c}{I_c}$$

I : Moment of inertia of the strip section (mm⁴)

$$I = \frac{SW * t_s^3}{12}$$

SW : Equivalent strip width which can be computed for the positive moment case as:

$$SW = 660 + 0.55S = 660 + 0.55 * (4125) = 2929 \text{ mm}$$

Therefore:

$$I = \frac{2929 * 220^3}{12} = 2.6 * 10^9 \text{ mm}^4$$

And as the strip section is rectangular $c = \frac{t_s}{2} = 110$ mm , consequently:

$$\sigma = \frac{88.04 * 10^6 * 110}{2.6 * 10^9} = 3.725 \text{ MPa}$$

As expected, the stress value from the equivalent strip procedure (3.725 MPa) is higher than the finite element result (2.690 MPa) by 38.5%. The rest of the strips are also analyzed using the same procedure. Table 26 summarizes the finite element transverse stresses at each section in the reference bridge's deck slab with the corresponding stresses from the equivalent strip method, based on the AASHTO LRFD specifications.

Table 26: B1 deck slab transverse stresses for positive moment case

Strip No.	Girder spacing (m)	FE stress* (MPa)	Strip width SW (m)	Analytical approach stress* (MPa)	Percentage difference %
1	4.125	2.690	2.929	3.725	38.5
2	3.375	2.886	2.516	3.201	10.9
3	2.625	2.318	2.104	2.600	12.2

* Stress values include the multiple presence factor.

For negative moment, one or two truck loads are applied in the finite element model at the defined longitudinal locations for the negative moment case. Here the transverse tensile stresses at each considered section are taken at the top layer of the concrete deck slab solid elements. Different loading scenarios are checked, and the tuck position in the transverse direction is also changed in order to maximize the loading effect. However, the initial placement of the truck transversely is based on influence lines.

For the reference bridge, many loading scenarios in the transverse direction are tested in order to choose the most critical position for maximum moments, and then apply it to the rest of the considered bridges. At the section that is 1 m away from the support, whether at the wide or the narrow end of the bridge, the rear axle of one truck is placed centered above the first interior girder and then above the intermediate girder. The same procedure is repeated for two trucks, such that their rear axles are once centered above the first interior girder and once above the intermediate girder, with a minimum gap between the two trucks of 1.2 m. Also, two trucks, one at each extreme edge of the bridge near the parapets, is another scenario applied in the finite element model to potentially maximize the loading effect. Finally, at the section at mid span of the bridge two trucks with a gap of 1.2 m between them are placed above the first interior girder in order to check the maximum transverse stress at that section. Table 27 summarizes all the tested scenarios for the reference bridge negative moment with the corresponding stress values multiplied by the corresponding multiple presence factor for one or two trucks.

It can be concluded that at the narrow end (Section 3) loading with one truck govern; because of the small girder spacing at the narrow end of the bridge. Also, it can be noticed that in all scenarios loading the deck slab above the first interior girder results in higher stress values than over the intermediate interior girder. For the wide-end strip (Section 1), it is obvious that loading the bridge with two trucks centered above the first interior girder with 1.2 m distance between them gives the maximum transverse stress (4.075 MPa) due to negative moment, as shown in Figure 67. The deflected shape of the entire bridge due to this loading scenario is shown in Figure 68 together with the transverse stress contours.

Table 27: Deck slab loading scenarios for interior negative moment case

| Strip No. | Location | Loading scenario | | Stress* |
		No. of trucks	Position	
1	1 m away from wide end support	1	Centered above 1st interior girder	2.302
			Centered above intermediate girder	1.993
		2	Centered above 1st interior girder (1.2 m away)	4.075
			Centered above 1st interior girder (1.8 m away)	3.223
			Centered above Intermediate girder (1.2 m away)	3.7074
			Centered above Intermediate girder (1.8 m away)	3.061
			One truck at each extreme edge	1.3402
3	1 m away from narrow end support	1	Centered above 1st interior girder	1.379
			Centered above intermediate girder	1.280
		2	Centered above 1st interior girder (1.2 m away)	1.474
			Centered above 1st interior girder (1.8 m away)	N.A**
			Centered above Intermediate girder (1.2 m away)	1.04
			Centered above Intermediate girder (1.8 m away)	1.096
			One truck at each extreme edge	0.751
2	At mid span	2	Centered above 1st interior girder (1.2 m away)	0.978

* Stress values include the multiple presence factor.

** Because of the geometry of the bridge at this section, it is impossible to fit two trucks 1.8 m away from each other above the first interior girder.

Figure 67: Max stress in deck slab in B1 for interior negative moment at sec 1
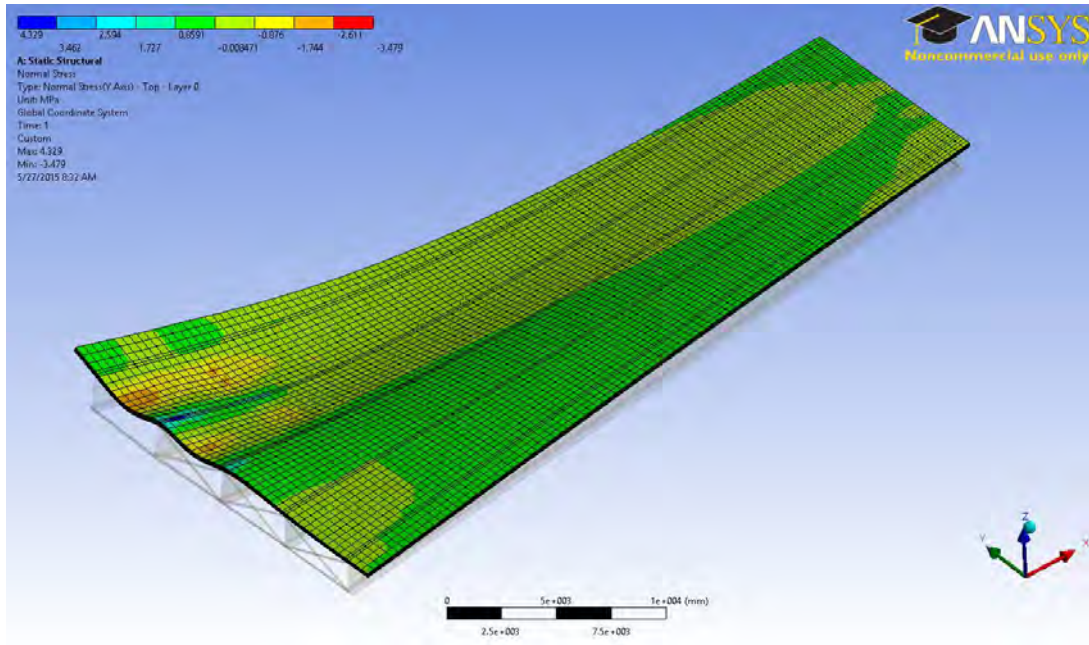
Figure 68: Stress contours in deck slab for interior negative moment at sec 1

Similar to the positive moment case, each strip is analyzed analytically using the AASHTO LRFD strip method as a continuous beam loaded by the heaviest axle of the truck. The maximum negative moment and corresponding maximum stress is calculated based on the strip cross-section at the considered location. For the strip at the wide end of the reference bridge, the maximum negative moment is equal to -88.33 KN-m, which is a result of two trucks positioned in opposite girder spacing from the first interior girder. This moment value is multiplied by the multiple presence factor for two trucks, and it can be converted into a stress by using the equivalent strip section at the negative moment region, as explained in the following:

$$\sigma = \frac{M.c}{I_c}$$

$$I = \frac{SW * t_s^3}{12}$$

SW : Equivalent strip width which can be computed for the negative moment case as:

$$SW = 1220 + 0.25S = 1220 + 0.25 * (4444) = 2331 \text{ mm}$$

Therefore:

$$I = \frac{2331 * 220^3}{12} = 2.068 * 10^9 \text{ mm}^4$$

And as the strip section is rectangular $c = \frac{t_s}{2} = 110 \text{ mm}$, consequently:

$$\sigma = \frac{88.33*10^6*110}{2.068*10^9} = 4.698 \text{ MPa}$$

It is clear that the stress value using the equivalent strip procedure (4.698 MPa) is higher than the finite element result (4.075 MPa) by 15.3%. The same procedure is applied for the rest of the strips in the reference bridge. Table 28 compares the finite element transverse stresses with the stresses from the equivalent strip method at the three sections chosen for the negative moment case in the reference bridge. The reason why there is a large difference between the finite element and equivalent strip method at strip 2 is because at that location the girders are free to deflect which causes some of the negative moment in the deck slab to be reduced.

Table 28: B1 deck slab transverse stresses for interior negative moment case

Strip No.	Girder spacing (m)	FE stress* (MPa)	Strip width SW (m)	Analytical approach stress* (MPa)	Percentage difference %
1	4.444	4.075	2.331	4.698	15.3
2	3.375	0.978	2.064	3.645	272.6
3	2.306	1.379	1.797	2.508	81.8

* Stress values include the multiple presence factor.

The overhang is also analyzed at three different sections along the span of the bridge (Sections 1, 2, and 3), which are the same as those used for the positive moment case. However, in order to maximize the negative moment in the overhang, a single truck is placed parallel to the parapet at a distance of 300 mm. In the reference bridge at the section close to the wide end of the bridge (Section 1), the maximum stress value due to the negative moment in the overhang equals 1.834 MPa, as shown in Figure 69. However this stress value should be multiplied by a multiple presence factor for 1 truck which equals to 1.2, and consequently the maximum transverse stress becomes equal to 2.201 MPa. Figure 70 shows the transverse stress contours in the slab with the deflected shape of the bridge due to truck loading for maximum overhang negative moment at Section 3.
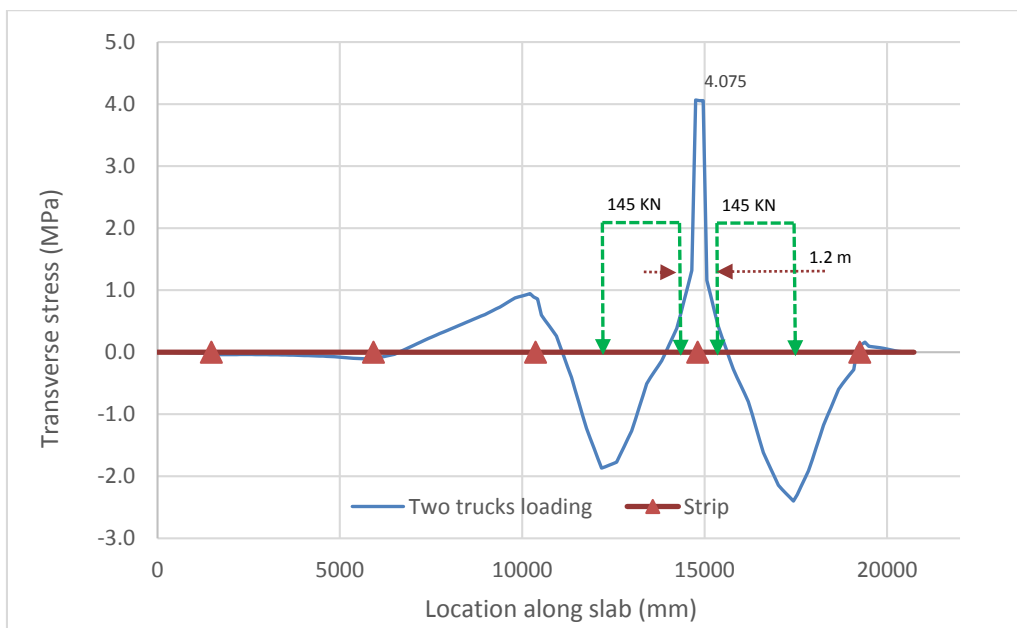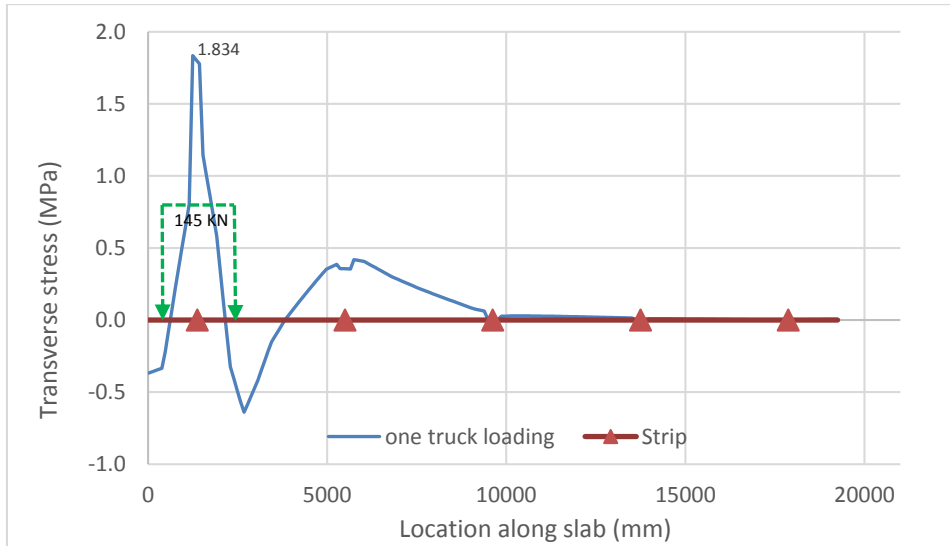
Figure 69: Max stress in deck slab in B1 for overhang negative moment at sec 1
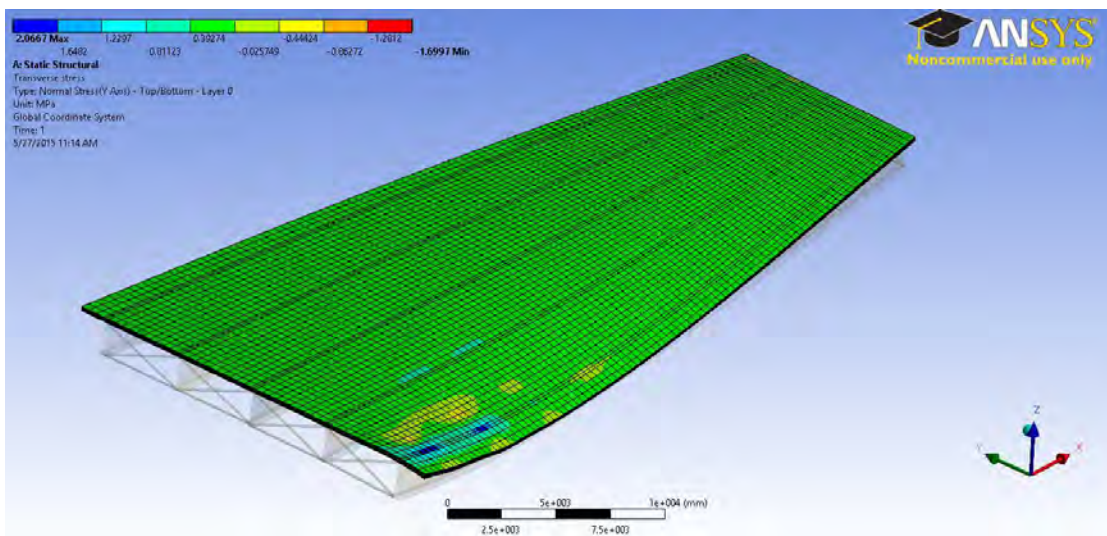
Figure 70: Stress contours in deck slab for overhang negative moment at sec 1

The overhang is then analyzed analytically as a cantilever loaded by the truck wheel on a distance of 300 mm from the parapet using statics. Using the equivalent strip width, the maximum transverse stress value at the overhang is computed based on the maximum negative moment resulting from the analytical solution of the overhang. For section 1 in the reference bridge, the overhang negative moment equals 67.425 KN-m, after factoring it using the multiple presence factor for one truck (1.2). The stress value resulting from the equivalent strip method is computed as follows:

$$\sigma = \frac{M.c}{I_c}$$

90

$$I = \frac{SW * t_s^{\ 3}}{12}$$

SW: Equivalent strip width which can be computed for the overhang negative moment case as:

$$SW = 1140 + 0.833X = 1220 + 0.833*(775) = 1786 \text{ mm}$$

Therefore:

$$I = \frac{1786*220^3}{12} = 1.585*10^9 \text{ mm}^4$$

And as the strip section is rectangular $c = \frac{t_s}{2} = 110 \text{ mm}$, consequently:

$$\sigma = \frac{67.425*10^6 *110}{1.585*10^9} = 4.681 \text{ MPa}$$

The above result shows that the stress value using the equivalent strip procedure (5.325 MPa) is much higher than the finite element result (2.201 MPa). The same procedure is applied for the rest of the strips considered for the overhang in the reference bridge. This is not a surprising result since design codes are usually very conservative when dealing with non-redundant, statically determinate elements, such as the deck slab overhang, where re-distribution of internal forces is limited or does not exist at ultimate. Table 29 compares the finite element transverse stresses with the stresses from the equivalent strip method at the three sections chosen for the overhang negative moment case in the reference bridge.

Table 29: B1 deck slab transverse stresses for interior negative moment case

Strip No.	Overhang distance (m)	FE stress* (MPa)	Strip width SW (m)	Analytical approach stress* (MPa)	Percentage difference %
1	1.375	2.201	1.786	4.681	113
2	1.125	1.684	1.577	3.590	113
3	0.875	1.134	1.370	2.166	91

* Stress values include the multiple presence factor.

4.5 Dead Load Effect in Reference Bridge

Dead load in bridge structures is never less important than live load, and it has a huge effect on bridge behavior. However, it does not get much attention by researchers because it is often easier to predict than the live load. This may be true for girder bridges, but may not be obvious for splayed girder bridges. Dead load in bridges is in general the permanent load that remains on the bridge for the whole service life without much change in magnitude. Such load is caused by the self-weight of the structure, future wearing surface (FWS), barriers or parapet weight, and stay-in-place metal deck form. The future wearing surface is usually taken as a pressure on the surface of the bridge with a 1.0 to 1.5 kPa magnitude, while the parapet or barrier load depends on the material density and cross-section dimensions. In this study, the future wearing surface is assumed to have 1.5 kPa magnitude, and the parapet, which is 300 mm in width, is assumed to have 10 KN/m magnitude along both edges of the bridge span. Two cases of composite construction methods should be considered when analyzing dead load effect in composite slab-on-girder bridges. The two methods are shored and un-shored construction. Shored construction occurs when the steel girders are supported by temporary falsework during the concrete deck slab casting. After concrete in the slab is hardened, the composite section is formed, and the shoring is removed. In this case the composite section resists the self-weight of the deck slab and the girder (if shoring is used under girders) beside the superimposed loads represented by FWS and parapet weight. On the other hand, in un-shored construction the steel girder is not supported when the deck slab is constructed. Therefore, the non-composite girder resists girders and deck slab weight, and the composite girder resists only the superimposed loads. Figure 71 shows a typical shored versus un-shored construction for steel girder bridges.
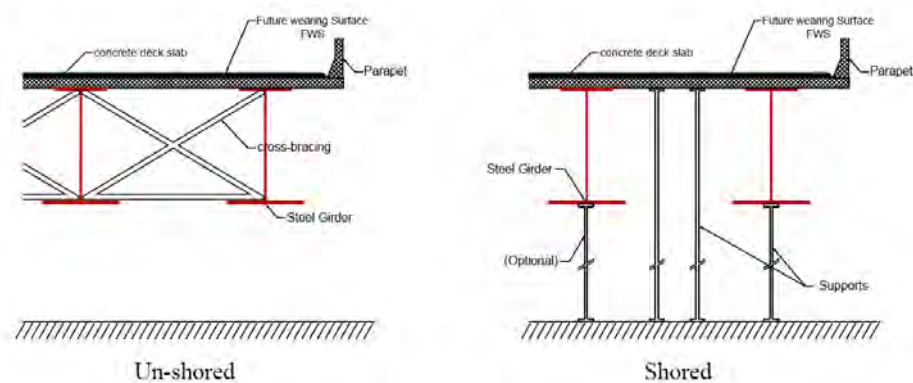
Figure 71: Typical shored vs. un-shored construction method

4.5.1   Girders.

In this study both shored and un-shored construction methods are studied and applied in this section to the reference bridge. A finite element model by ANSYS is developed for both cases and the results are compared with hand calculations for the composite girder of the bridge loaded with the same dead loads based on the tributary area concept.

4.5.1.1 Shored construction.

In shored construction, the composite girder resists all dead loads from elements' self-weight, FWS, stay-in-place metal deck form, and parapet weight. In the analytical approach, a single composite girder of the bridge is loaded with the concrete deck slab self-weight, where deck slab width is taken as half of the girder spacing from each side resulting in a width equal to the girder spacing which changes along the span length, resulting in a trapezoidal load on the composite girder. The steel girder self-weight is also represented by a uniform load along the composite girder assuming the girder was supported during erection. Regarding the superimposed load from parapet weight and future wearing surface, the AASHTO LRFD specifications suggest distributing it equally between the girders. Therefore, the parapet weight is represented by a uniform load along the span and its magnitude equals the summation of parapet loads at both edges of the bridge divided by the number of girders. However, due to the bridge splayedness, the FWS load varies along the girder span, and it is represented by a trapezoidal load with a magnitude at any section equal to the total FWS load per unit width at that section divided by the number of girders. Cross-bracing, if present, is represented by point loads along the span of the composite girder; these loads vary in magnitude from one point to another based on the cross-bracing weight where it changes because of the change in girder spacing along the span. The composite girder dead load for the reference bridge B1 is shown in Figure 72.

The composite girder is then analyzed, and the moment at the mid span is computed to find the stress at the bottom flange of the girder in the composite section at the mid span. Then the resulting stress is compared with the one concluded from the finite element results at mid span as shown in Table 30.
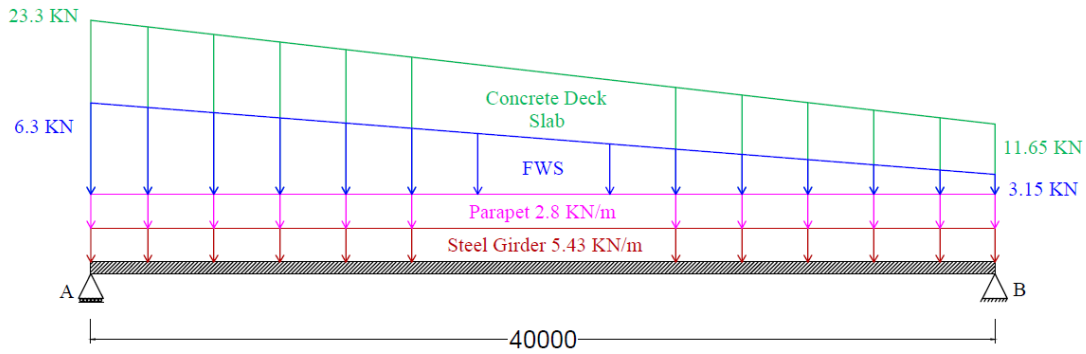
Figure 72: Composite girder dead load in shored construction

Table 30: Shored construction method dead load results

Girder	Analytical calculations	FE Exterior girder (G1)	FE First Interior girder (G2)	FE Intermediate girder (G3)
Stress (MPa)	**77.77**	78.572	74.511	73.444

Figure 73 shows the longitudinal stress contours in the girder with the deflected shape of the bridge due to dead load in the case of shored construction.

Figure 73: Longitudinal stress and deflected shape due to dead load – shored

It is obvious that the results are very close to each other. The stress value resulting from the analytical approach using the composite girder is greater than the stress value from the FE model by 4.2% and 5.5% for first interior girder and the intermediate girders, respectively. However, it was only 1% lower than the FE stress for the exterior girder, which indicates that using the analytical approach is an accurate approximation to calculate the dead load effect when using the shored construction method.

94

4.5.1.2 Un-shored construction.

In the un-shored construction case, the composite girder resists loads only from FWS and parapet weight. The non-composite girder resists all other loads including its own self-weight and weight of the deck slab. Therefore, in the analytical approach, the composite girder is only loaded by the trapezoidal load representing the FWS and the uniform load representing the parapet weight. Both load components are assumed to be distributed equally among the bridges' girders as suggested by the AASHTO LRFD specification, and computed in the same manner as was presented back in the shored construction method. Figure 74 shows the composite girder loading in the un-shored construction case. Structural analysis of the bare steel girder subjected to loads on the non-composite section is not considered here since there is no interaction from other girders.
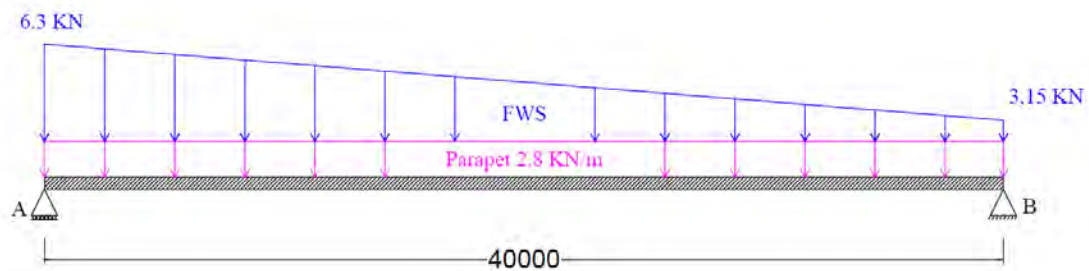
Figure 74: Composite girder dead loads in un-shored construction

The composite girder is then analyzed, and the midspan moment and corresponding stress are computed again in the same manner as in the shored construction method. The analytical results are compared with the finite element findings at mid span as shown in Table 31.

Table 31: Un-shored construction method dead load results

Girder	Analytical calculations	FE Exterior girder (G1)	FE First Interior girder (G2)	FE Intermediate girder (G3)
Stress (MPa)	**19.23**	21.00	20.25	19.20

It is obvious that the results are very close to each other. However, the stress value conducted from the analytical approach using the composite girder is slightly greater than the stress value from the FE model by only less than 1% for the intermediate girder. For the first interior and exterior girders it was lower by 5.3% and 9.2%, respectively. This shows that distributing the dead load equally between all girders, as suggested by the AASHTO LRFD specifications, in the un-shored

construction method might not be that accurate, as the parapet load is very close to the exterior girder; thus the girders nearby receive a larger percentage than girders away from the edge. Figure 75 shows the longitudinal stress contours in the girder with the deflected shape of the bridge due to dead load for the un-shored construction case.
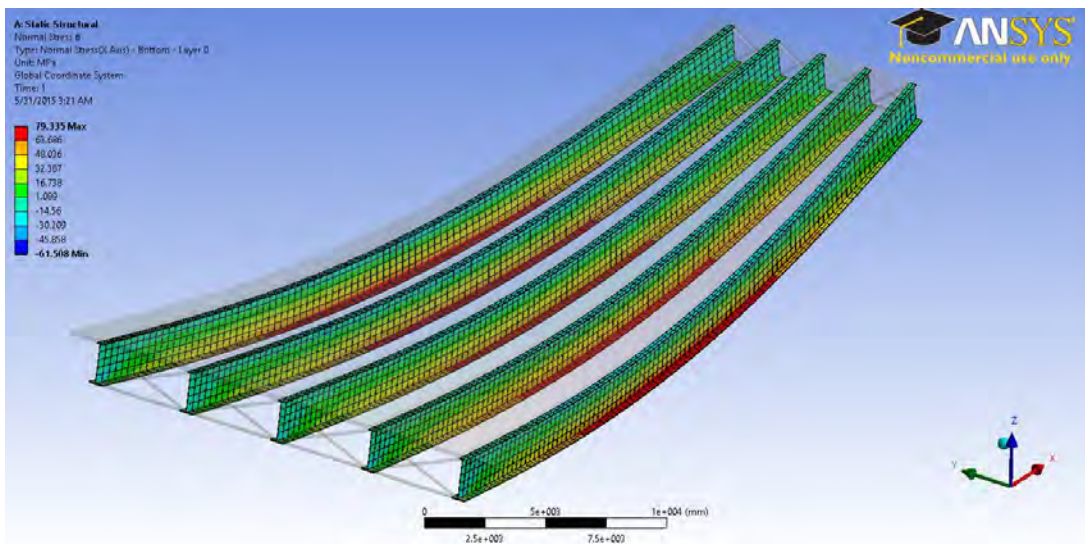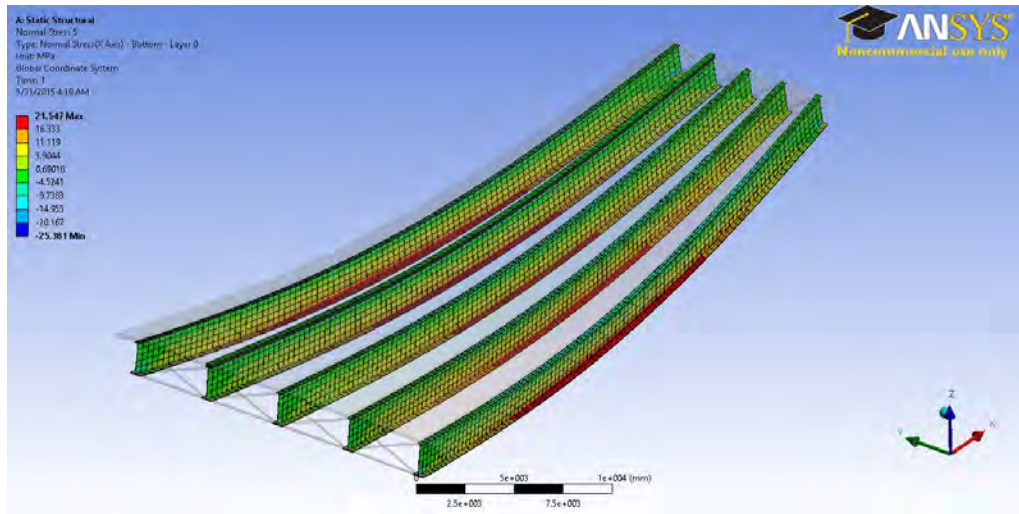

Figure 75: Longitudinal stress and deflected shape due to dead load – unshored

4.5.2   Deck slab.

Although dead load does not have as much impact on the deck slab as live load, nevertheless it has to be considered. To study its effect on the slab, the common shored construction method is considered. In this method, the concreted deck slab is affected by its own self-weight, the parapet weight, and the FWS weight. A finite element model of the reference bridge (B1) is considered to investigate the dead load effect on the deck slab in splayed girder bridges in detail.
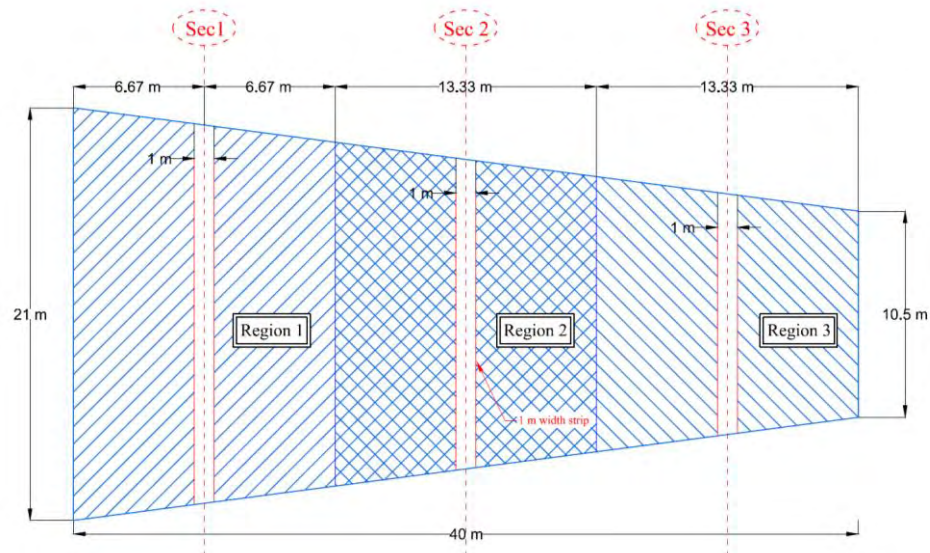
Figure 76: Deck slab considered strips for dead load

96

Here a 1 m strip of the slab is taken at three different locations along the centerline of the bridge as shown in Figure 76. The stresses in the overhang portion and the positive and negative interior regions are recorded. It should be noted that as the strip width is 1 m, any recorded stress value is taken as the average between the nodal stresses within the strip.

The finite element results are compared with the analytical solution of the same strips, analyzed as a continuous beam with rectangular sections of unit width. The overhang is analyzed separately as a cantilever loaded with the deck slab self-weight, the parapet weight, and the FWS, as shown in Figure 77. The continuous beam that represents the strip (without the overhangs at both ends) is loaded with its own self-weight and the FWS. The computed moment couple due to the overhang weight is also added at both ends of the beam as shown in Figure 78. It should be noted that AASHTO considers the future wearing surface separate from the self-weight due to the difference in load factors. In this study their effect is added together at the service level.
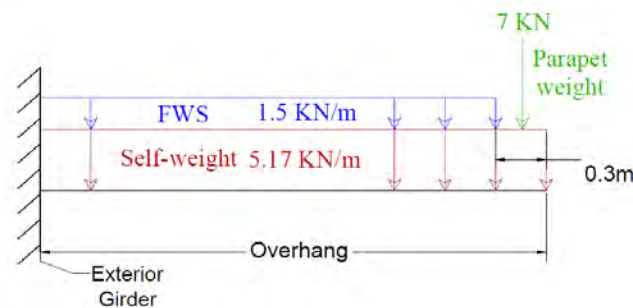
Figure 77: Deck slab overhang dead load
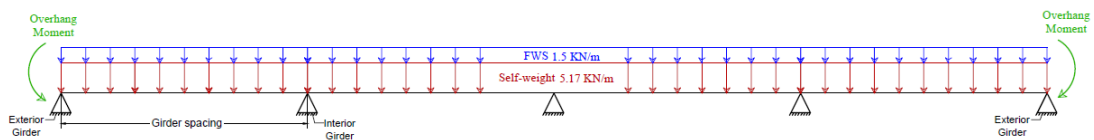
Figure 78: Deck slab strip dead load

Table 32 compares the finite element stress results with the analytical solution at each considered strip. It is clear that the analytical approach, which assumes the girders are on rigid supports to the slab, often gives higher stresses compared with the finite element method. It is obvious that by moving toward the narrow end of the bridge the stress values drop because of the decrease of load and spacing between the girders due to bridge splayedness. However, it is noted that the stress values from the finite element analysis are closer to the analytical values when the chosen strip is closer to the support due to the increased rigidity of the structure at that location. By moving

97

toward the mid span of the bridge, the girders start to deflect and, as a result, the stresses due to positive moment drop, and the effect of the parapet weight becomes significant.

Table 32: Deck slab stress results due to dead load

Strip No.	location	Girder spacing (m)	Overhang (m)	Method	Stress (MPa)		
					Positive moment region	Negative moment region	Overhang
1	6.67 m away from the wide end support	4.125	1.375	FE	0.374	0.802	1.284
				Analytical	0.632	1.260	1.776
2	At mid span of the bridge	3.375	1.125	FE	-0.023*	0.784	0.963
				Analytical	0.434	0.862	1.315
3	6.67 m away from the Narrow end support	2.625	0.875	FE	0.008	0.509	0.822
				Analytical	0.254	0.506	0.690

* The negative sign means that compression stresses are developed at the bottom of the slab.

Chapter 5: Findings and Discussion: Girders

5.1 Introduction

In this chapter, the live load distribution in splayed girder bridges is analyzed and discussed in depth. The flexure and shear effects in both interior and exterior girders are studied. The discussion is carried out through a parametric study, where six different parameters that affect the splayed girder bridge behavior are considered through fifteen different bridges modeled using the finite element method. Each parameter is isolated to understand its effect by freezing the other parameters and changing it by increasing and decreasing its value by a certain percentage. The live load flexure and shear effects are represented by the GDF. Therefore, the GDF results from the finite element models for the different bridges are discussed, and then compared with the equivalent GDF values computed using the proposed approximate approach for splayed girder bridges using the AASHTO LRFD expressions.
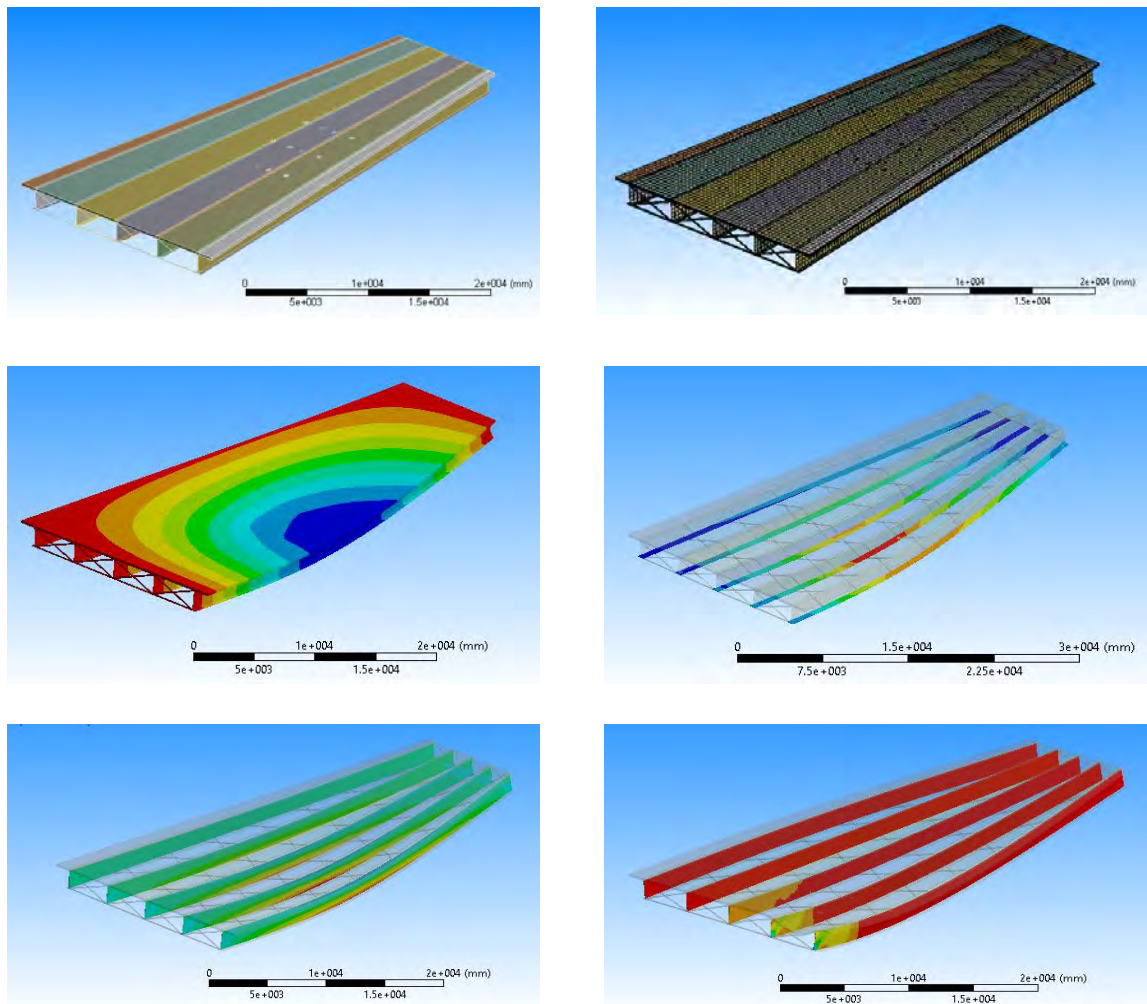

Figure 79: Reference bridge finite element model

5.2 Flexural Effect

The reference bridge (B1) was presented and analyzed back in Sections 4.4.1 and 4.4.3.1 using FEM and the Equivalent GDF approach, respectively. After comparing the GDF from both methods for interior and exterior girders, it was concluded that the Equivalent GDF approach is very promising, especially since the difference between the FEM results and the Equivalent GDF was very small, where for the interior girder the difference was about 4% and for the exterior girder it was only 3%. Hence, Bridge B1 is set as a benchmark for all bridges studied. To check if the Equivalent GDF approach gives reasonable results for the other bridges, it is compared with the finite element findings for the same bridge models.

5.2.1 Effect of girder spacing.

Girder spacing is the most critical parameter in the distribution of live load from the deck slab to the supporting girders. Because of the complex geometry of splayed girder bridges, two splayedness measures are considered. The first one is the splayedness ratio $(S_2-S_1)/L$ that represents the degree of splayedness of the bridge, and the second one is the girder spacing ratio S_1/S_2. In the latter case, the splayedness ratio $((S_2-S_1)/L)$ is kept constant. Hence, four bridges in total are considered for the effect of girder spacing, two for each aspect.

5.2.1.1 Splayedness ratio $(S_2-S_1)/L$ effect.

Figure 80 shows a plan view of bridges B1, B2, and B3 with the corresponding $(S_2-S_1)/L$ values, and truck positioning for maximum flexure effect. It is obvious that decreasing the splayedness ratio in bridge B2 is a result of increasing the width of the bridge at the narrow end, while increasing the splayedness in bridge B3 is a result of decreasing the width of the bridge at the narrow end. Therefore, the girder spacing increases in bridges B2 over the one in bridges B1 due to the reduced splayedness, while it decreases in bridge B3 due to the increased splayedness.

The increase in girder spacing for the considered bridges varies along the span of the bridge. It starts with 0% at the wide end of the bridge and finishes with 33% at the narrow end of the bridge, which gives different changes in girder spacing at each truck axle position. The difference in girder spacing at each is illustrated in Table 33.
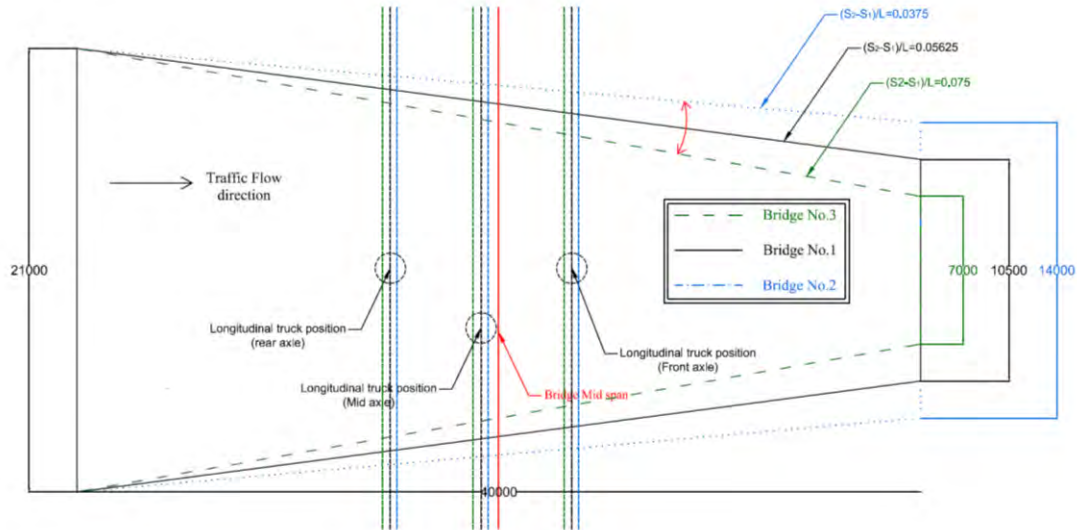
Figure 80: Bridges B1, B2, and B3 plan view - flexure

Table 33: % Difference in girder spacing B1, B2 and B3 - flexure

Bridges	Girder Spacing difference %			Notes
	Rear axle	Middle axle	Front axle	
B1 and B2	7.30	10.20	13.45	increased
B1 and B3	-6.85	-9.70	-12.90	decreased

It should be noted that although the change in splayedness between bridges B1 and B2, and between bridges B1 and B3 are the same, the girder spacing difference at the truck axles does not. This is because of the different longitudinal truck positioning computed for each bridge based on its splayedness. However, the difference for the considered bridges is very small and can be neglected.

Figure 81 below shows the GDF for bridges B1, B2, and B3 for interior and exterior girder results from the finite element analysis versus the bridge splayedness ratio $(S_2-S_1)/L$. It can be noticed that the points have almost a linear trend. For interior girders, increasing the splayedness ratio by 33% led to a 7.254% reduction in GDF value, while decreasing splayedness ratio by 33% also led to a 7.252% increase in the GDF value. For the exterior girders, increasing splayedness by 33% led to an 8.12% reduction in GDF value, while decreasing splayedness ratio by 33% led to a 6.93% increase in the GDF value.
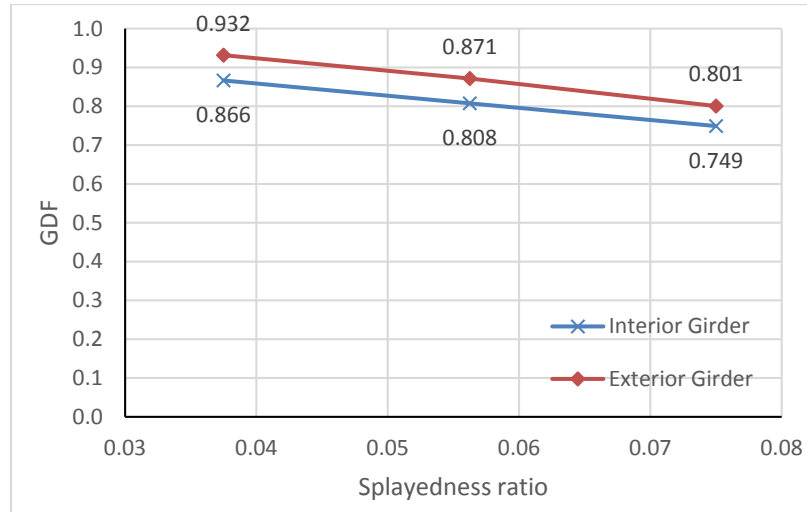
Figure 81: Flexure FEM GDF versus splayedness ratio

It can be concluded that increasing the splayedness ratio in a given bridge results in a reduction in the GDF values for both interior and exterior girders. This is because any changes in splayedness mean changes in the girder spacing, which is the most critical parameter in the distribution of live load to supporting girders. To compare the changes in girder spacing due to the changes in splayedness with the GDF values, an average value of the change in girder spacing at each truck axle position is needed. Because the front axle load represents only 10.8% of the truck's total weight, a weighted average of the changes in girder spacing at each axle is used. Therefore, increasing the splayedness ratio by 33% causes the girder spacing to decrease by 8.77% in bridge B3, while decreasing the splayedness ratio by 33% causes the girder spacing to increase by 9.25%. Figure 82 presents the change in GDF against the changes in girder spacing due to difference in splayedness. It shows an almost linear trend for the changes in both interior and exterior girders.
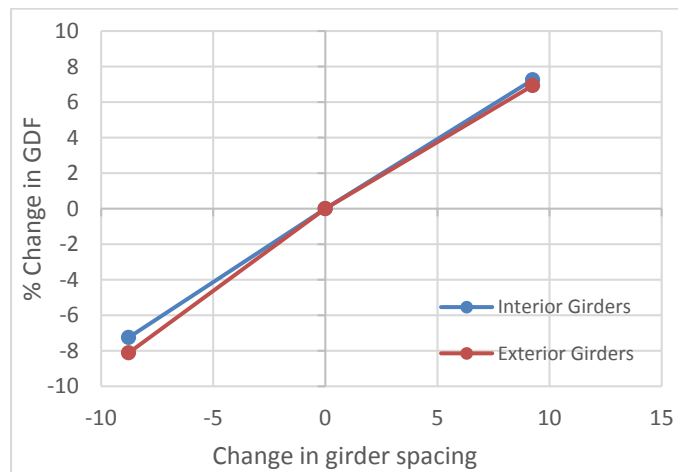
Figure 82: Girder spacing changes vs. flexure GDF changes due to splayedness

102

Figure 83 presents the GDF for bridges B1, B2, and B3 for interior and exterior girders computed using the Equivalent AASHTO LRFD GDF approach against the bridge splayedness $(S_2-S_1)/L$. It can be noted that the points have a linear trend for interior and exterior girders. For interior girders, increasing splayedness by 33% led to a 6.50% reduction in the GDF, while decreasing splayedness by 33% also led to a 6.70% increase in the GDF. For the exterior girders, increasing splayedness by 33% led to a 10.01% reduction in GDF value, while decreasing splayedness by 33% led to a 10.91% increase in the GDF value. In general, the results are comparable to the finite element findings in Figure 81.
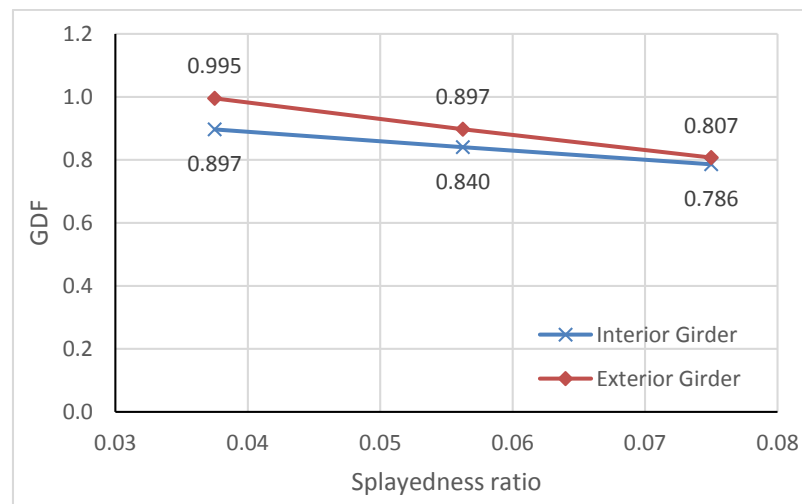

Figure 83: Flexure Equivalent GDF versus splayedness ratio

Figure 84 illustrates the GDF results for interior girders in bridges B1, B2, and B3 by both FE and AASHTO LRFD. It shows that the equivalent GDF for the three bridges is very close to the GDF from the finite element results, with some conservatism. The percentage difference between the results of the two methods is less than 5% for the considered bridges.
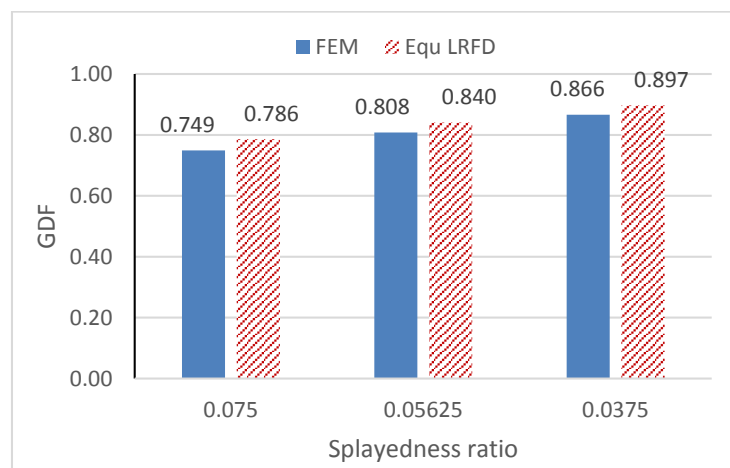
Figure 84: Interior flexure FEM GDF versus Equ GDF - B1, B2, B3

Figure 85 illustrates the GDF for exterior girders in bridges B1, B2, and B3 by finite element analysis and equivalent LRFD. The results are similar in nature to those for the interior girders.
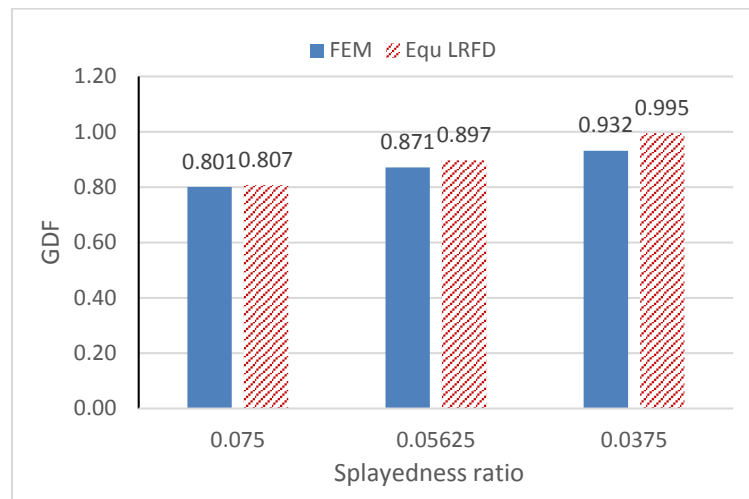
Figure 85: Exterior flexure FEM GDF versus Equ GDF - B1, B2, B3

5.2.1.2 Girder spacing ratio S_1/S_2 effect.

Figure 86 shows a plan view of bridges B1, B4, and B5 with their corresponding S_1/S_2 values, while the girder splayedness ratio $(S_2-S_1)/L$ is the same in all bridges and equals 0.05625. For the reference bridge, the S_1/S_2 ratio equals 0.5; in bridge B4 the ratio is decreased to 0.4 resulting a reduction in girder spacing equal to 750 mm at any section along the span, while in bridge B5 the ratio is increased to 0.5714 resulting in an increase in girder spacing equal to 750 mm at any section along the span. This means that the percentage change in girder spacing is not constant along the span of the considered bridges.
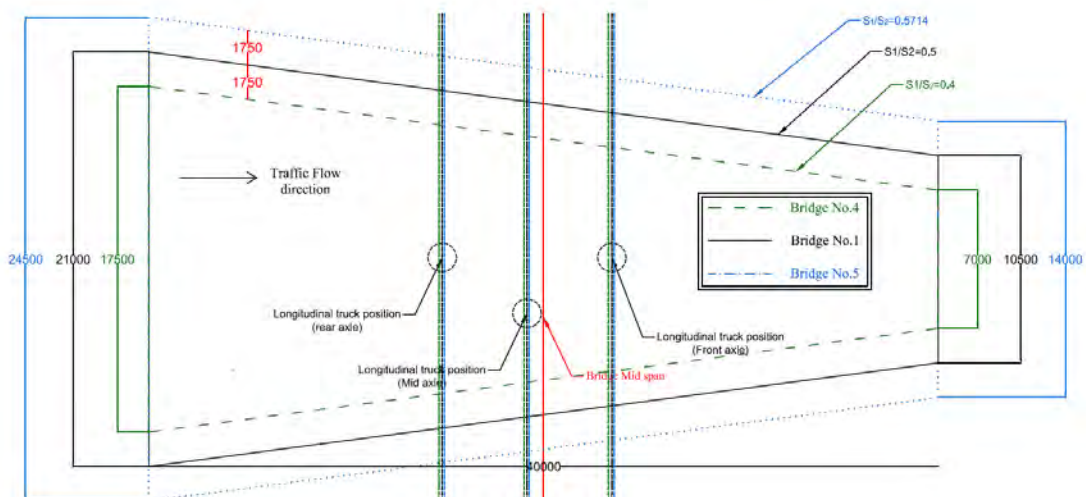
Figure 86: Bridges B1, B4, and B5 plan view - flexure

The percentage change in girder spacing is illustrated in Table 34 for each truck axle position in bridges B4 and B5, in relation to bridge B1.

Table 34: % Difference in girder spacing between bridges B1, B4, B5 - flexure

Bridges	Girder Spacing difference %			Notes
	Rear axle	Middle axle	Front axle	
B1 and B4	-20.5	-21.9	-23.6	decreased
B1 and B5	20.5	21.9	23.6	increased

Figure 87 illustrates the GDF for bridges B1, B4, and B5 in interior and exterior girders from the finite element analysis versus the girder spacing ratio S_1/S_2. It can be noticed for the interior girders that increasing the S_1/S_2 ratio by 14.3% leads to a 15.05% increase in the GDF value, while decreasing the S_1/S_2 ratio by 20% leads to a 16.39% reduction in the GDF value. For the exterior girders, increasing the S_1/S_2 ratio by 14.3% leads to a 15.17% growth in GDF value, while decreasing the S_1/S_2 ratio by 20% leads to a 17.41% reduction in the GDF value. Although the S_1/S_2 ratio increased by 14.3% and then decreased by 20%, they resulted in almost equal percentages of change in the GDF for the interior and exterior girders. This is because changing the S_1/S_2 ratio was based on changing the girder spacing of the reference bridge by the same value up and down in the development of bridges B4 and B5. The small difference between the percent growth and reduction of the GDF, whether in the interior or exterior girder, is caused by changing the truck longitudinal location among bridges B1, B4, and B5 in order to maximize the GDF for flexure.
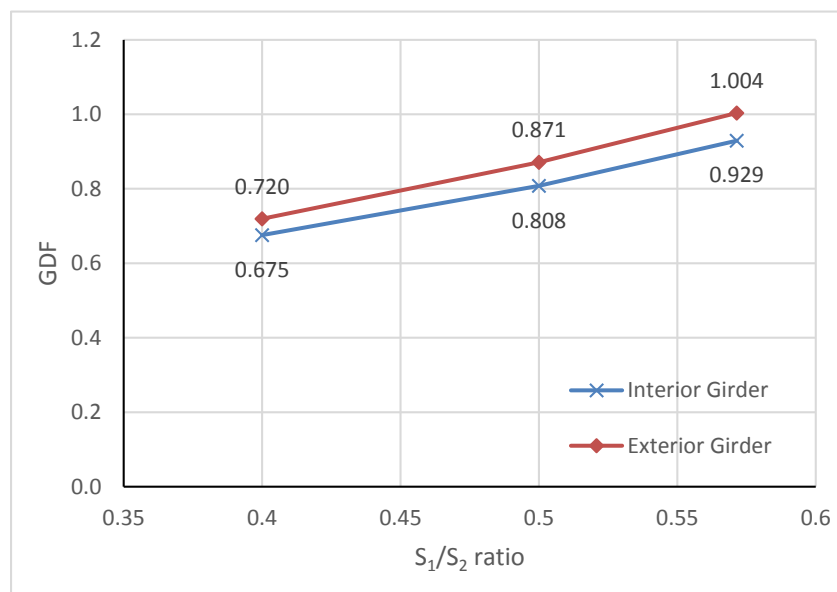
Figure 87: Flexure FEM GDF versus $S1/S2$ ratio

To compare the change in girder spacing due to the changes in the S_1/S_2 ratio with the GDF values, a weighted average of the change in girder spacing at each axle is used for comparison, similar to what was used in section 5.2.1.1. Using this approach, by increasing the S_1/S_2 ratio by 14.3%, the girder spacing increased by 21.44% in bridge B5, whereas decreasing the S_1/S_2 ratio by 20% caused the girder spacing to decrease by 21.44%. Figure 88 presents the change in GDF against the changes in equivalent girder spacing due to changes in the S_1/S_2 ratio. It shows a linear trend for the changes in both interior and exterior girders, and they almost overlap on each other, which means that the effect of changing the equivalent girder spacing due to the S_1/S_2 ratio changes is almost equal in both the interior and exterior girders.
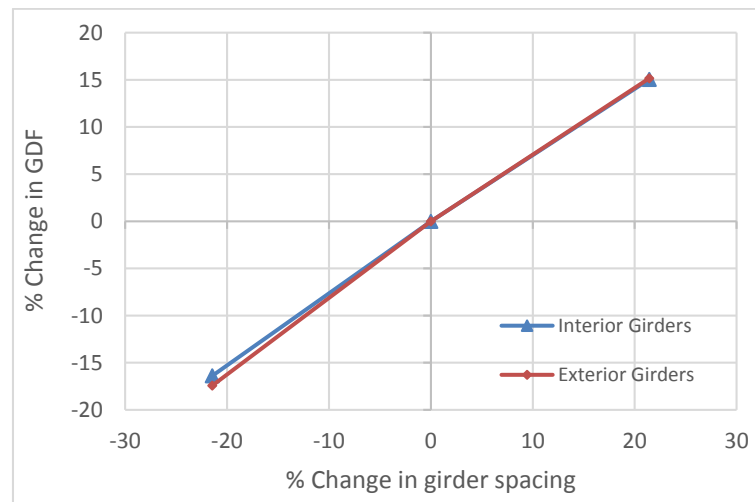
Figure 88: Girder spacing changes vs. GDF changes due to S_1/S_2 ratio - flexure

Figure 89 illustrates the equivalent AASHTO LRFD GDF for bridges B1, B4, and B5 for the critical interior and exterior girders computed against the S_1/S_2 ratio. For interior girders, the results show that increasing the S_1/S_2 ratio by 14.3% in bridge B5 leads to a 15.21% rise in GDF value, while decreasing the S_1/S_2 ratio by 20% in bridge B4 results in a 15.82% reduction in the GDF value, which is in line with the finite element results. For the exterior girder, increasing the S_1/S_2 ratio by 14.3% in bridge B5 leads to a 24.75% rise in GDF value, while decreasing the S_1/S_2 ratio by 20% in bridge B4 results in a 22.77% reduction in the GDF value. This shows that changes in the S_1/S_2 ratio impact the GDF in the exterior girder a little more than they affect exterior girders.
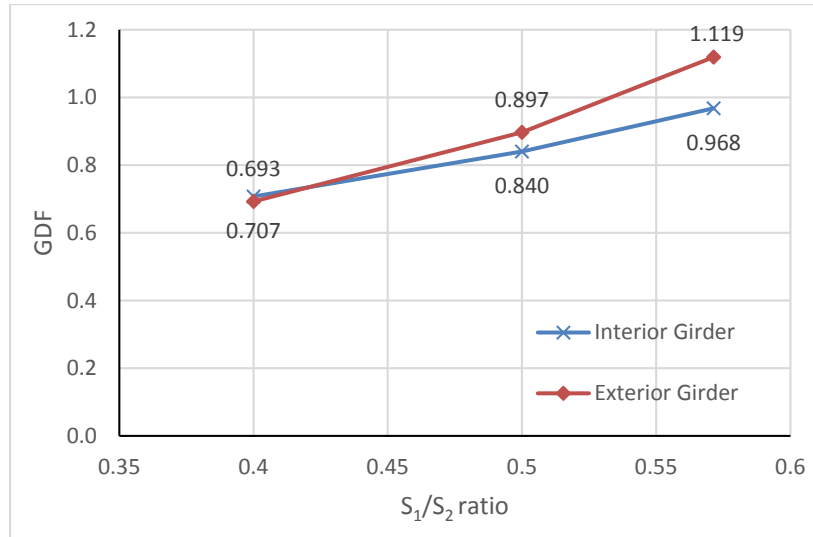
Figure 89: Flexure equivalent GDF versus S_1/S_2 ratio

Figure 90 illustrates the FEM and equivalent AASHTO GDF for interior girders in bridges B1, B4, and B5. The results show that the GDF values from the equivalent GDF approach in the three bridges are very close to the GDF values from the finite element analysis of the same bridges, but with a little conservatism. The percentage difference between the results of the two methods in all cases is less than 5%.
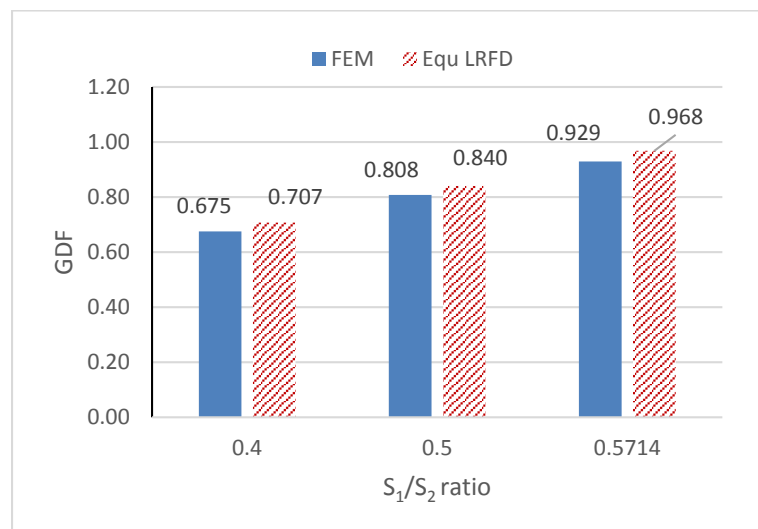
Figure 90: Interior flexure FEM GDF vs. Equ GDF - bridges B1, B4, B5

Figure 91 shows a comparison of the GDF values in bridges B1, B4, and B5 for the exterior girders. The results suggest that the equivalent AASHTO GDF values for the three bridges are close to the GDF from the finite element results. For the case of the S_1/S_2 ratio being equal to 0.4, the finite element results are higher than the equivalent GDF value by 3.71%. However, in the case of the S_1/S_2 ratio being equal to 0.5 and 0.5714, the simple AASHTO approach gave a slightly higher GDF value than FEM.
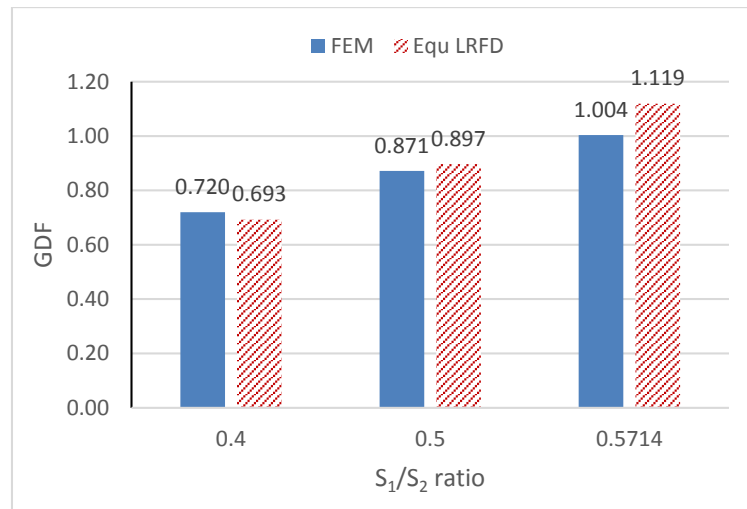
Figure 91: Exterior flexure FEM GDF vs. Equ GDF - bridges B1, B4, B5

It is known that the change in any splayedness parameters is a change in the girder spacing of the bridge, and any change that leads to increasing the girder spacing will result in an increase in the GDF in both the exterior and interior girder. Figure 92 shows the increase in equivalent GDF due to an increase in the average girder spacing ($S_{avg} = (S_1+S_2)/2$) for the four bridges analyzed above and the reference bridge. In all cases, the exterior girders are slightly more impacted by the increase in average girder spacing than the interior girders. Also, the equivalent AASHTO GDF approach is a good predictor of the live load distribution in the girder with some margin of safety compared to FEM.
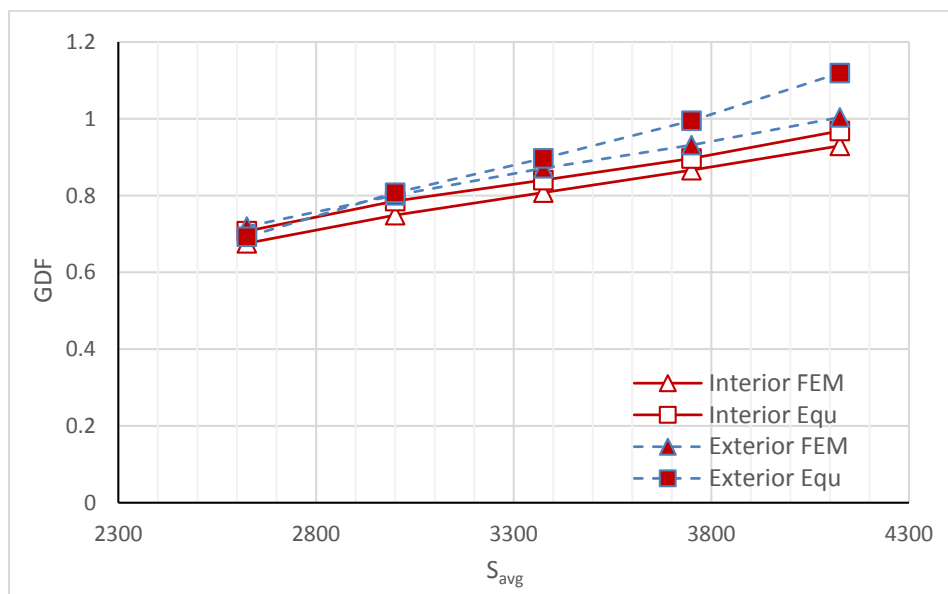
Figure 92: Flexure GDF versus average girder spacing

108

5.2.2 Effect of slab thickness.

The reference bridge B1 has a reinforced concrete deck slab thickness equal to 220 mm. By decreasing the thickness to 150 mm (31.8%) while keeping all other parameters constant, bridge B6 is developed. In contrast, by increasing it to 300 mm (36.4%) while keeping the other parameters constant, bridge B7 is obtained.

Figure 93 shows the GDF for the interior and exterior girders computed from the finite element results versus the slab thickness for bridges B1, B6, and B7. For the interior girders, it's clear that by increasing the slab thickness by 36.4% the GDF drops by 5.12%, and decreasing it further by 31.8% results in a further 6.67% reduction in the GDF value. This is because decreasing the slab thickness leads to a drop in the stiffness of the member that receives the load and transfers it to the supporting girders. This results in less sharing of the live load, which leads to higher GDF as in bridge B6, while in contrast more load sharing leads to a lower GDF as in bridge B7. The exterior girder did not act in a similar way, where increasing the slab thickness by 36.4% results in just a 0.98% drop in GDF, and reducing the slab thickness by 31.8% caused just a 1.15% reduction in the GDF. The reason why the GDF of the exterior girders was not affected much by the slab thickness is because the load on such elements is mainly coming from one truck placed mostly in the overhang or just above the girder. The system is equivalent to a statically-determinate element where slab thickness is irrelevant.
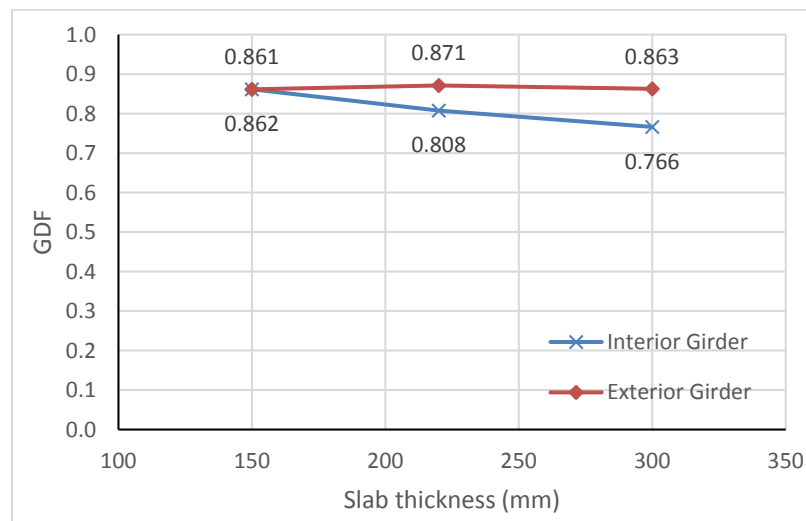
Figure 93: Flexure FEM GDF versus Slab thickness

Figure 94 shows the GDF for bridges B1, B6, and B7 for interior and exterior girder calculated using the Equivalent AASHTO LRFD GDF approach versus the slab thickness. In interior girders, a reduction of 31.8% in slab thickness results in a 10.5%

increase in the GDF, whereas an increase of 36.4% leads to a 7.6 % reduction in the GDF. In exterior girders, reducing the slab thickness by 31.8% increases the GDF by 10.47%, and increasing it by 36.4% decreases the GDF by 7.58%. It can be noticed that the equivalent GDF in the exterior girders has the same pattern as that in the interior girders. This is because the GDF is based on the AASHTO LRFD formulas where the exterior GDF is a product of the interior girder GDF and a factor related only to the overhang distance which remains constant in bridges B6 and B7.
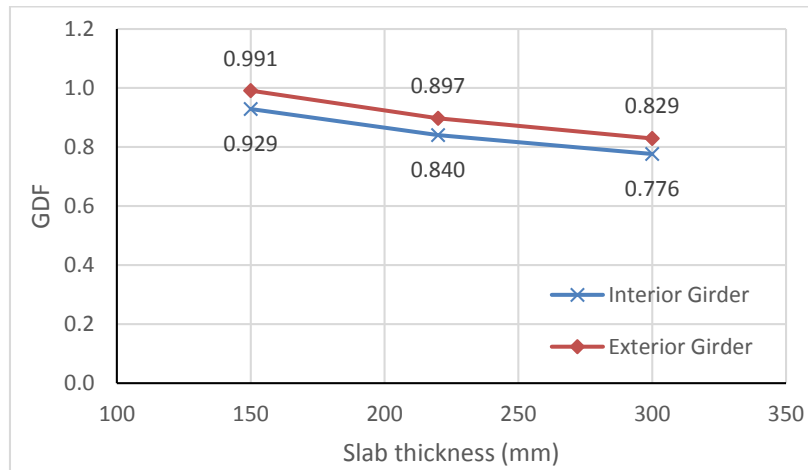
Figure 94: Flexure Equivalent GDF versus slab thickness

Figure 95 summarizes the GDF for interior girders in bridges B1, B6, and B7, where it appears that the GDF values computed using the equivalent GDF approach are close and a little conservative compared to the GDF values resulting from the finite element analysis. The percentage difference between the results of the two methods is 4.03%, 7.79%, and 1.30% for bridges B1, B6, and B7, respectively.
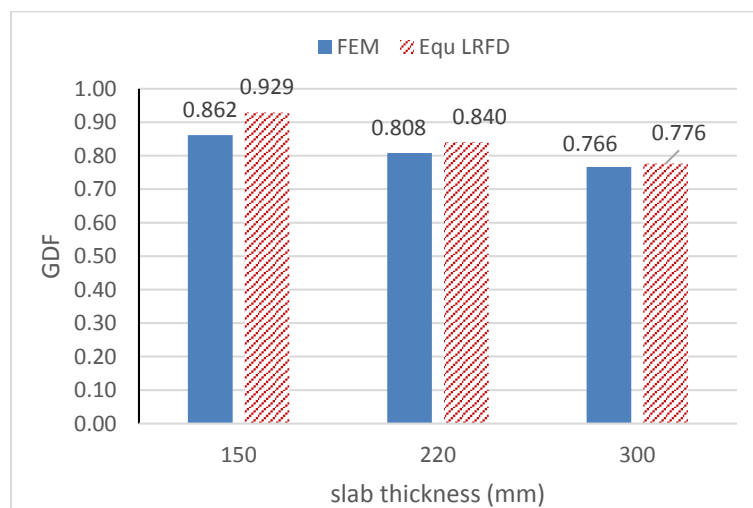
Figure 95: Interior FEM GDF vs. Equ GDF - bridges B1, B6, B7

Figure 96 presents a summary of the GDF for the exterior girders in bridges B1, B6, and B7 that have different slab thicknesses. The results show that the reference bridge's equivalent GDF is slightly conservative by 2.96% compared with the finite element results. For bridge B6 with a thin slab, the equivalent GDF is higher than the finite element results by 15.07%. In contrast, a thicker slab as in bridge B7 results in a 3.90% lower equivalent GDF compared to the one calculated from finite element results and this is because the AASHTO LRFD formulas for the exterior girder do not account for the rigid body rotation effect since the considered bridge has cross-bracing only at the supports. It should be noted that most bridges have slab thicknesses in the 180 – 250 mm range. Hence, the equivalent AASHTO GDF for the exterior girder will be close, with some conservatism with the FE findings.
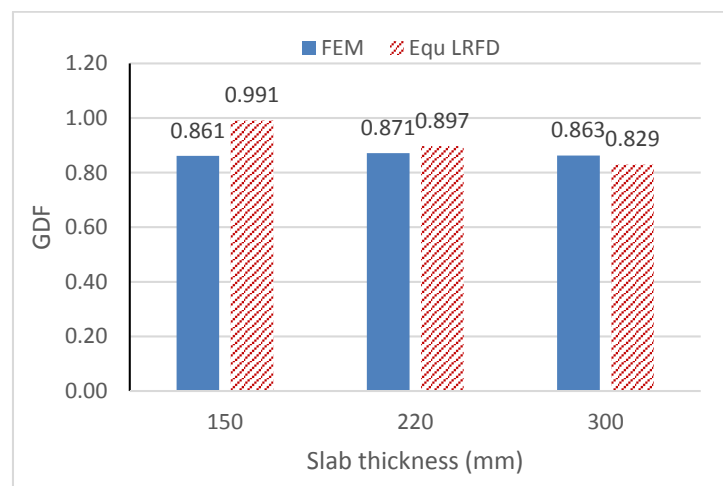
Figure 96: Exterior FEM GDF vs. Equ GDF - bridges B1, B6, B7

In conclusion, changing the slab thickness in splayed girder bridges affects interior girders more than exterior girders. The interior girder results are close with some conservatism in the equivalent AASHTO GDF. Compared with the finite element results, a conservative value for the equivalent GDF is obtained in a thin slab (B6), while a slightly lower GDF using the same approach is caused by a thick slab (B7).

5.2.3   Effect of cross-bracing presence and spacing.

As the AASHTO LRFD formulas used to calculate the GDF are designed based on bridge models without accounting for diaphragms or cross-bracings [46], the reference bridge in this study is assumed to have cross-bracing only at the ends of the bridge (40 m). However, two other bridges with different cross-bracing spacings are developed to address the cross-bracing effect on splayed girder bridges. Bridge B8 has

a cross-bracing spacing equal to 5 m, and bridge B9 has a cross-bracing spacing equal to 10 m. Figure 97 shows the change in GDF due to the movement of two trucks in adjacent lanes in the transverse direction for the case of cross-bracing only at the supported ends (reference bridge B1), and the case of using cross-bracing at spacing equal to 5 m (B8). It should be noted that the size and shape of the cross bracing have little effect on live load distribution; however, spacing is most important. The cross-bracing used in this study is described back in Section 4.2 and Figure 28.
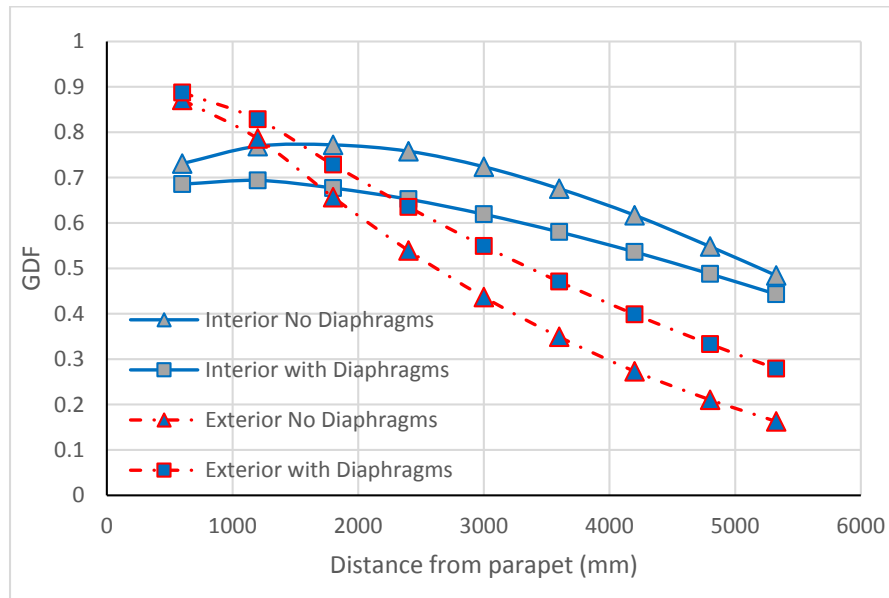
Figure 97: GDF versus distance from parapet bridges B1 and B8 - 2 trucks

It is clear that the GDF values in the interior girder without cross-bracing (B1) are higher than the GDF when using cross-bracing in B8 at a 5m spacing. In contrast, the presence of cross-bracing in B8 resulted in higher GDF values in exterior girders than the ones resulting from the same bridge with no cross-bracing (B1). Adding cross-bracing to a bridge results in a more uniform deflection across all girders, resulting in more load distribution among the interior girders and less GDF in the interior girders as a result. But increasing the rigidity of the cross-section with the addition of cross-bracing increases the effect of rigid body rotation in the exterior girder where a single girder is placed on the overhang, away from the center line of the bridge, which results in a higher GDF in the exterior girders.

Figure 98 illustrates the GDF values for bridges B1, B8, and B9 for the interior and exterior girders. It demonstrates that for the interior girders, adding cross-bracing affects the GDF values, although the spacing of the cross-bracing is not a significant aspect. Adding intermediate cross-bracing to the reference bridge negligibly affects the

GDF of the exterior girder by less than 2%. This behavior is a result of increasing the bridge's cross-section rigidity, which allows more load sharing in the interior girders, thus leading to lower GDF values. The rigid body rotation of a splayed girder does not occur as much in splayed girder bridges as it does in parallel girder bridges due to the resistance of the flared girders against superstructure twisting.
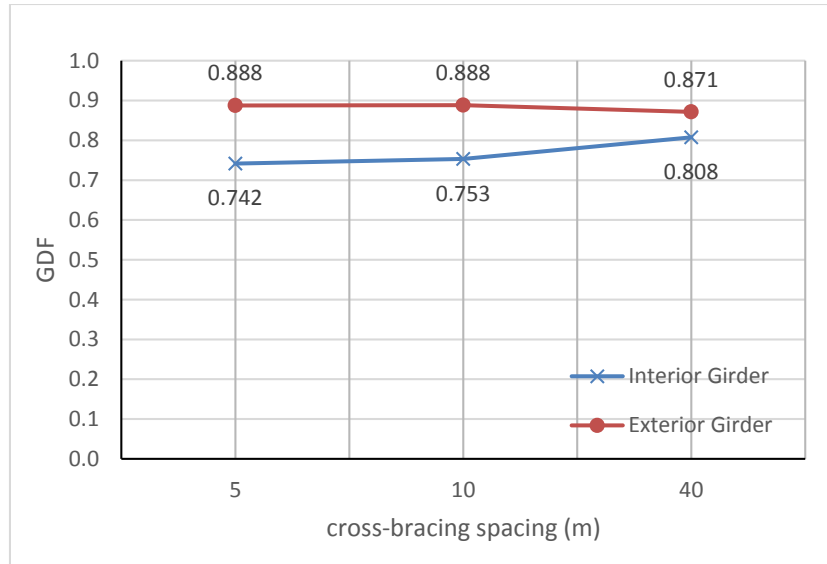
Figure 98: FEM GDF versus cross-bracing spacing

AASHTO LRFD formulas do not account for the presence of cross-bracing. Therefore, the equivalent GDF values for the interior or exterior girders are equal for bridges with or without cross-bracing, where the equivalent GDF for the interior girders equals 0.840, and the equivalent GDF for the exterior girders equals 0.897. It should be noted that AASHTO LRFD requires exterior girders to be checked for rigid body rotation if cross-bracing is present.

Figure 99 compares the equivalent AASHTO LRFD GDF in the interior girders in bridges B1, B8, and B9 with the finite element results. It shows that with or without cross-bracing, the GDF values from the equivalent GDF approach are a little conservative compared with the finite element results. The percentage difference between the results of the two methods is 4.03%, 13.32%, and 11.54% for bridges B1, B8, and B9, respectively. This shows that the AASHTO GDF values at the axle locations can be conservatively used to design splayed girder bridges with or without diaphragms.

113
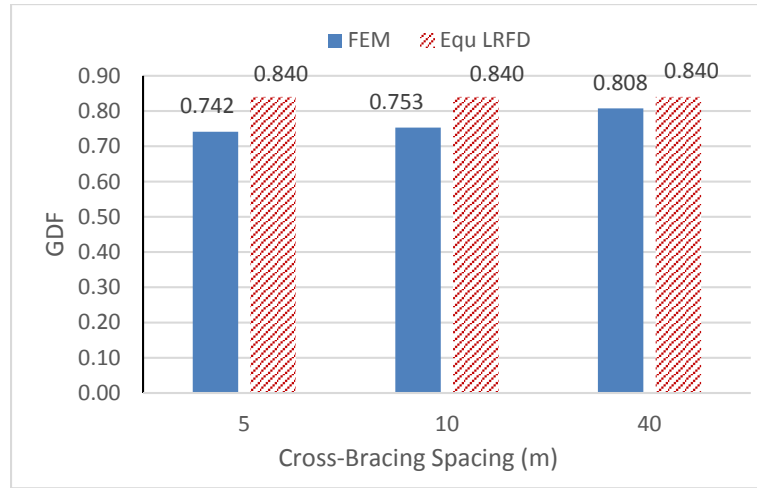
Figure 99: Interior flexure FEM GDF vs. Equ GDF - bridges B1, B8, B9

Figure 100 displays the GDF in the exterior girders in bridges B1, B8, and B9. Because adding cross-bracing results slightly increase the GDF value as discussed above, the gap between the equivalent AASHTO GDF value and the GDF from finite elements decreases. The percentage difference between the results of the two methods is 2.96%, 1.08%, and 1% for bridges B1, B8, and B9, respectively.

Figure 100: Exterior flexure FEM GDF vs. Equ GDF - bridges B1, B8, B9

It can be concluded that adding cross-bracing to a splayed girder bridge will affect the GDF values, for the interior girders, by reducing them. The corresponding difference in GDF for the exterior girder is negligibly small.

5.2.4 Effect of number of girders.

The reference bridge (B1) consists of 5 girders. By reducing the number of girders to 3 while keeping all parameters including the girder spacing constant, bridge

B10 is developed. Likewise, by increasing the number of girders to 7, bridge B11 is produced.

Figure 101 shows the difference between the GDF results from the finite element analysis of bridges B1, B10, and B11 for the interior and exterior girders due to a change in the number of girders. It is clear that reducing or increasing the number of girders in the reference bridge by two girders affects mostly the exterior girders. For the interior girders, reducing the number of girders to 3 increases the GDF by 1.07%, while increasing it to 7 reduces the GDF by 1.44%. In exterior girders, reducing the number of girders to 3 resulted an increase of 1.93% in the GDF value, but increasing the number of girders to 7 reduced the GDF in the same girders by 6.78%.
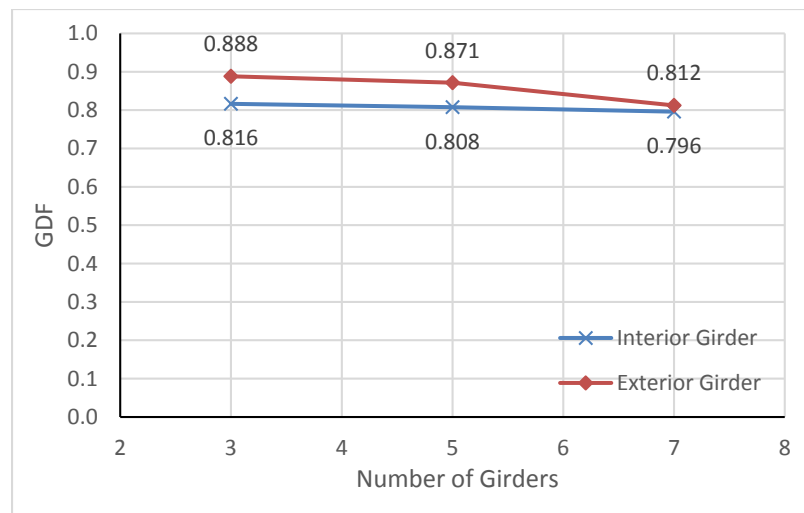
Figure 101: Flexure FEM GDF versus cross-bracing spacing

AASHTO LRFD formulas do not consider the number of girders explicitly in a bridge, but it suggests using the lever rule if the number of girders is 3, as in bridge B10. However, for consistency the equivalent GDF is used for all bridges in the study, even for the one with three girders, which results in an equal equivalent GDF in all three bridges with different numbers of girders. The results gave for interior girders an equivalent GDF equals 0.840, and for exterior girders the equivalent GDF equals 0.897.

Figure 102 shows the equivalent GDF for interior girders in bridges B1, B10, and B11 versus the finite element results. It shows that the number of girders does not affect the results by much, and the equivalent GDF values are a little bit conservative compared with the finite element ones. The percentage difference between the results of the two methods are 4.03%, 2.93%, and 5.55% for bridges B1, B10, and B11, respectively.
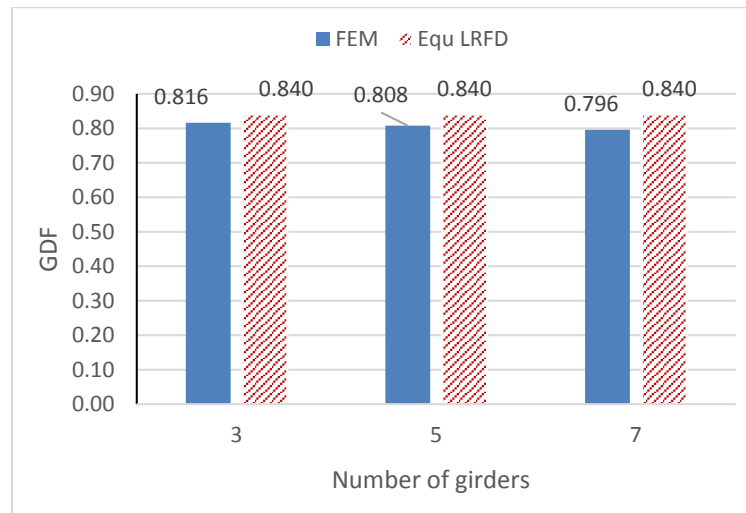
Figure 102: Interior flexure FEM GDF vs. Equ GDF - bridges B1, B10, B11

Figure 103 illustrates the equivalent GDF for the exterior girders in bridges B1, B10, and B11 against the finite element results. Once again, the equivalent GDF by AASHTO yields close values with some conservativeness compared to the finite element results. However, as the number of girders in the bridge increases, the results of the equivalent GDF become more conservative. The percentage difference between the results of the two methods are 2.96%, 1.00%, and 10.44% for bridges B1, B10, and B11, respectively.
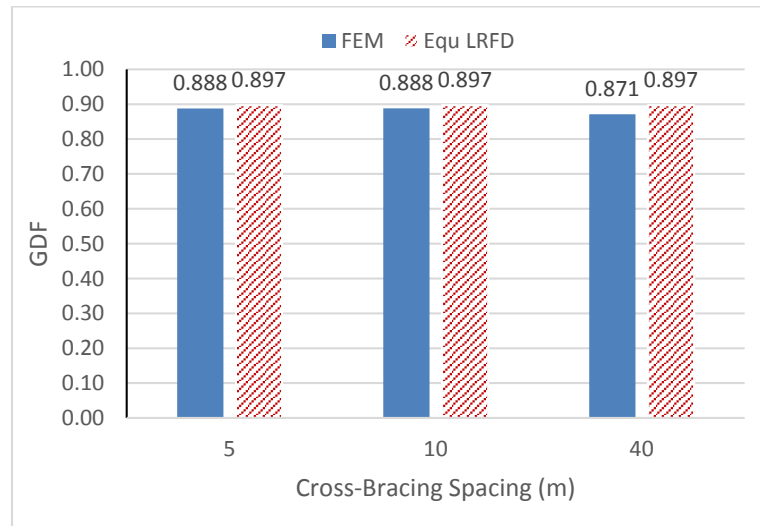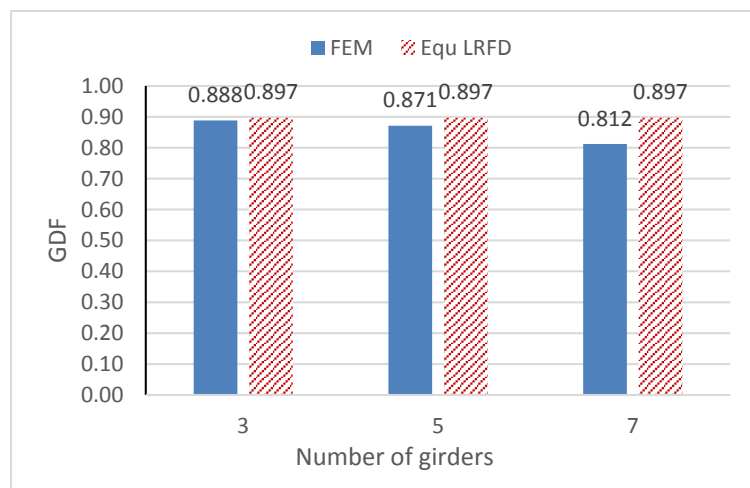

Figure 103: Exterior flexure FEM GDF vs. Equ GDF - bridges B1, B10, B11

It can be concluded that the number of girders in a splayed girder bridge is not a critical parameter that affects its behavior in flexure. Further, using the equivalent AASHTO GDF approach to find the GDF values for the interior or exterior girders gives good and somewhat conservative results compared with the finite element ones. However, the AASHTO LRFD specification does not allow the use of GDF formulas to compute interior or exterior GDF value for a bridge with only three girders as in

bridge B10. Instead it suggests using the lever rule to calculate it in both interior and exterior girders. But compared to the finite element results of bridge B10, the equivalent GDF value gives close results that are higher than the finite element values by 2.93% for interior girders and 1.00% for exterior girders. On the other hand, using the lever rule to compute an equivalent GDF resulted in much higher values, where in interior girders the GDF value was equal to 1.14 which is 40% more conservative, and in exterior girders the GDF value was equal to 1.045 which is 18% more conservative than the corresponding finite element results. The AASHTO LRFD requires using the lever rule in the case of three girders because it gives more conservative results for less redundant bridges, where failure in one of the girders is very critical and can cause failure of the entire bridge.

5.2.5   Effect of girder stiffness.

The girder stiffness was varied in the study by changing the depth of the steel girder web within the bridge. In the reference bridge (B1) the girder depth is 1700 mm. By reducing the girder depth by 17.65%, bridge B12 is developed with 1400 mm girder depth. By increasing the girder depth by the same percentage, bridge B13 is produced with 2000 mm girder depth. Note that the girder stiffness in AASHTO is considered through the K_g parameter in the GDF where K_g is the longitudinal stiffness factor.

Figure 104 presents the GDF values for bridges B1, B12, and B13 versus the steel girder depth. It can be noticed that in the interior girders the GDF values slightly increase by 1.71% when increasing the girder depth by 17.65% in bridge B13, while decreasing the girder depth by the same percentage in bridge B12 results in a small drop of 2.12% in the GDF value. On the other hand, reducing or increasing the girder depth by 300 mm negligibly affects the GDF in the exterior girders.
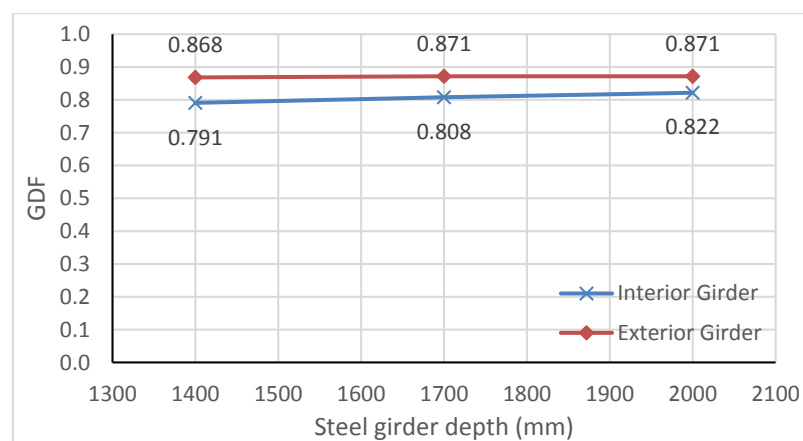
Figure 104: Flexure FEM GDF versus steel girder depth

117

Figure 105 illustrates the equivalent AASHTO GDF values for bridges B1, B12, and B13 against the steel girder depth. It shows that the equivalent GDF values have the exact same trend in the interior and exterior girders. For both the interior and exterior girders, reducing the girder depth in bridge B1 by 17.65% leads to a 3.65% increase in GDF, while increasing the girder depth by the same percentage reduces the GDF by 3.31%. This duplicate behavior in the interior and exterior girders is a result of computing these equivalent GDFs based on the AASHTO LRFD formulas that present the exterior GDF as a product of multiplying the interior GDF value by a factor relating only to the overhang distance. Despite increasing and decreasing the girder depth by the same percentage (17.65%), the percentage difference in the equivalent GDF varies between 3.65% and 3.31% in both the interior and exterior girders, respectively. This slight difference developed because changing the girder depth changes the longitudinal stiffness parameter K_g used in the AASHTO LRFD formulas. By reducing the girder depth in this study by 17.65%, a 33.80% reduction in K_g is obtained, while increasing the girder depth by the same percentage resulted in an increase of 43.44% in K_g.
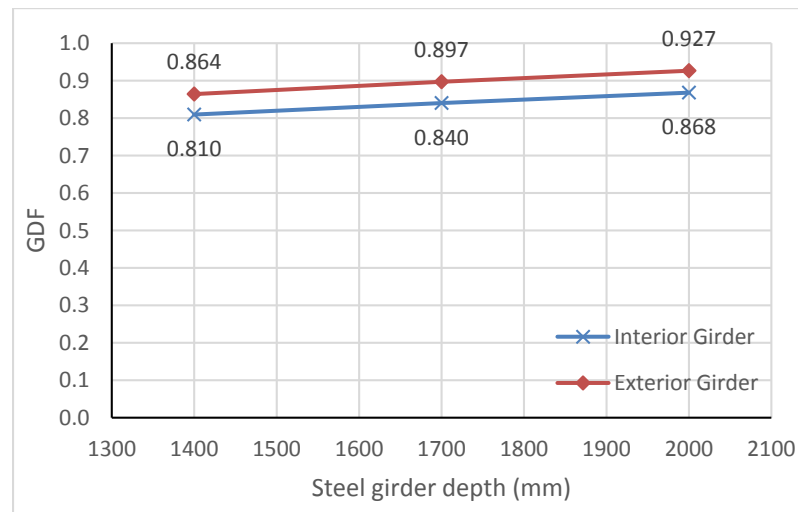
Figure 105: Flexure Equivalent GDF versus girder depth

Figure 106 presents the computed equivalent AASHTO GDF in the interior girders in bridges B1, B12, and B13 versus the finite element results. It shows that the equivalent GDF values are slightly higher than the ones computed from finite element models; thus, the simple procedure is a good predictor of live load distribution. Also, it demonstrates that the GDF computed using the approximate approach has the same trend as the GDF values computed from the finite element models. The percentage difference between the results of the two methods is 4.03%, 2.41%, and 5.67% for bridges B1, B12, and B13 respectively.
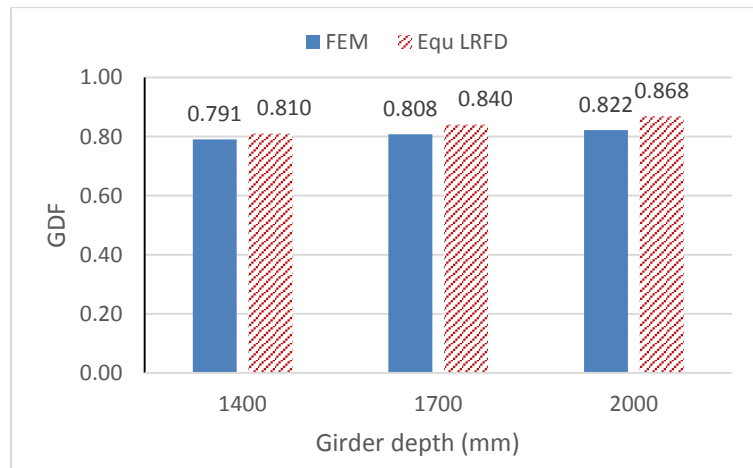
Figure 106: Interior flexure FEM GDF vs. Equ GDF - bridges B1, B12, B13

Figure 107 compares the equivalent AASHTO GDF values for the exterior girders in bridges B1, B12, and B13 with the GDF values from finite element analysis. It's obvious that the results of the two methods are very close. However, as explained above the finite element results did not change by much for the exterior girders, while the equivalent GDF values went up a little with an increase in girder depth. Therefore, in bridge B12 the finite element result was higher than the one computed using the equivalent GDF by 0.45%, while in bridge 13 the equivalent GDF value was more conservative by 6.35%.
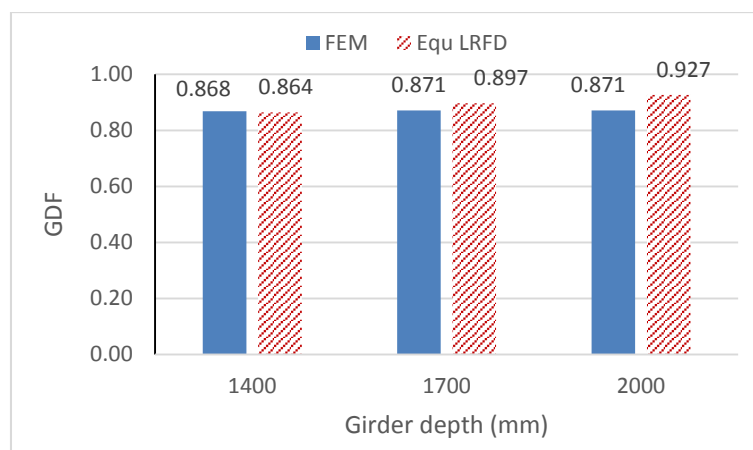
Figure 107: Exterior flexure FEM GDF versus Equ GDF - bridges B1, B12, B13

Based on the previous analysis, it can be concluded that changing the cross-section stiffness in a splayed girder bridge by changing the girder depth slightly affects the GDF values. Increasing the girder depth results in an increase in the GDF values in both the interior and exterior girders. However, when comparing the finite element results with the equivalent AASHTO GDF approach, the equivalent GDF for the interior girders gave closer results than the ones for the exterior girders. Besides that, a

reasonable conservatism was recorded in the interior and exterior girders' equivalent GDF.

5.2.6 Effect of span length.

Figure 108 presents the plan view of bridges B1, B14, and B15 with the corresponding span lengths. The reference bridge span length is 40 m. Bridge B14 is 25% shorter and bridge B15 is 25% longer. Although changing the bridges' span length affects splayedness of the bridge and consequently the girder spacing, at the truck axle positions the maximum change in the girder spacing recorder is 2.5% which is small when considering the effect of span length on splayed girder bridges.
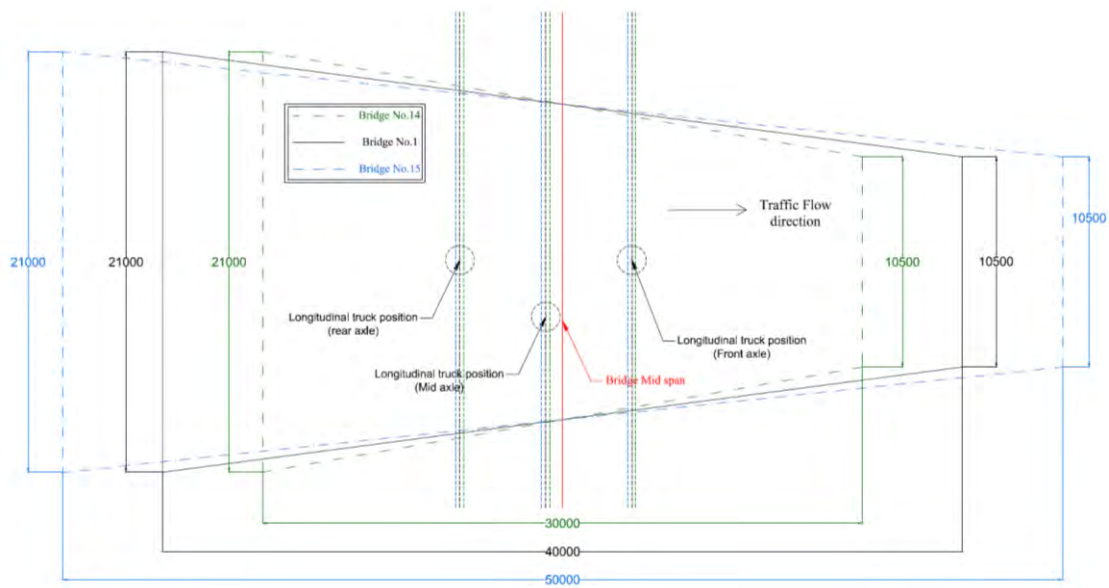
Figure 108: Bridges B1, B14, and B15 plan view - flexure

Figure 109 illustrates the GDF for bridges B1, B14, and B15 in the interior and exterior girders resulting from the finite element analysis versus the span length. It can be noticed that in the interior girders, reducing the span length by 25% leads to a 5.69% growth in the GDF value, while increasing the span length by 25% results in a 4.26% drop in the GDF value. The finite element results showed that the exterior girders did not act in the same manner. In this case, decreasing the span length by 25% results in a 1.77% reduction in the exterior girder GDF value, while increasing the span length by the same percentage leads to a reduction of less than 0.5% in the GDF value. This means that the interior girders' GDF decreases with increasing the span length, but the exterior girder does not change significantly by changing the span length.
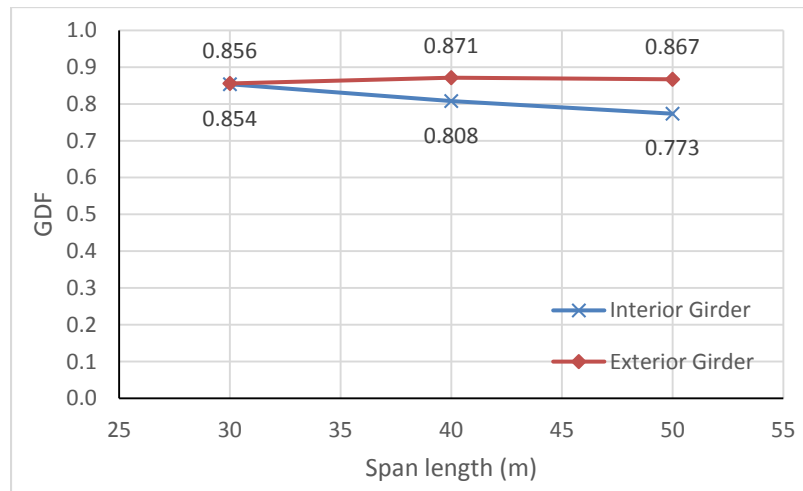
Figure 109: Flexure FEM GDF versus span length

Figure 110 presents the equivalent AASHTO GDF values for bridges B1, B14, and B15 against the span length. It shows that the equivalent AASHTO GDF values in the interior and exterior girders have the same trend. For the interior girder, reducing the span length by 25% increases the equivalent GDF by 8.62%, while increasing the span length by the same percentage leads to a 6.18% drop in the equivalent GDF value. For exterior girders, reducing the span length by 25% results in an 8.38% increase in the equivalent GDF value, and an increase in span length by the same percentage results in a drop in the equivalent GDF by 6.05%. This similar behavior of interior and exterior girders is as explained before due to the fact that the exterior GDF in AASHTO is a product of the interior GDF with a parameter related to the overhang.
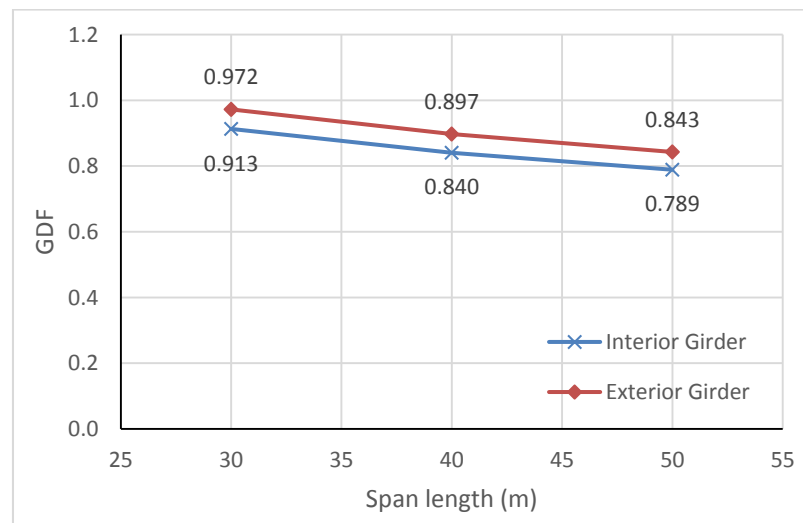
Figure 110: Flexure Equivalent GDF versus span length

Figure 111 shows the computed equivalent AASHTO GDF in the interior girders in bridges B1, B14, and B15 versus the finite element GDF. It shows that the

121

equivalent GDF values are slightly higher than the ones computed from finite element analysis, which is acceptable in practice. Also, it clarifies that the GDF computed using the equivalent approach has the same trend as the values from the finite element models. The percentage difference between the results of the two methods is 4.03%, 6.92%, and 2% for bridges B1, B14, and B15, respectively.
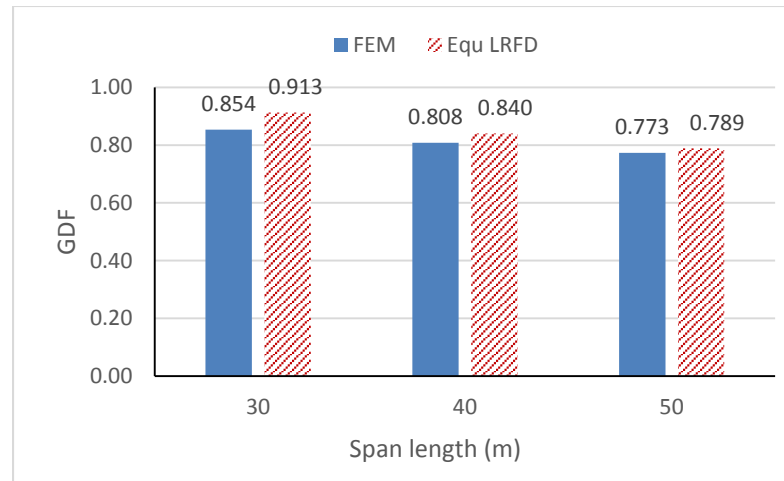
Figure 111: Interior flexure FEM GDF vs. Equ GDF - bridges B1, B14, B15

Figure 112 compares the equivalent exterior GDF values for bridges B1, B14, and B15 with the finite element exterior GDF. It's obvious that the results of the two methods are very close. In bridge B15 the finite element results were higher than the equivalent GDF by 2.81%, and in bridge B14 the equivalent GDF value was higher by 13.59%.
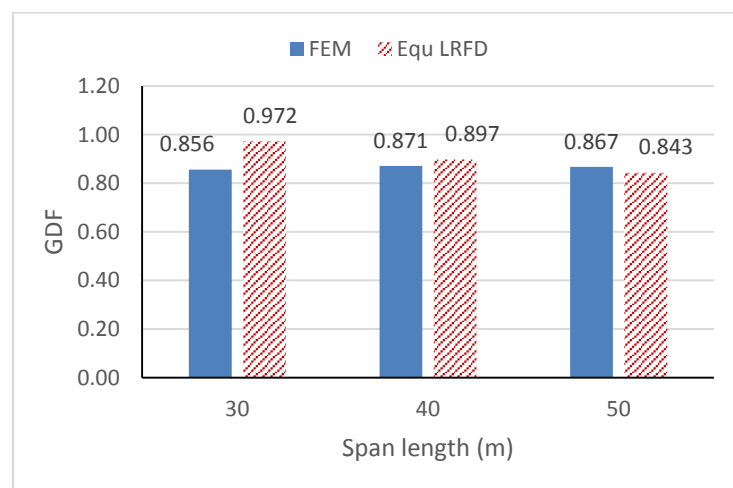
Figure 112: Exterior flexure FEM GDF vs. Equ GDF - bridges B1, B14, B15

5.2.7   Summary.

Previous results showed that for all of the fifteen bridges analyzed for flexure, the equivalent GDF based on the AASHTOL LRFD expressions for flexure were very

close to the GDF values obtained from the finite element analysis, for both interior and exterior girders. Figure 113 compares both methods for interior and exterior girders. There are very few cases in which that the equivalent AASHTO GDF slightly underestimates the GDF values obtained from the finite element analysis. For all practical purposes, equivalent GDF based on the AASHTO LRFD specifications is a good approach for analyzing splayed girders in flexure.
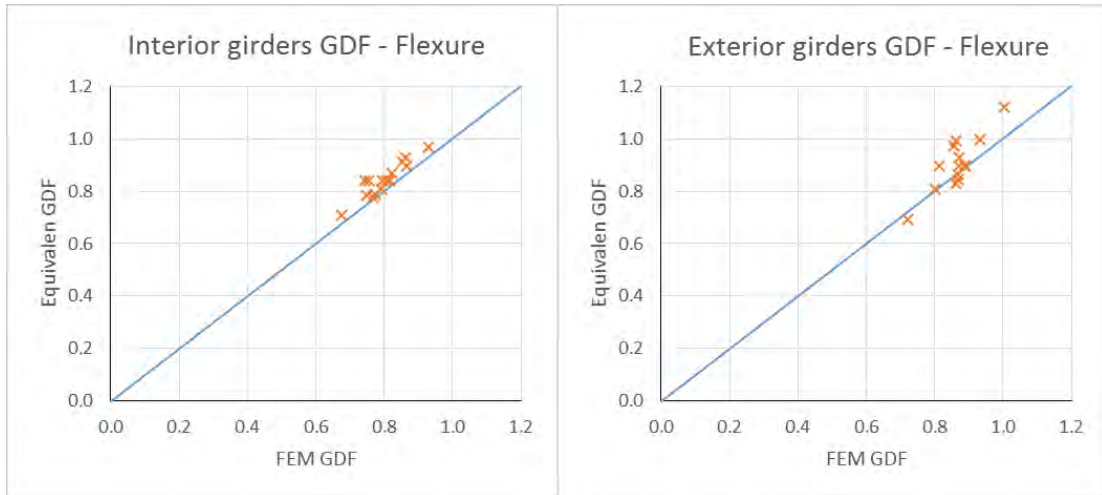
Figure 113: Summary of all flexure GDF results

5.3 Shear Effect

The reference bridge (B1) was presented and studied in depth under the effect of shear back in Sections 4.4.2 and 4.4.3.2 using FEM and the Equivalent GDF approach, respectively. It was observed that computing the GDF using the AASHTO LRFD formulas for shear gives 5.12% lower GDF values in interior girders compared with the GDF value resulting from the FE analysis, while in exterior girders it gives 18.08% more conservative results. Consequently, the lever rule was suggested to be used in computing the equivalent GDF, and by applying it on the reference bridge it gave more promising results, where for interior girders there was no difference in GDF value compared with FE results, and in the exterior girders the GDF value was only 6.46% more conservative. Therefore, in this parametric study both methods are applied to all the considered splayed girder bridges to study shear effect in splayed girder bridges, and to choose the more adequate method for calculating the equivalent GDF. Bridge B1 is the benchmark for all considered bridges, and to prove that the Equivalent GDF approach gives accurate results, the final aim of this section is to compare all GDF

results from FEM with the ones resulting from the Equivalent AASHTO GDF approach for the same bridges.

5.3.1 Effect of girder spacing.

Girder spacing is the most critical parameter in distribution of live load for both flexure and shear. Therefore, just as explained for the flexural effect back in Section 5.2.1, the same two aspects $(S_2-S_1)/L$ and S_1/S_2 ratio are considered in studying the effect of splayed girders on shear. Hence, the same four bridges (B2, B3, B4, and B5) that were studied for flexure are studied again for shear.

5.3.1.1 Splayedness ratio $(S_2-S_1)/L$ effect.

Figure 114 presents a plan view of bridges B1, B2, and B3 with the corresponding $(S_2-S_1)/L$ values, together with the truck position to maximize the shear effect. Changing the splayedness ratio $(S_2-S_1)/L$ results in changes in bridge width along the span length, and consequently changes in the corresponding girder spacing. However, because the longitudinal position of the trucks(s) to maximize shear effect is at the wide end of the bridge, changes in girder spacing are not significant if the maximum girder spacing is considered. Therefore, at the rear axle position as shown in Figure 114 there is no change in girder spacing due to changes in the splayedness ratio between bridges B1, B2, and B3. Furthermore, there are only $\pm 2\%$ and $\pm 4\%$ changes in the girder spacing at the location of the middle and front axles, respectively.
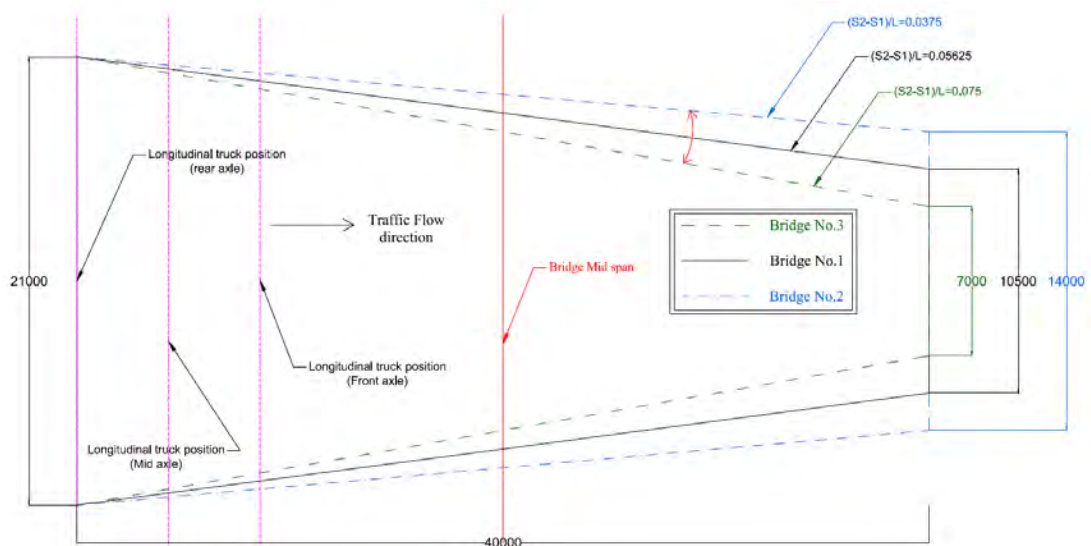
Figure 114: Bridges B1, B2, and B3 plan view - Shear

124

Figure 115 presents the shear GDF for bridges B1, B2, and B3 in the interior and exterior girders computed from the FE analysis versus the bridge splayedness ratio. It can be observed that there are almost no changes in the GDF values in both the interior and exterior girders for the three bridges. However, the slight change in GDF values tends to be descending when increasing the splayedness ratio, and this is because of the very small decrease in girder spacing at truck axles when increasing the splayedness ratio.
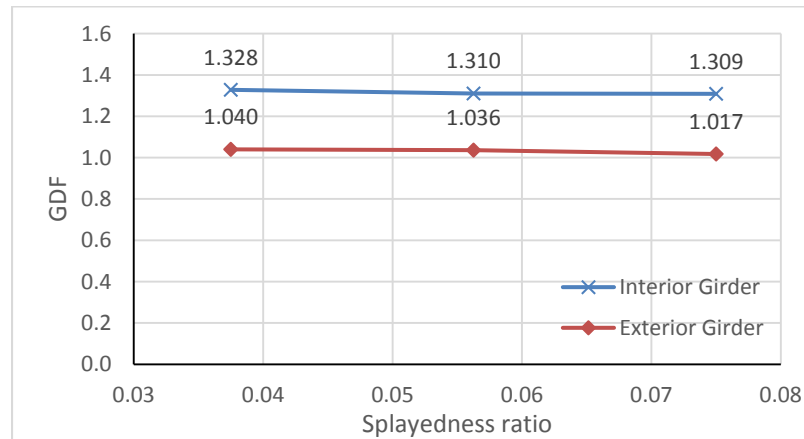
Figure 115: Shear FEM GDF versus splayedness ratio

Figure 116 shows the shear AASHTO equivalent GDF for bridges B1, B2, and B3 in interior and exterior girders, once using the lever rule and another time using LRFD procedures, versus the bridge splayedness ratio. It is obvious that both methods have the same trend as FE analysis, where by increasing the splayedness ratio there is a small drop in the shear GDF. The reduction percentage in the LRFD equivalent GDF does not exceed 1.3%, and in the lever rule equivalent GDF it is less than 0.7%. However, it can be noticed that the LRFD equivalent GDF in the interior and exterior girder are almost the same, which is a result of the chosen geometry (girder spacing, overhang width) of the bridges considered.
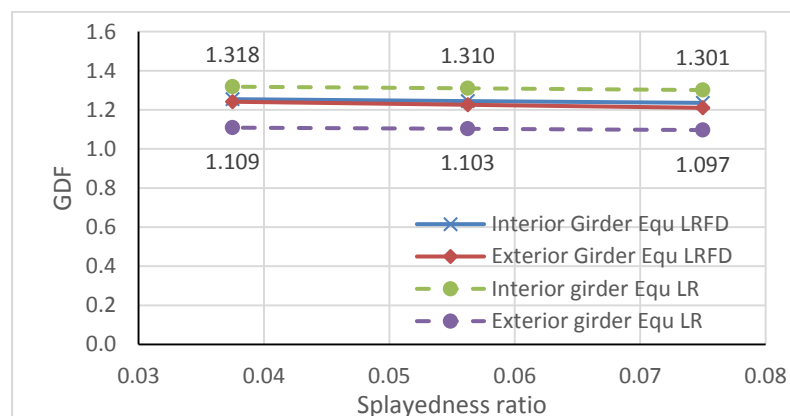
Figure 116: Shear Equivalent GDF versus splayedness ratio

125

Figure 117 presents the difference in shear GDF between the FE results and the two equivalent GDFs proposed for the interior girders in bridges B1, B2, and B3. It shows that the LRFD equivalent GDF are lower than the FE results by 5.12%, 5.64%, and 5.79% in bridges B1, B2, and B3, respectively. The lever rule equivalent GDF is closer to the FE results, but still are either equal or slightly smaller than the FE results by 0.77% and 0.6% in bridges B2 and B3, respectively. The GDF values from all three methods give the same trend, where by increasing the splayedness ratio, the girder spacing is a little reduced and therefore the GDF values slightly drop.
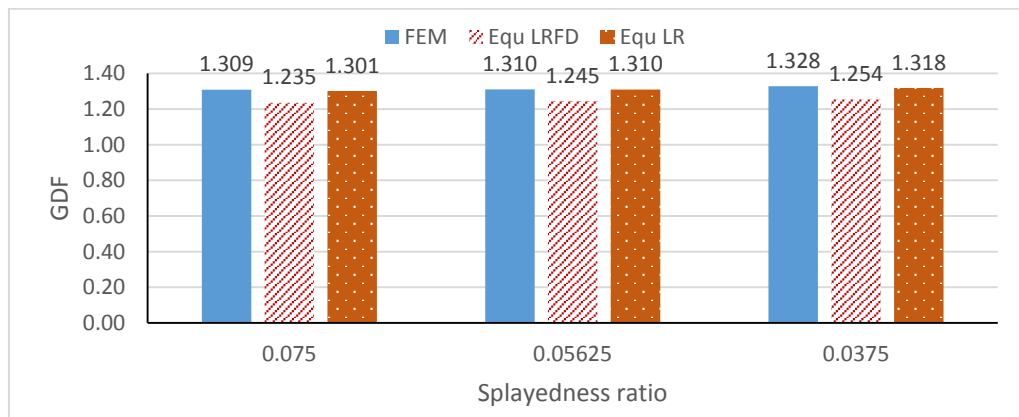
Figure 117: Interior shear FEM GDF vs. Equ GDF - bridges B1, B2, B3

Figure 118 compares the shear GDF computed from the FE analysis with the two equivalent GDFs in AASHTO using the formulas and lever rule approach for the exterior girders in bridges B1, B2, and B3. It shows that the LRFD equivalent GDF values are higher than the FE results by 18%, 19.2%, and 18.7% in bridges B1, B2, and B3, respectively. The lever rule equivalent GDFs are closer to the FE results with some conservatism of 6.5%, 6.6%, and 7.8% in bridges B1, B2 and B3, respectively. Also, as in the interior girders, the GDF values for the exterior girders from all three methods have the same trend, where increasing the splayedness ratio results in a small reduction in girder spacing and, therefore, the GDF values drop slightly.
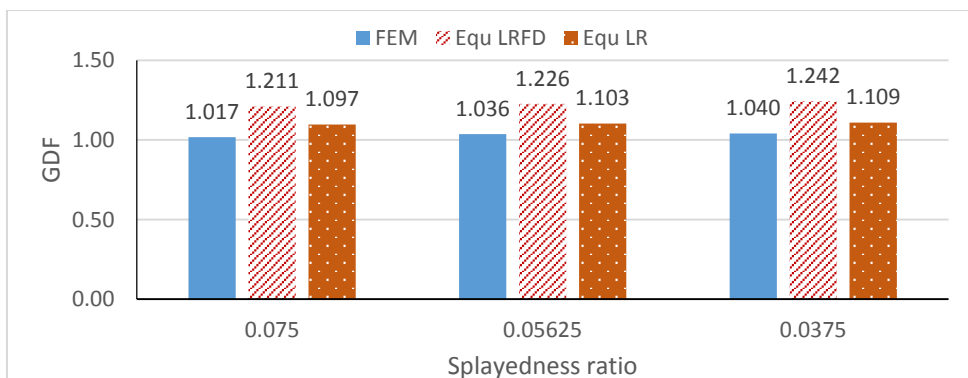
Figure 118: Exterior shear FEM GDF vs. Equ GDF - bridges B1, B2, B3

It can be concluded that changing the splayedness ratio does not have significant changes on GDF in both interior and exterior girders, for the case of shear in girders. However, the small difference in GDF values between the three bridges is caused by the very slight change in girder spacing at the position of the trucks middle and front axles since the girder spacing at the rear axle is the sane in all girders. On the other hand, the lever rule can predict the shear GDF results more accurately than using the LRFD shear formulas in both the interior and exterior girders.

5.3.1.2 S_1/S_2 effect.

Figure 119 shows a plan view of bridges B1, B4, and B5 with the corresponding S_1/S_2 values. In all cases, the girder splayedness ratio is kept constant and equals 0.05625 for all three bridges. In the reference B1, the S_1/S_2 ratio equals 0.5, and in bridge B4 this ratio is decreased to 0.4 resulting a reduction in girder spacing equal to 750 mm, while in bridge B5 the ratio is increased to 0.5714 resulting in an increase in girder spacing equal to 750 mm.
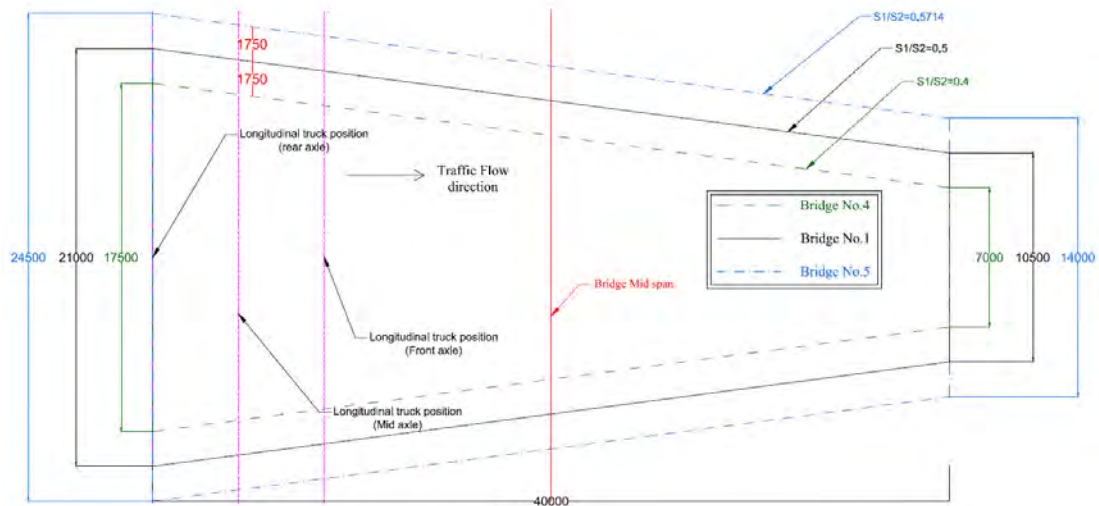
Figure 119: Bridges B1, B4, and B5 plan view - Shear

At the longitudinal truck location for maximum shear shown in Figure 119, the girder spacing changes at each truck axle by different percentages as presented in Table 35.

Table 35: % Difference in girder spacing between bridges B1, B4, B5 - shear

Bridges	Girder Spacing difference %			Notes
	Rear axle	Mid axle	Front axle	
B1 and B4	-16.7	-17.6	-18.7	decreased
B1 and B5	16.7	17.6	18.7	increased

Figure 120 presents the shear GDF for bridges B1, B4, and B5 in the interior and exterior girders computed using the FE analysis against the S_1/S_2 ratio. In interior girders, increasing the S_1/S_2 ratio by 14.3% resulted in a 10.54% increase in GDF value, while decreasing the S_1/S_2 ratio by 20% led to a 12.88% reduction in GDF value. The same trend is observed in the exterior girders, where increasing the S_1/S_2 ratio by 14.3% causes a growth of 7.8% in GDF value, while reducing the S_1/S_2 ratio by 20% resulted in an 11.86% drop in the GDF value. It can be noticed that all bridges acted like normal bridges, where by increasing girder spacing the shear GDF increased somewhat linearly.
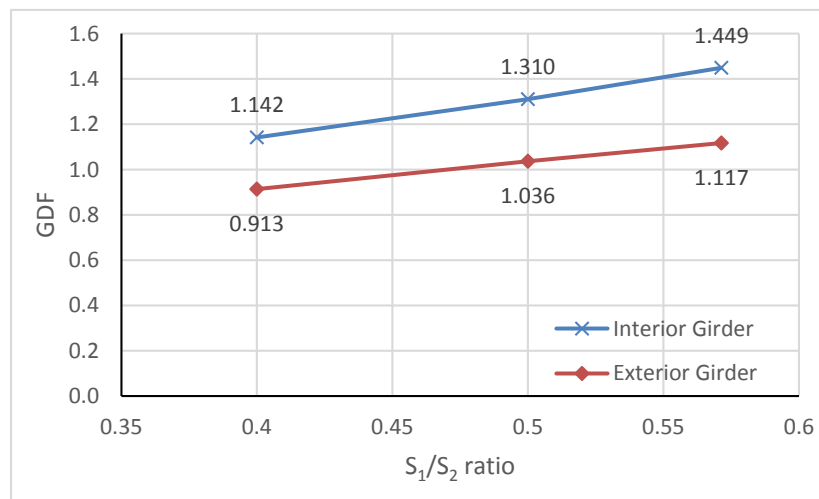
Figure 120: Shear FEM GDF versus S_1/S_2 ratio

Figure 121 and Figure 122 present the shear equivalent GDF for bridges B1, B4, and B5 in interior and exterior girders calculated based on the AASHTO LRFD formulas and the lever rule, respectively. Both methods agree on the trend that the shear GDF increases when the girder spacing is increased. However, the shear equivalent AASHTO GDF computed using the LRFD formulas for bridge B5 does not match the trend of bridges B1 and B4, where in both bridges the GDF value for the interior girder is higher than the one for the exterior, which also matches with the FE results. The GDF value for bridge B5 for the exterior girder is higher than that for the interior one. This due to the high girder spacing in bridge B5 at the wide end of the bridge, where it exceeds the applicability limits set by AASHTO LRFD to use shear GDF formulas, but more importantly due to the corresponding very high overhang width (taken as one-third of the corresponding girder spacing). On the other hand, using the lever rule to

compute the shear equivalent GDF gives more consistent results which are closer to the FE results despite the large girder spacing and overhang width value in bridge B5.
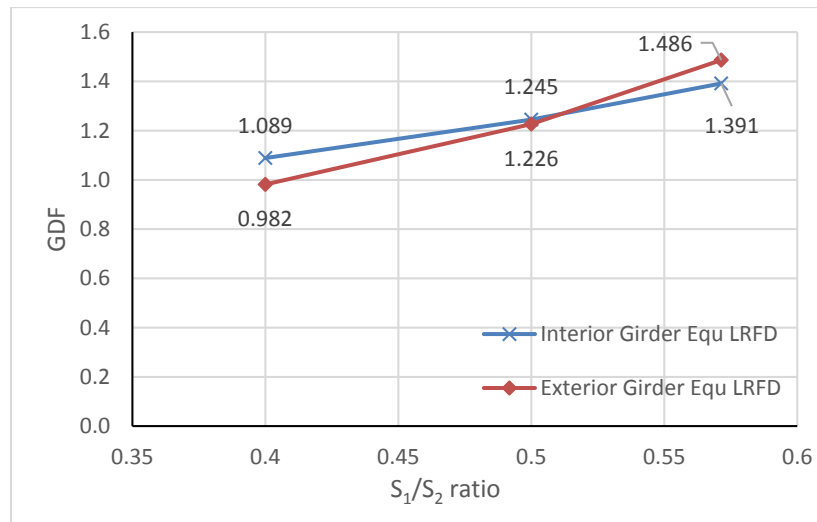
Figure 121: Shear LRFD Equivalent AASHTO GDF versus S_1/S_2 ratio
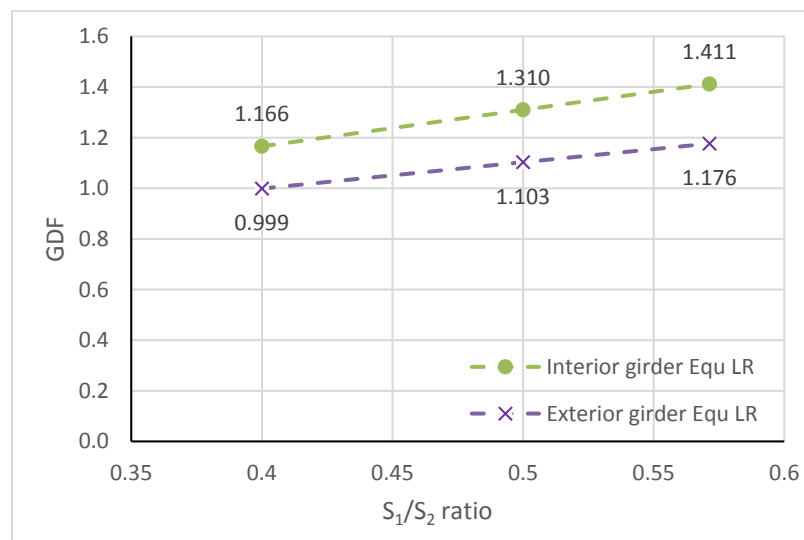
Figure 122: Shear lever rule Equivalent GDF versus S_1/S_2 ratio

Figure 123 and Figure 124 compare the shear equivalent GDF with the FE results in the interior and exterior girders, respectively, for bridges B1, B4, and B5. For the interior girders it is obvious that the equivalent GDF based on the AASTO LRFD formulas for shear fails to predict GDF values higher than the FE ones in any S_1/S_2 ratio. The least difference between the two methods is recorded in bridge B4 with an S_1/S_2 ratio equal to 0.4, resulting in a value more than 4% lower than the FE results. However, the shear equivalent GDF values based on the lever rule gave reasonable results in all cases. It is 2.57% more conservative in bridge B4, and only 2.5% less than the FE results in bridge B5. On the other hand in the exterior girders, the LRFD

equivalent GDF values are greater than the FE results by a minimum of 7.23% where the S_1/S_2 ratio equals 0.4 (bridge B4), and a maximum of 32.8% at the S_1/S_2 ratio equals 0.5714 (bridge B5). By using the lever rule, more consistent values for the equivalent GDF were recorded. Compared with the FE results, the lever rule gave more conservative results by 9.4% and 5.3% in bridges B4 and B5, respectively.

Figure 123: Interior shear FEM GDF vs. Equivalent GDF - bridges B1, B4, B5

Figure 124: Exterior shear FEM GDF vs. Equivalent GDF - bridges B1, B4, B5

As known, the shear GDF is mostly affected by the girder spacing at the rear axle longitudinal location for maximum shear effect, which is at the wide supported end of splayed girder bridges. By changing the splayedness ratio while keeping the girder spacing at the wide supported end constant (bridge B2 and B3), the shear GDF of the considered bridges did not change appreciably for the interior and exterior girders. On the other hand, increasing and decreasing the girder spacing at the same location, as in bridges B4 and B5 compared to B1 resulted in significant changes in shear the GDF.

Regarding the computation of equivalent GDF using a simple approach, it is concluded that using the AASHTO LRFD formulas to compute the equivalent GDF leads to inconsistent results, where in interior girders it is lower than the finite element

results, and in exterior girders it is much more conservative. Therefore, the lever rule is recommended to be used to calculate the shear equivalent GDF, because it gave very close results to the FE with little conservatism in exterior girders, while in interior girders the results were almost equal. Figure 125 presents the shear GDF for bridges B1 to B5 against the average girder spacing ($S_{avg} = (S_2+S_1)/2$) obtained from finite element analysis and the lever rule procedure.
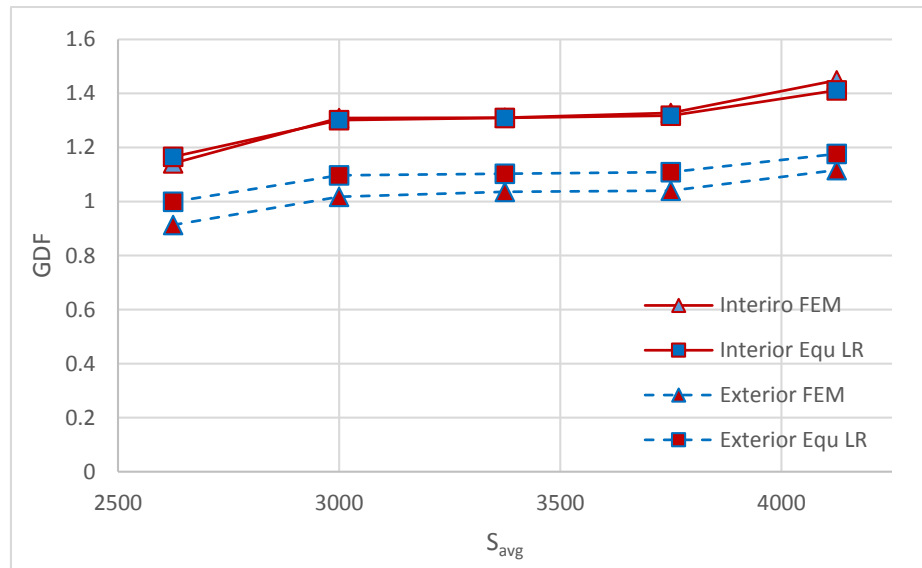
Figure 125: Shear GDF vs. AVG girder spacing

5.3.2 Effect of slab thickness.

Two bridges besides the reference bridge are considered to study the slab thickness effect which varies between 150 mm and 300 mm. Figure 126 presents the shear GDF for bridges B1, B6, and B7 computed from the FE analysis in the interior and exterior girders versus the slab thickness. It is obvious that in exterior girders there is almost no change in GDF values due to slab thickness changes, where increasing the slab thickness to 300 mm (36.4%) caused only a 2% reduction in GDF value, whereas a drop in the slab thickness to 150 mm (31.8%) led to only a 0.8% increase in GDF. This is an expected result since the GDF for shear in the exterior girder is mainly affected by the overhang and girder spacing between the exterior and first interior girders. In the interior girder the effect was a little higher, where increasing the slab thickness decreased the GDF value by 3.25% while decreasing the slab thickness increased the GDF value by 2.53%. This very small effect is a result of changing the bridge's cross-section stiffness due to changing the slab thickness, where when reducing the thickness of a slab the GDF rises because the girders share less load.

131

However, because the truck is exactly at the girders supports, the slab thickness effect on shear GDF is very small, and this is why it is not considered in the AASHTIO LRFD shear formulas.
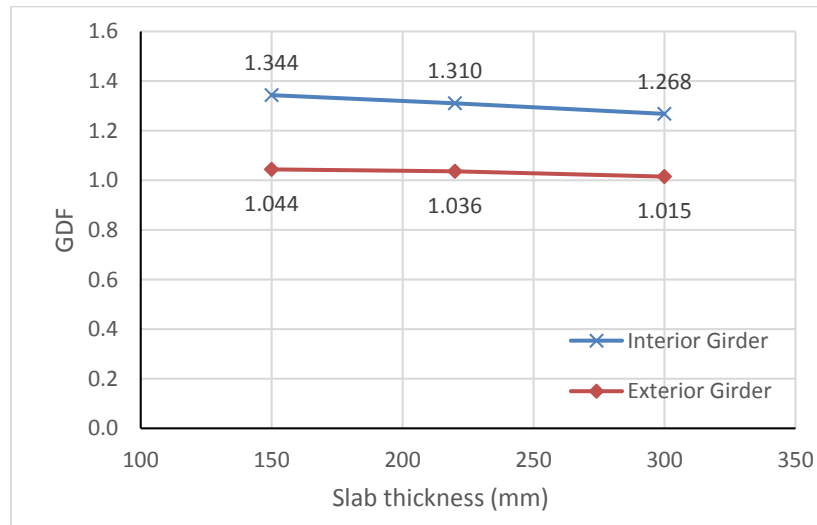
Figure 126: Shear FEM GDF versus slab thickness

The AASHTO LRFD formulas do not take slab thickness into account in the expressions of the shear GDF. Therefore, the shear equivalent GDF computed using the LRFD formulas gives the same value for bridges B1, B6, and B7, which is equal to 1.245 for the interior girder and 1.226 for the exterior girder. Similarly, and for the same reasons, the shear equivalent GDF computed using the lever rule has the same value for bridges B1, B6, and B7, which equals 1.310 for the interior girders and 1.103 for the exterior girders.

Figure 127 compares the shear GDF from the FE results with the equivalent GDF resulting from both the AASHTO LRFD formulas and the lever rule for interior girders. For interior girders, the equivalent GDF based on the AASTO LRFD formulas for shear underestimate the GDF values in all three bridges with different slab thicknesses. In bridge B6 with a slab thickness of 150 mm, the shear GDF was about 7.5% lower than the FE results, and in bridge B7 it was 1.95% lower as well. However, the lever rule based shear equivalent GDF provided better results. It gave a 3.3% more conservative value in bridge B7, and it gave a 2.51% lower value compared with the FE results in bridge B6. As illustrated in Figure 128, for exterior girders the LRFD equivalent GDF is greater than the FE results by 17.2% in bridge B6, and by 20.5% in bridge B7. Using the lever rule to compute shear equivalent GDF resulted in more

132

reasonable results, where compared with the FE results, it was conservative by 5.63% and 8.65% in bridges B6 and B7, respectively.
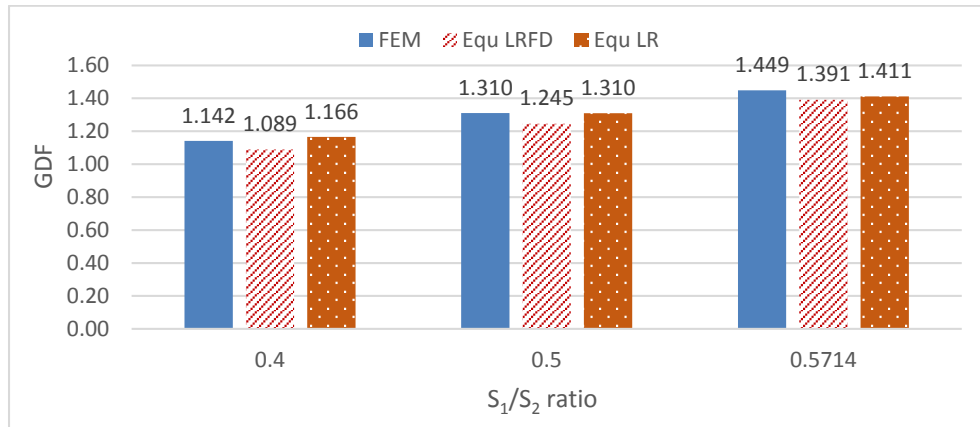

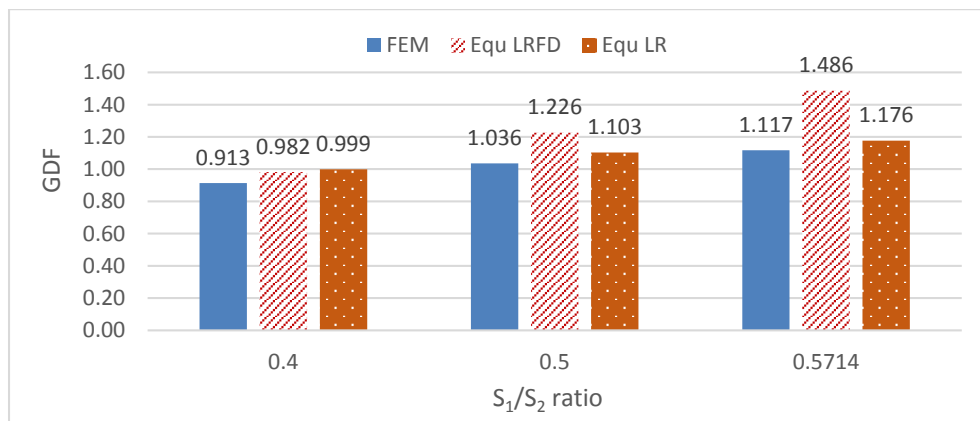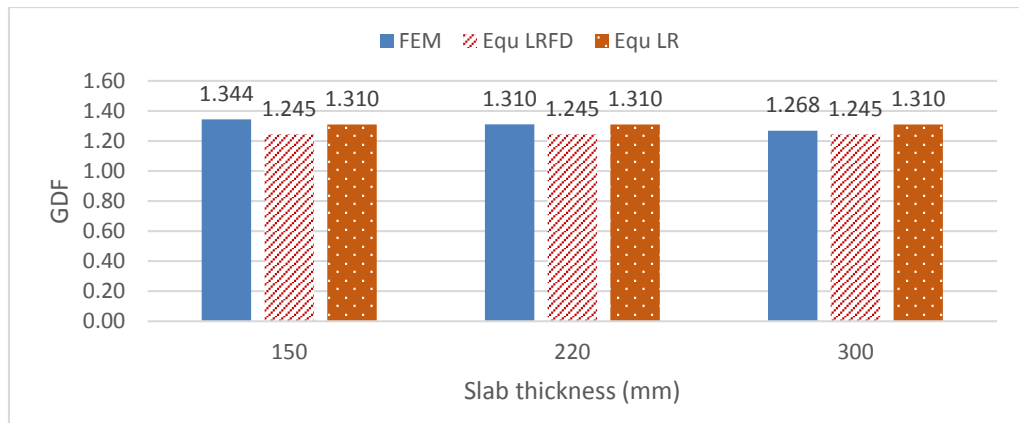Figure 127: Interior shear FEM GDF vs. Equ GDF - bridges B1, B6, B7
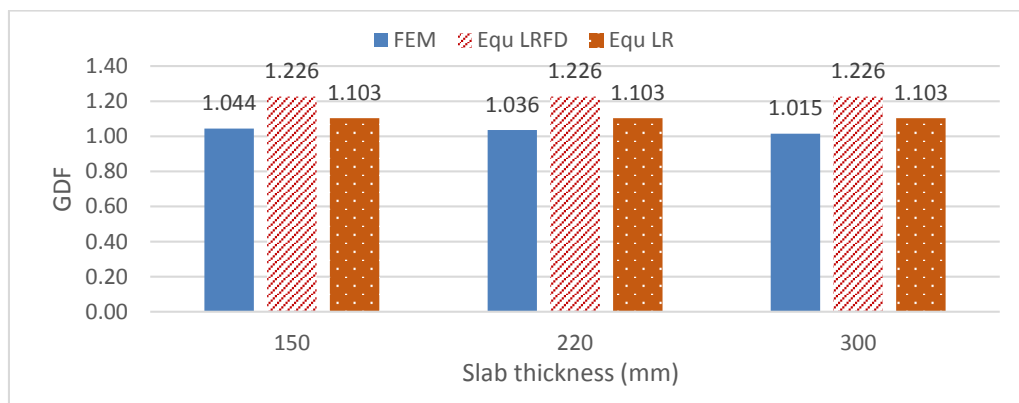
Figure 128: Exterior shear FEM GDF vs. Equ GDF - bridges B1, B6, B7

It can be concluded that the slab thickness effect on shear GDF in interior and exterior girders of splayed girder bridges is very minimal and can be neglected. Using the AASHTO LRFD formulas to compute the equivalent GDF for bridges with different slab thicknesses leads to inconsistent results, where in interior girders they give slightly low values compared with the FE results and in exterior girders they result in very conservative values. On the other hand, using the lever rule to calculate the shear equivalent GDF gives very close values to the FE results.

5.3.3 Effect of cross-bracing presence and spacing.

Two bridges, B8 and B9, besides the reference bridge B1 are considered to study the cross-bracing effect in splayed girder bridges. Note that the AASHTO LRFD formulas for shear GDF were developed based on bridge models without diaphragms or cross-bracings.

Figure 129 shows the FE shear GDF for bridges B1, B8, and B9 in interior and exterior girders against cross-bracing spacing. It is clear, especially in interior girders, that adding cross-bracings in splayed girder bridges reduces the shear GDF values. Adding cross-bracing at 10 m spacing (bridge B9) resulted in a 2% and 3.46% reduction in shear GDF in the exterior and interior girders, respectively (bridge B8). By doubling the cross-bracing and making the spacing equal to 5 m only, a 3.78% and 8.76% drop in shear GDF is recorded in the exterior and interior girders, respectively.

Adding cross-bracing results in a stiffer superstructure cross-section for the bridge, and consequently more load sharing between the girders, and therefore less shear GDF in the girder under consideration. However, cross-bracing spacing is more critical for shear than it is for flexure, where it should be noticed that as the truck's longitudinal position is at the supported end, adding only 10 m spaced cross-bracing means that the mid axle of the truck does not have cross-bracing beneath it, while the front axle, which has the least portion of the truck's load, has one close to it. On the other hand, using a 5 m spaced cross-bracing means that each truck axle has a cross-bracing close to it, and therefore the bridge cross section is stiffer under each truck axle position resulting more load sharing in less GDF as a result.
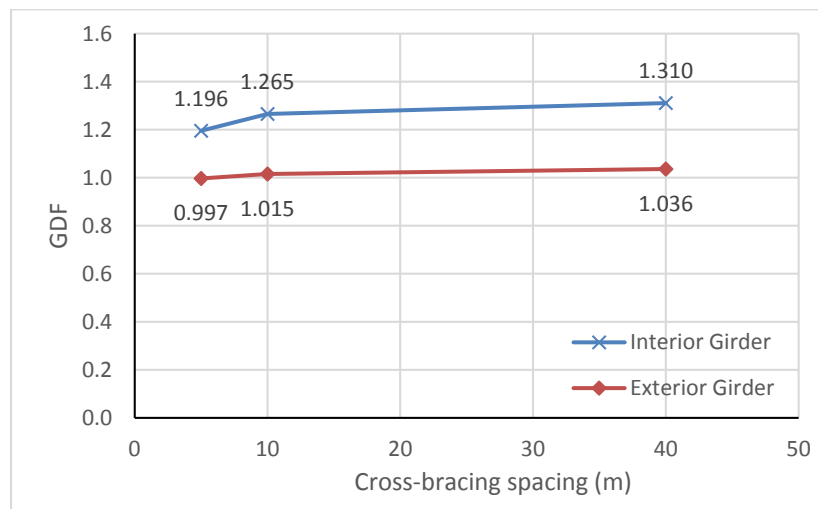
Figure 129: Shear FEM GDF versus cross-bracing spacing

Figure 130 compares the FE shear GDF with the equivalent GDF resulting from the AASHTO LRFD formulas and the lever rule method for interior girders. The AASHTO LRFD formulas do not account for the cross-bracing presence or spacing; consequently, the shear equivalent GDF computed based on these formulas is the same for bridges B1, B8, and B9, and it is equal to 1.245. Therefore, the computed equivalent

134

GDFs are inconsistent with the FE results, where for bridges with cross-bracing spacing of 40 m and 10 m, shear GDF was lower than the FE results, but by decreasing the spacing to 5 m, the equivalent shear GDF becomes 4% higher than the FE results. On the other hand, using the lever rule to find the shear equivalent GDF gave more reliable results for interior girders, where with only cross-bracing at the ends (bridge B1) the equivalent GDF is equal to the FE results, and by adding 10 m and 5 m spaced cross-bracing, the equivalent GDF became 3.53% and 9.55% more conservative, respectively. The exterior girder results are illustrated in Figure 131, which shows that the LRFD equivalent GDFs for shear are much greater than the FE results in all cases, where they reached 22.73% and 20.5% conservatism in bridges B8 and B9, respectively. But by using the lever rule, the equivalent GDF for shear in the exterior girders was only 10.65% more conservative in bridge B8 and 8.65% more conservative in bridge B9.

Figure 130: Interior shear FEM GDF vs. Equ GDF - bridges B1, B8, B9
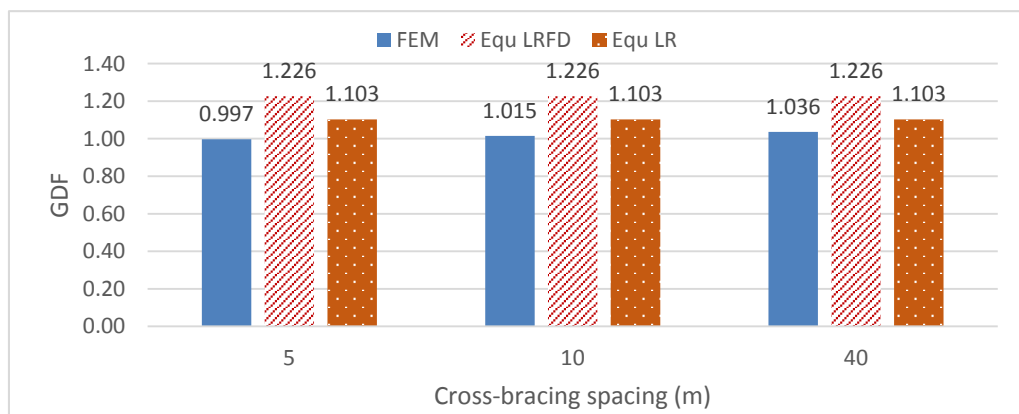
Figure 131: Exterior shear FEM GDF vs. Equ GDF - bridges B1, B8, B9

It can be concluded that cross-bracing has little effect on GDF for shear in splayed girder bridges especially for exterior girders. In addition, the cross-bracing spacing has important effect on shear GDF for interior girders only if the cross-bracing is smaller than 10 m. Regarding the equivalent AASHTO GDF, it can be concluded that

using the LRFD formulas to calculate the equivalent GDF for bridges with different cross-bracing spacing leads to inconsistent results, where in interior girders they give nonconservative and conservative results depending on the cross-bracing spacing, while in exterior girders they consistently give very conservative values. However, using the lever rule to calculate the shear equivalent GDF in splayed girder bridges gave very close results compared with the FE results, with some conservatism.

5.3.4   Effect of number of girders.

Two bridges, B10 and B11, besides the reference bridge B1 are considered to study the effect of number of girders in splayed girder bridges. The bridges considered are bridge B10 with only 3 girders, and bridge B11 with 7 girders.

Figure 132 shows the FE shear GDF for bridges B1, B10, and B11 in interior and exterior girders versus the bridge's number of girders. It can be noticed that in exterior girders the GDF values are very close to each other, and they slightly decrease (by less than 2%) with an increase in the number of girders. In interior girders, the shear GDF drops by 5.17% when increasing the number of girders from 3 to 5, while by adding 2 more girders, for a total number of 7 girders, almost no changes occurred in the GDF value. The explanation for these changes is that in bridge B10 there are only 3 girders (2 exterior and 1 interior) and they all share the loads of 2 trucks to maximize the shear effect, while bridge B1, which has 5 girders (3 interior and 2 exterior) is also loaded by 2 trucks to maximize the shear effect. Therefore, the two bridges are loaded with the same number of trucks but one has only one interior girder, and the other one (bridge B1) has 3 interior girders, which can share more load and consequently the girder under consideration has a lower shear GDF.
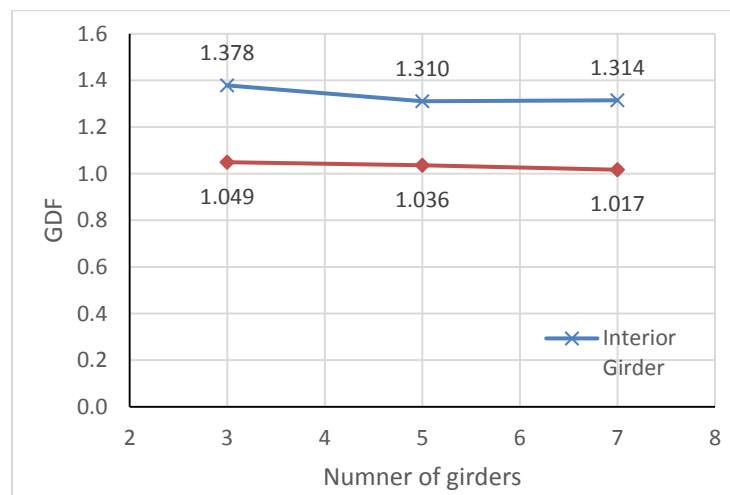
Figure 132: Shear FEM GDF versus number of girders

The AASHTO LRFD formulas do not consider the number of girders in calculations of shear GDF in interior and exterior girders. These formulas are applied to regular bridges having four or more girders. For bridges with three girders, the AASHTO specifications recommend the use of the lever rule. In this section, both methods are applied to compute the shear equivalent GDF regardless of the number of girders in the bridge. The shear equivalent AASHTO GDF computed using the LRFD formulas gives the same value for bridges B1, B10, and B11, equal to 1.245 for the interior girder, and to 1.226 for the exterior girder. Similarly, the shear equivalent GDF computed using the lever rule is equal to 1.310 for interior girders and 1.103 for exterior girders.

Figure 133 shows the shear GDF computed from FE analysis and the equivalent GDF using the AASHTO LRFD formulas and the lever rule for interior girders. The LRFD equivalent GDF underestimates the GDF values in the three bridges. In bridge B10 which consists of 3 girders, the shear GDF was about 9.8% lower than the FE results, and in bridge B11 it was 5.4% lower as well. However, the equivalent GDF for shear that is based on the lever rule method gave better results. Compared with the FE results, it almost matched the results in bridges B1 and B11, while it was less than 5% lower than the FE results in bridge B10. Additionally, Figure 134 presents the shear GDF from the three methods for the exterior girders. The LRFD equivalent GDF based on the AASHTO formula gave very large values compared with the FE results, where it exceeded 16.5% in bridge B10, and 20% in bridge B11. By using the lever rule to compute shear equivalent GDF, the results were more consistent, where compared with the FE results they were more conservative by 5.18% and 8.5% in bridges B10 and B11, respectively.
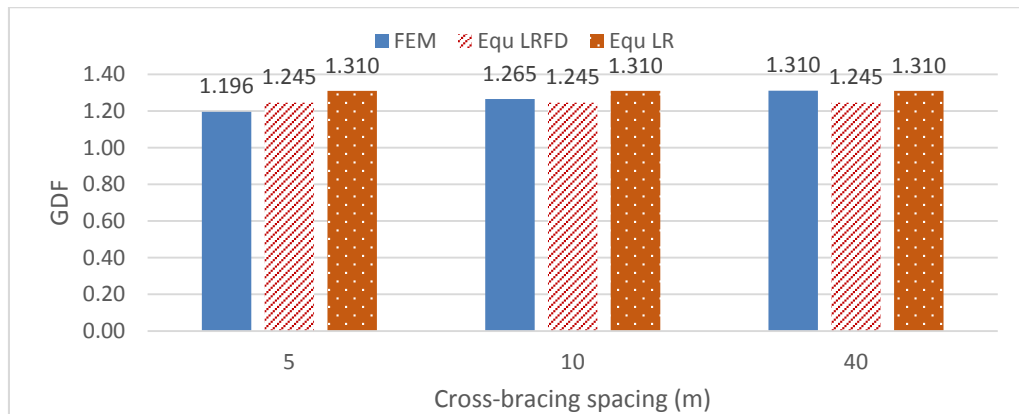

Figure 133: Interior shear FEM GDF versus Equ GDF - bridges B1, B10, B11

Figure 134: Exterior shear FEM GDF vs. Equ GDF - bridges B1, B10, B11

It can be concluded that in splayed girder bridges, the shear GDF in both the interior and exterior girder is not significantly affected by the number of girders when the number of girders is large (more than 5). However, bridge B10, which consists of only 3 girders, showed higher GDF values because of the few number of girders to share the load. Using the AASHTO LRFD formulas to compute the equivalent GDF for splayed girder bridges with different number of girders leads to unreliable results, where in interior girders give low values compared with the FE results and in exterior girders they result in very conservative results. Instead, using the lever rule to compute the shear equivalent GDF gave very close results compared with the FE findings. In exterior girders, the equivalent GDF gave conservative values, and in interior girders the results were almost equal to the FE values, except for bridge B10 which gave slightly lower results.

5.3.5 Effect of girder stiffness.

Two bridges besides the reference bridge are considered to study the stiffness effect in splayed girder bridges. The bridges considered are bridge B12 with only 1400 mm girder depth, and bridge B13 with 2000 mm girder depth.

Figure 135 presents the FE shear GDF for bridges B1, 12, and B13 in the interior and exterior girders against the girder depth. It is very clear that in both the interior and exterior girders the GDF values are very close to each other and they are almost equal, where the greatest GDF difference does not exceed 0.5%.

Figure 135: Shear FEM GDF versus girder depth

Figure 136 and Figure 137 present the difference between the shear GDF computed from FE analysis and the equivalent GDF resulting from both the AASHTO LRFD formulas, and the lever rule for the interior and exterior girders, respectively. From the FE analysis, bridges B1, B12, and B13 have almost the same shear GDF value. In addition to that, both the AASHTO LRFD formulas and the lever rule do not consider girder stiffness in calculations of shear GDF in interior and exterior girders. Therefore, the difference between the three methods is the same in bridges B1, B12, and B13, and similar to the reference bridge, the LRFD equivalent GDF gives low values for interior girders compared with the FE results, and very conservative results for exterior girders. In contrast, the lever rule equivalent GDF gives more reliable results, where it is almost equal or slightly higher than the FE results for interior girders, and more conservative for exterior girders.
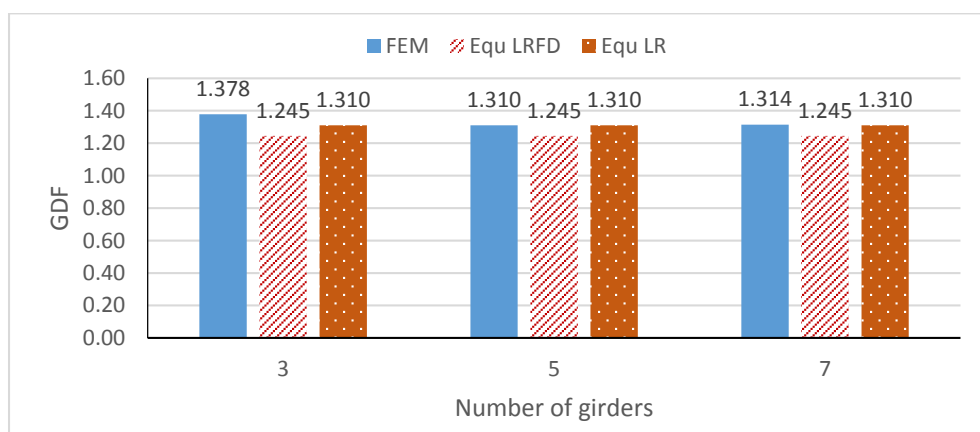

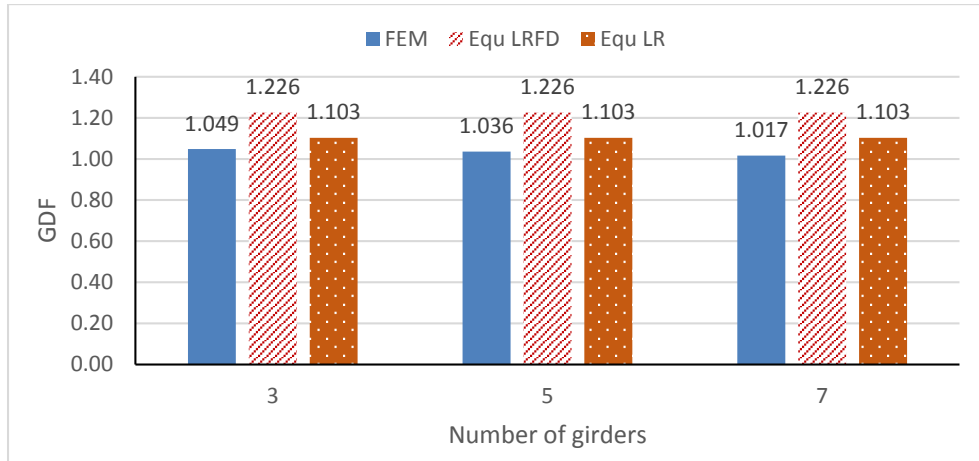Figure 136: Interior shear FEM GDF vs. Equ GDF - bridges B1, B12, B13
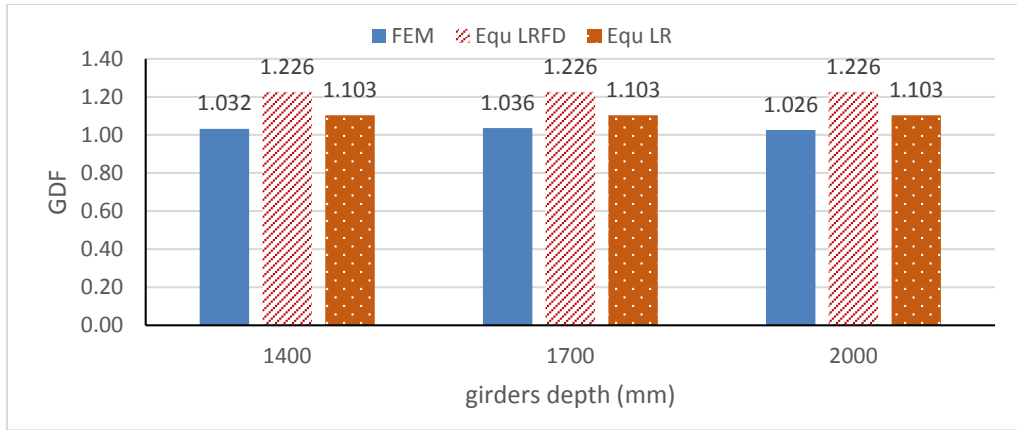
Figure 137: Exterior shear FEM GDF vs. Equ GDF - bridges B1, B12, B13

It can be concluded that for splayed girder bridges, the shear GDF in both interior and exterior girders is not affected by changing girder stiffness. And regarding the equivalent GDF, just like in the reference bridge, using the AASHTO LRFD formulas to compute the equivalent GDF leads to unreliable results as explained before. In contrast, using the lever rule to compute the shear equivalent GDF gives very close results compared with the FE results.

5.3.6 Effect of span length.

Besides the reference bridge two bridges are considered to study the span length effect in splayed girder bridges. The considered bridges are bridge B14 a span of 30 m, and bridge B15 with 50 m span length.

Figure 138 presents the FE shear GDF for bridges B1, 14, and B15 in the interior and exterior girders against the span length. It is obvious that in the interior and exterior girders the GDF values are very close to each other and they are almost equal, where the difference does not exceed 2%.
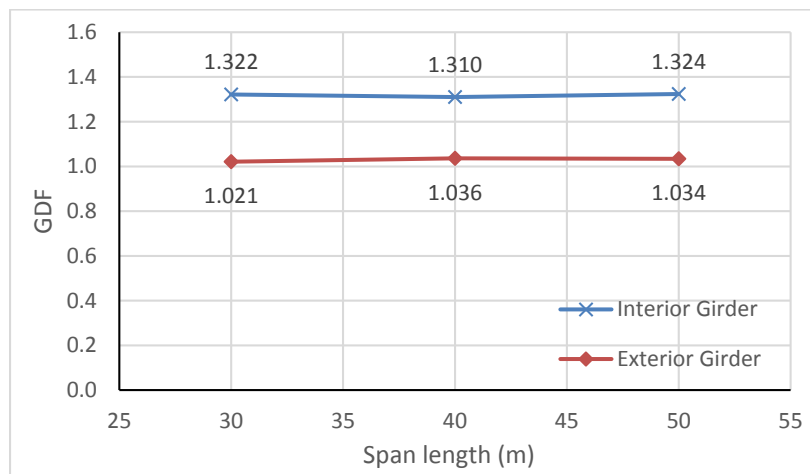
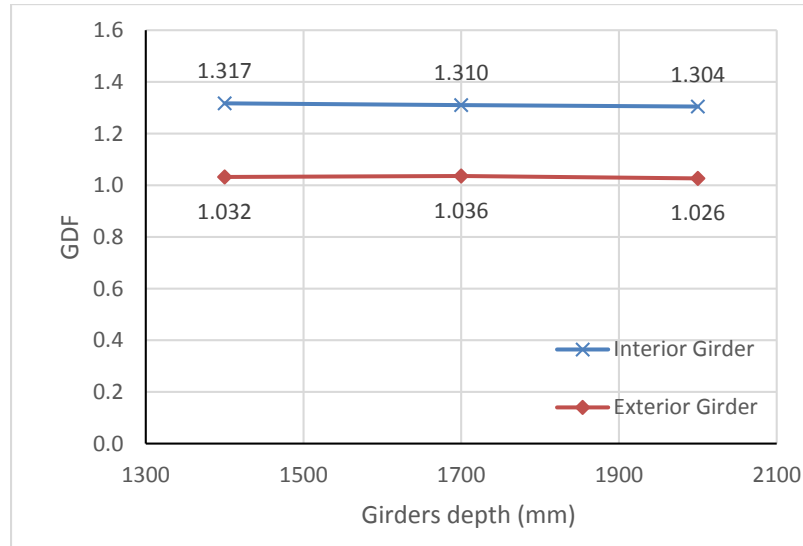Figure 138: Shear FEM GDF versus span length

140

Figure 139 and Figure 140 compares the shear GDF resulted from the FE analysis with the equivalent GDF resulting from both the AASHTO LRFD formulas, and the lever rule for the interior and exterior girders, respectively. From the FE analysis, bridges B1, B14, and B15 have almost the same shear GDF value. Both the AASHTO LRFD formulas and the lever rule do not consider span length directly in calculations of shear GDF in interior and exterior girders. However, changing the span length in a splayed girder bridge leads into a slight change in the splayedness and consequently changes in the girder spacing. Therefore, very small difference in the shear GDF between the three bridges is noticed. Similar to the previously examined bridges the AASHTO LRFD expressions underestimate the shear GDF for interior girders, and give very conservative results for exterior girders when compared with the finite element finings. However, the lever rule showed more reasonable results, where for interior girders the results are almost equal, and for exterior girder the shear GDF are slightly conservative.

It can be concluded that for splayed girder bridges, the effect of changing the span length on the shear GDF in both interior and exterior girders is almost negligible. Regarding the equivalent GDF, similar to the reference bridge, using the AASHTO LRFD formulas to compute the equivalent GDF leads to unreliable results as explained before. However, using the lever rule to calculate the shear GDF gives much close results compared with the FE results.
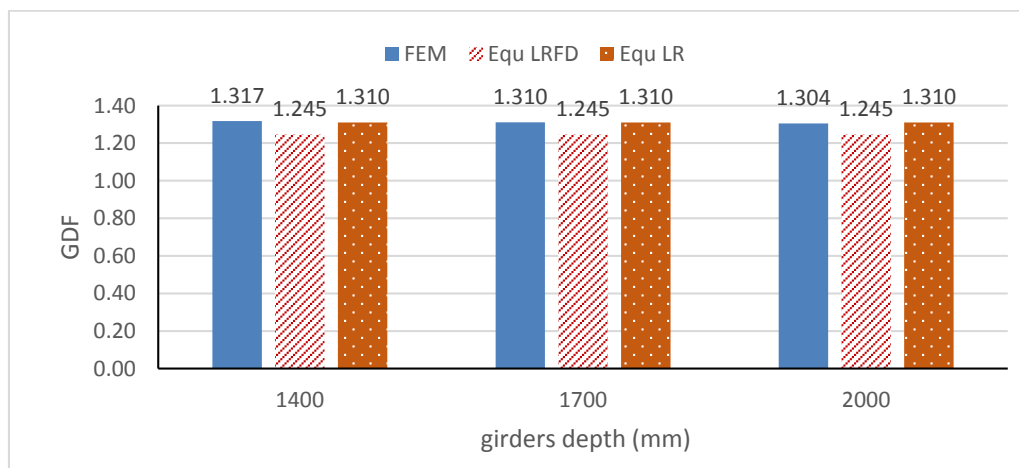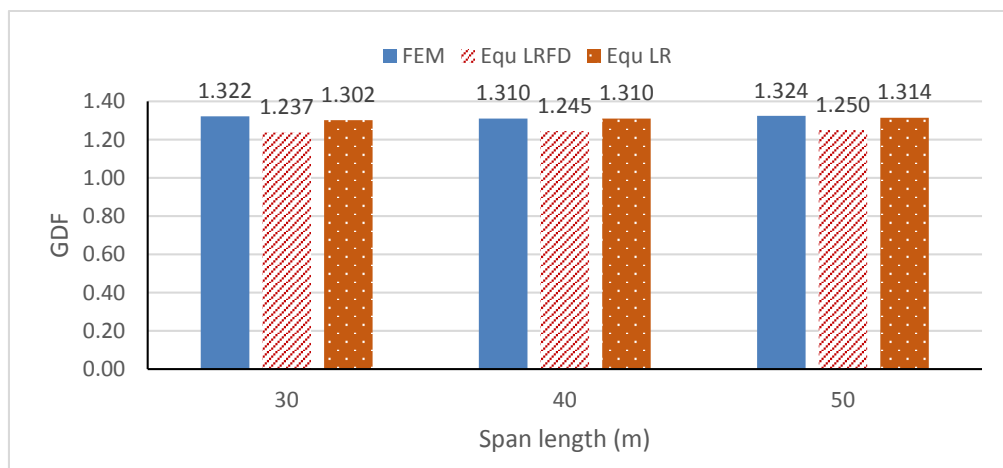

Figure 139: Interior shear FEM GDF vs. Equ GDF - bridges B1, B14, B15
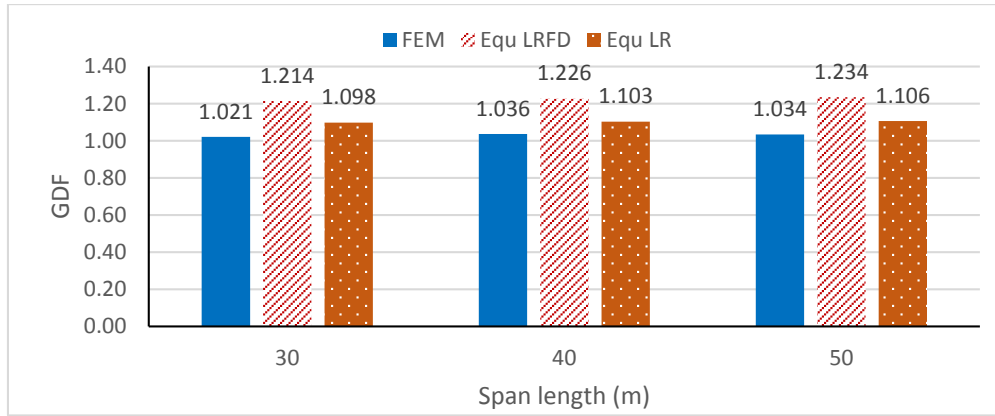
Figure 140: Exterior shear FEM GDF vs. Equ GDF - bridges B1, B14, B15

5.3.7 Summary.

Previous results showed that for of the fifteen bridges analyzed for shear, using the lever rule gives more reasonable results than using the AASHTO LRFD expressions to compute the shear GDF in both interior and exterior girders when compared with the finite element results. Figure 141 compares the ANSYS shear GDF values with the corresponding shear GDF values that are based on the lever rule for both the interior and exterior girders. It can be concluded that almost in all the considered cases, the shear GDF obtained from using the lever rule were reasonably very close to the finite element findings. For all practical purposes it is concluded that the GDF based on the lever rule is a good and simple approach for analyzing splayed girder bridges in shear.
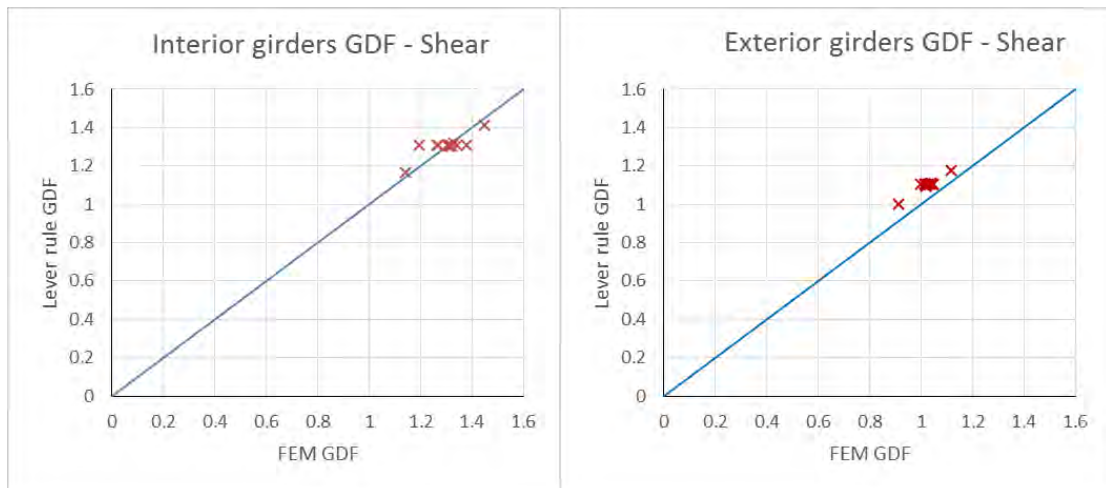
Figure 141: Summary of all shear GDF result

142

Chapter 6: Findings and Discussion: Deck Slab

In this chapter, the live load effect on the concrete deck slab of splayed girder bridges is discussed and analyzed. According to AASTHO LFD or LRFD specifications, the deck slab in bridges is generally analyzed for flexure only, because past experience showed that shear does not apply if minimum slab thickness is chosen. Here, three splayed girder bridges are analyzed using finite element program ANSYS to investigate the deck slab behavior in three critical cases: (1) positive moment in interior regions, (2) negative moment in interior regions, and (3) negative moment in the overhang. The results from finite element models are compared with the strip method suggested in AASHTO LRFD to design concrete deck slabs in bridges.

6.1 Positive Moment in Interior Region

The stress due to the positive moment case in each of the considered bridges is computed at three different longitudinal locations along the span of the bridge as described in Section 4.3.2. These locations are considered because they address different locations of the concrete deck slab in splayed girder bridges. The equivalent strip method suggested by the AASHTO LRFD specifications assumes that the strip taken in the transverse direction of the bridge is rigidly supported by the girders. This is true at the ends of a simply-supported bridge where the girders are supported by the abutment. However, the girders deflect within the span of the bridge, which changes this condition especially at the mid span of the bridge. The vertical relative deflection between the girders re-distributes some of the bending moment in the deck slab. Therefore, before analyzing the splayed girder bridges, a 40 m long simply-supported bridge with parallel girders spaced at 3.375 m and 220 mm slab thickness is modeled by ANSYS and then loaded once at each longitudinal location specified earlier for splayed girder bridges as shown in Figure 142. This bridge will shed insight and provide information into why splayed girder bridges differ from regular bridges with parallel girders.

The regular bridge is loaded by a number of trucks in the transverse direction at each specified section, and the maximum transverse stress due to this loading is recorded. For all sections, loading with one truck only resulted in the maximum transverse stress value including the multiple presence factor. The maximum transverse

143

stress values due to positive moment (M^+) are 2.418 MPa, 3.00 MPa, and 2.34 MPa at sections 1, 2, and 3, respectively.
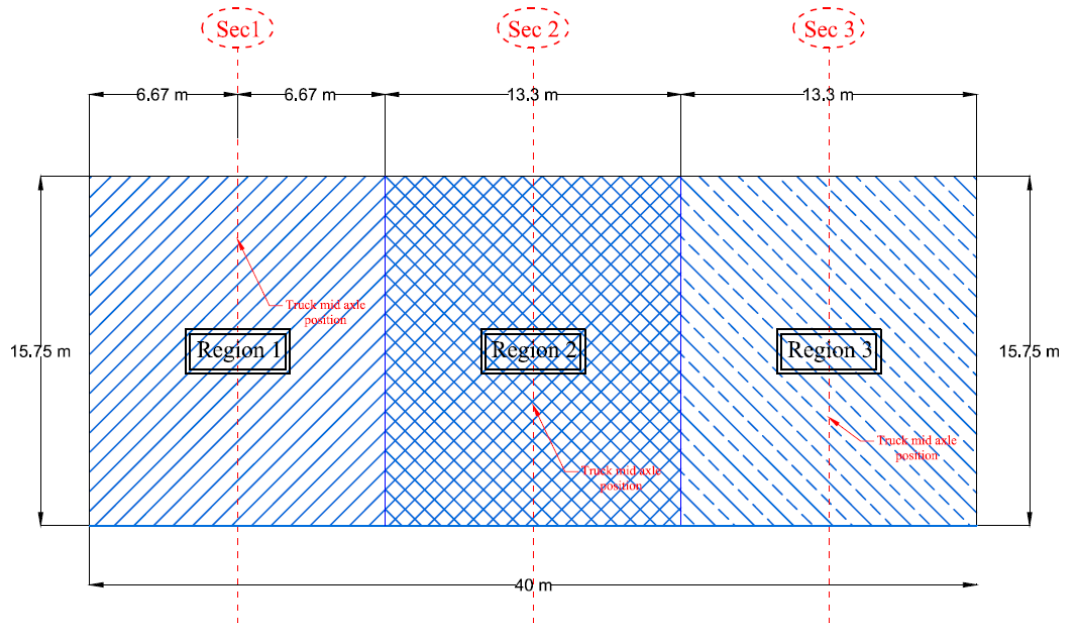
Figure 142: Regular bridge deck slab plan

Using the equivalent strip method, the maximum tensile transverse stress at the bottom layer of the slab equals 3.201 MPa at any section, because all sections have the same girder spacing, and the girders are assumed as rigid supports. It is obvious that the finite element results in any section are lower than the corresponding ones from the equivalent strip method. However, the finite element results differ from each other, as they give a maximum value at Section 2 at the mid span of the bridge, and by moving toward the supported ends of the bridge (Section 1 and 2) the critical stress value decreases. This is mainly because of the deflection of the supporting girders, where for a simply-supported bridge the maximum deflection is at the mid span. This indicates that the maximum transverse stress in the deck slab for the positive moment case (M^+) can be expected in the mid span of a simply-supported bridge with parallel girders.

Starting with the reference splayed bridge (B1), Figure 143 compares the transverse stresses resulting from the finite element analysis with the stresses computed using the equivalent strip (ES) method at each section considered for the positive moment case along the span of the bridge.

144
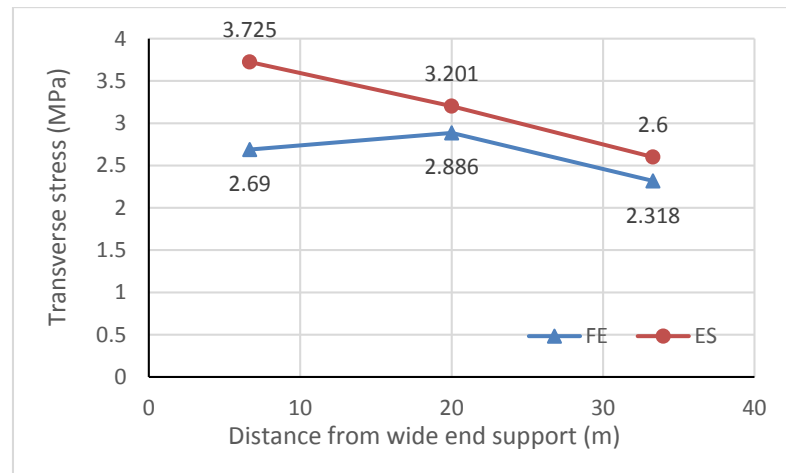
Figure 143: Deck slab transverse stresses in case of M$^+$ for reference bridge

The stress values computed using the ES method show a linear trend, where by moving towards the narrow end of the bridge the stress value drops. Note that the strip method is mainly related to the girder spacing at each section where stress due to positive moment decreases due to the splayedness of the bridge. However, this is not the case for the FE stresses, where the maximum transverse stress value occurs at the mid span of the bridge equal to 2.886 MPa. Although the girder spacing at Section 1 (6.67 m from the wide end) is greater than at the mid span, the FE stress at the mid span is greater by 6.8%. This is caused by the deflection of the girders along the span of the bridge which leads to higher stress values at the mid span of the bridge due to release in stresses in negative moment region toward positive moment regions. At the narrow end of the bridge, the girder spacing is lower than the one at the mid span, plus the deflection of the girder is also less. Therefore, the transverse stress value is 19.7% lower than the one at the mid span of the bridge. In all cases the stress values using the ES method are higher than the finite element results. Figure 144 shows the transverse stress results in bridge B4, which has a minimum girder spacing of 1500 mm and a maximum girder spacing of 3750 mm due to positive moment (M$^+$) in the deck slab. The stresses resulting from the ES method have also a linear trend similar to the reference bridge (bridge B1). The finite element findings also gave a similar trend to the finite element results of the reference bridge. The maximum transverse stress value of 2.792 MPa occurs at a section located at the mid span of the bridge. This stress value is 10.74% greater than the stress value at Section 1 (6.67 m from the wide end), and it is greater than the one at Section 3 (6.67 m from the narrow end) by 23.9%. However, by comparing the FE results with the ES method results, it can be noticed that the finite element transverse stress at Section 2 (at the mid span) resulted in a 6.77% greater stress

145

value compared with the equivalent strip method, and at Section 3 it was still greater by 2.73%.
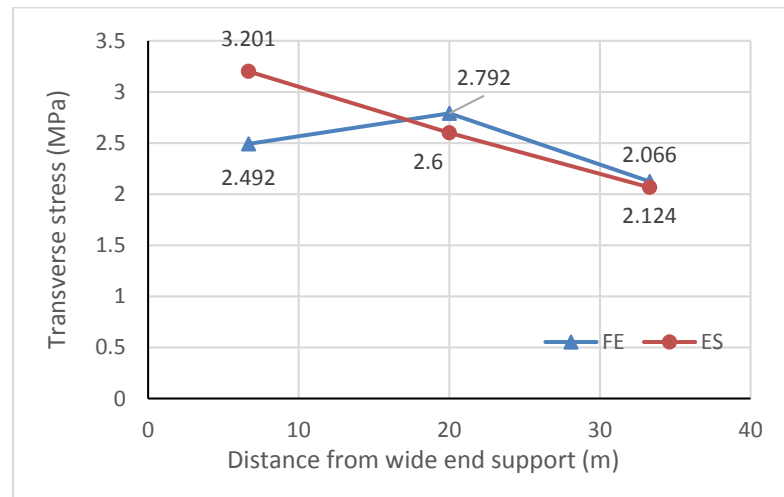
Figure 144: Deck slab transverse stresses in case of M$^+$ for B4

Figure 145 illustrate the transverse stress results in bridge B5 for the case of positive moment (M$^+$) in the deck slab. Note that bridge B5 has a maximum girder spacing of 5250 mm and a minimum girder spacing of 3000 mm. Here, the bridge has large girder spacing, which gave high transverse stress values in both methods. As expected, the stress values from the ES method have linear trend, in which the stress decreases with the decrease in the girder spacing along the span of the bridge. However, unlike bridge B1 and B4, where the maximum FE transverse stress is at a section through the mid span of the bridge, here the maximum FE stress value (3.826 MPa) results at the greater girder spacing at section 1. This value is greater than the stress at the mid span by 15.8%. Also, it is obvious that the stress values from the ES method are always greater than the FE results.
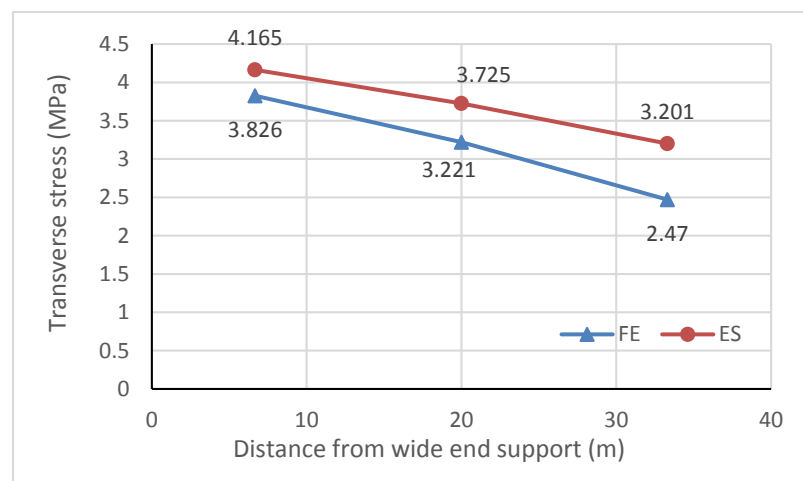
Figure 145: Deck slab transverse stresses in case of M$^+$ for B5

146

Each of the three considered bridges (B1, B4, and B5) have a section with a girder spacing of 3.375 m at different locations longitudinally. In bridge B1, Section 2 at the mid span of the bridge h a girder spacing of 3.375 m, and the maximum transverse stress due to positive bending at this section is 2.886 MPa. In bridge B4 it is Section 1 with the same girder spacing but at 6.76 m from the wide supported end of the bridge, and the stress value equals 2.492 MPa. Finally, in bridge B5 Section 3 at 6.76 m from the narrow end of the bridge has a girder spacing of 3.375 m and the stress value equals 2.47 MPa. The section with 3.375 m girder spacing is close to the narrow end of bridge B5, and section with the same girder spacing is near to the wide end of bridge B4. Both sections resulted in almost the same value of the maximum transverse stress. By comparing the stresses at the same exact longitudinal locations, with the stress values in the bridge with parallel girders of spacing at 3.375 m, it can be noticed that there is a very small difference. At the mid span section the difference is almost 4%, and at 6.7 m from the support the maximum difference is 6%.

Based on these results, it can be concluded that in a splayed girder bridge the transverse stress in the deck slab due to the positive moment case can be affected by two main factors. The first one is the varying girder spacing along the span of the bridge, and the second one is the longitudinal location that affects the deflection of the girders that support the concrete deck slab. However, the girder spacing has a greater effect on the deck slab behavior, as found in bridge B5, where the high value of girder spacing gave high stress values compared with the equivalent strip method.

In most cases the equivalent strip method resulted in higher stress values compared with the finite element results, which indicates that in the case of positive moment the equivalent strip method can be a reliable approximate method to design the deck slab in splayed girder bridges.

6.2 Negative Moment in Interior Region

The same three bridges analyzed in the case of positive moment are now studied for interior negative moment case (M^-) under the effect of a live load. As described in Section 4.3.2, three longitudinal locations for each of the considered bridges are examined. There are two sections, each 1 m away from one of the bridge-supported ends, and a third one at the mid span of the bridge.

Starting with the reference bridge (B1), Figure 146 compares the stress values from the finite element model with the corresponding stress from the equivalent strip method for the case of interior negative moment in the deck slab. The transverse stress value significantly changed along the span of the bridge, where at a section near the wide end of the bridge the transverse stress value recorded was 4.075 MPa, and at the mid span of the bridge the maximum transverse stress decreased to 0.978 MPa, and at the narrow end of the bridge it is 1.379 MPa. Similar to the positive moment case, in a splayed girder bridge two major parameters affect the transverse stress values in the interior negative moment case. The first one is the girder spacing, where by decreasing the girder spacing along the span of the bridge, the stress drops. The second one is the longitudinal location of the loaded section, where in the negative moment case the transverse stress value dramatically decreases because of the girders' deflection due to live load which causes a significant reduction in negative moment in the interior region. Therefore, the maximum transverse stress values are recorded near the bridge ends where the deflection of the girders is minimal. Compared with the equivalent strip ES method, it can be noticed that at any section the stress values are higher than the ones obtained from finite element modeling because this method is based only on the girder spacing which gives the results this linear trend. Consequently, the ES method is conservative in bridge B1 compared with the finite element results, and at maximum girder spacing it is 15.3% more conservative.

Figure 146: deck slab transverse stresses in case of M⁻ for reference bridge

Bridges B4 and B5 showed exactly the same behavior recorded in bridge B1, as shown in Figure 147 and Figure 148. Because of the deflection of girders due to loading section 2 at the mid span, the transverse stress due to negative bending (M⁻) is too low. The maximum transverse stress value is recorded by loading section 1 (1 m away from

the wide end) because of the large girder spacing at the wide end of the bridge plus the small negative effect of girder deflection as the section is very close to the bridge supports. Also, it can be noted that in both bridges the ES method resulted in a higher stress value than the ones obtained from finite element models at all sections along the span of the bridge. This gave the results good conservativity, where at a section near to the wide end support of the bridge the transverse stress value is 33.3% more conservative in bridge B4, and it gave almost the same value as the finite element result at a similar section in bridge B5. It should be noted that bridge 5 has a girder spacing of 5.25 m at the wide end of the bridge, and it is not common to use this high girder spacing in bridges.

Figure 147: Deck slab transverse stresses in case of M⁻ for B4

Figure 148: Deck slab transverse stresses in case of M⁻ for B5

Based on these results, it can be concluded that in splayed girder bridges using the equivalent strip method for deck slab design in the case of interior negative moment results in conservative stress values, and it can be a reliable design approach for the deck slab.

6.3 Overhang Negative Moment

For overhang negative moment, the same three bridges are analyzed using the finite element method and the equivalent strip method suggested by the AASHTO LRFD. Similar to the positive and negative moment cases, three different sections are considered along the span of each bridge and each is once loaded with only one truck parallel to the parapet to maximize the moment at the overhang.

Figure 149 compares the finite element transverse stress results for bridge B1 with the results obtained from the equivalent strip method at three sections along the span of the bridge. It can be noticed that moving toward the narrow end of the bridge in both methods resulted in a reduction in the transverse stress values. This decrease in stress values is related to the overhang distance where by moving toward the narrow end of the bridge, the overhang distance decreases which reduces the truck wheel effect in the overhang. Also, using the equivalent strip method results in more conservative values compared with the finite element results. At a section that is 6.67 m away from the wide end of the bridge and has an overhang distance of 1.375 m, the transverse stress value using the ES method is 112% more conservative. This conservativity is because the ES method results are based on analyzing the overhang as a cantilever perfectly supported at the exterior girder of the bridge, and loaded with one truck wheel at the minimum distance from the parapet. However in the finite element model the entire truck load is applied with the mid axle at the specified section, which leads to deflections in the exterior girder that consequently results a reduction in the transverse stress values at the top layer of the deck slab at the exterior girder.
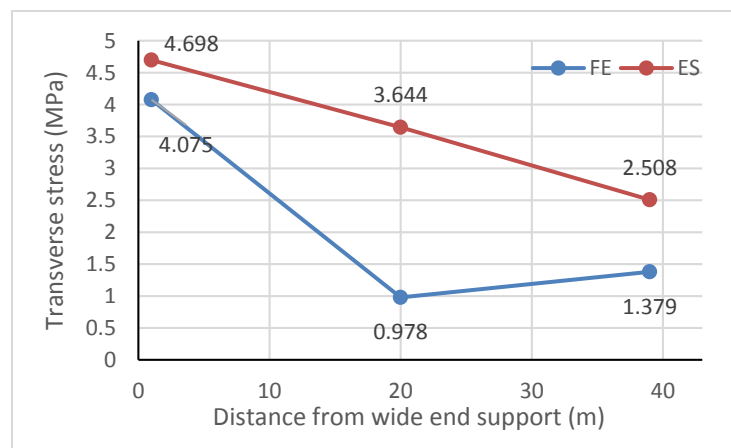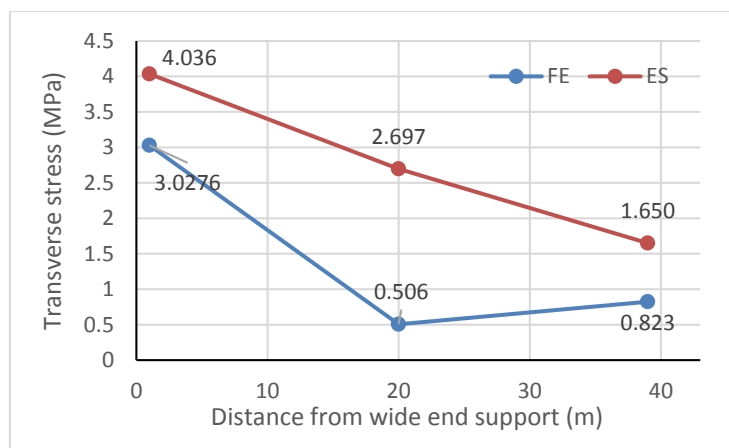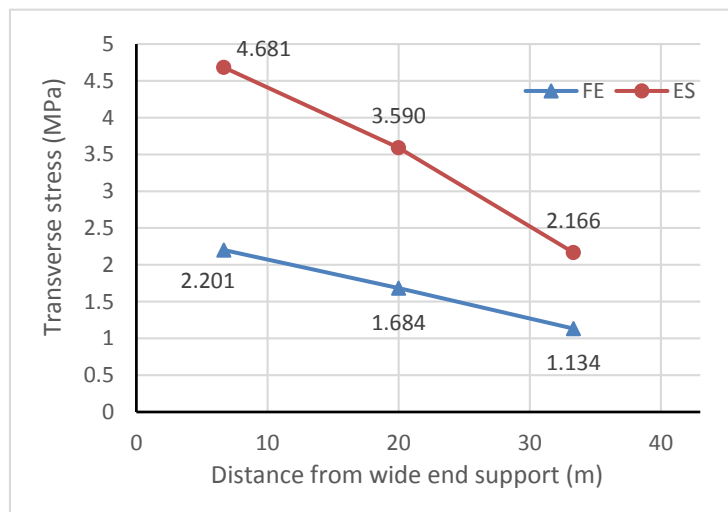

Figure 149: deck slab transverse stresses in case of OH⁻ for reference bridge

150

Bridges B4 and B5 shows a similar behavior to bridge B1 in the case of overhang moment. In both bridges, the stress values drop with decreasing the overhang distance along the span of the bridge. Also, the transverse stress values are higher using the ES method than the ones obtained from finite element models, where at Section 1 it is 114% and 113% more conservative in bridges B4 and B5, respectively.
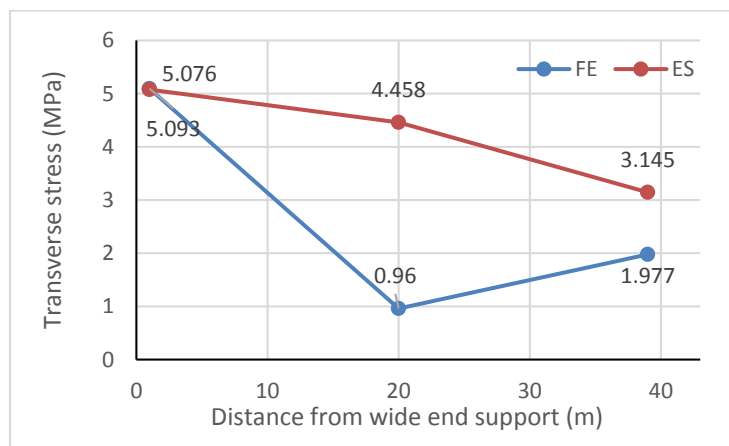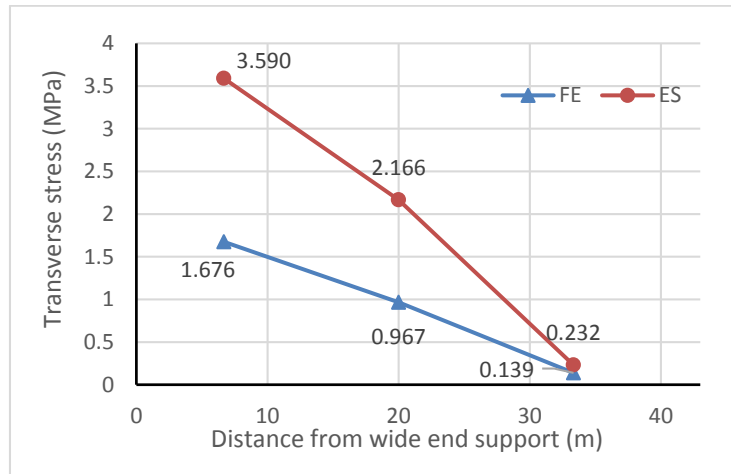

Figure 150: Deck slab transverse stresses in case of OH⁻ for B4

Based on these results, it can be concluded that in splayed girder bridges using the equivalent strip method for deck slab design in the case of overhang negative moment, results conservative stress values and it can be a viable design approach for the deck slab.
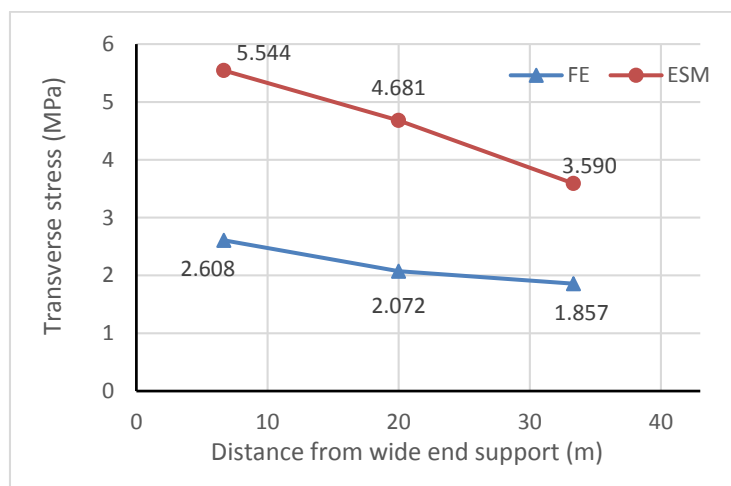
Figure 151: Deck slab transverse stresses in case of OH⁻ for B5

Finally, it can be concluded that in splayed girder bridges the equivalent strip method is a good approximate method to design the concrete deck slab, whether for positive moment, interior negative moment, or at the overhang. However, in order to

design the concrete deck slab in a more efficient and less conservative way, it is recommended to sub-divide the deck slab into a number of regions along the span of the bridge. Each region is designed based on the widest section which has the maximum girder spacing and overhang distance; then the design will be applied along this region. The number of regions can be taken based on the length of the span to make sure that the design in not very conservative (few number of regions), and not very complex (large number of regions) which can increase the complexity of constructing the deck slab.

Chapter 7: Conclusions and Recommendations

7.1 Summary

The use of splayed girder bridges can be a practical solution for problems encountered in complex transportation networks. Such a bridge consists of a nonprismatic thin concrete slab compositely attached to several nonparallel girders. A literature search on the subject of splayed girder structures revealed little published research on the topic. Therefore, it is imperative that such research be conducted on such irregular bridges. Traditionally, the AASHTO specifications have been leading the way in bridge analysis using simplified procedures, even with the recent publication of the LRFD version. However, the simple expressions of the girder distribution factors and approximate design procedures in the specifications are meant to be utilized with regular bridges, in which the girders are parallel and the deck slab width is constant. Since 3-dimensional computer modeling is expensive and demands time, bridge engineers whenever possible try to shy away from such an approach in favor of more simplistic procedures.

The aim of this study is to devise a simple approach that can be used to analyze the deck slab and supporting girders of a splayed girder bridge. It aims at checking if the AASHTO's LRFD girder distribution factors that were derived for regular bridges can be implemented for splayed girder bridges with modifications, if deemed necessary. It also attempts to find out if the equivalent strip method in the specifications for deck slab analysis can be safely used for splayed girder bridges, with some alterations if required.

This research utilizes the finite element computational method through the use of ANSYS. In the computer model, 4-node rectangular shell elements were used for the steel girder flanges and web, 2-node beam elements for the cross-bracing, and 8-node solid elements in the deck slab. As recommended by AASHTO, linearly-elastic material behavior is utilized and the model is verified against laboratory and field tests of actual bridges with reasonable findings. Fifteen composite steel girder superstructures are modeled in the study to consider the effects of the girder splayedness angle, girder spacing, number of girders, deck slab thickness, span length, girder stiffness and presence/spacing of cross-bracing. The parameters varied as follows: splayedness ratio 0.0375-0.075, smaller-to-larger girder spacing ratio 0.4-0.57, deck

slab thickness 150-300 mm, number of girders 3-7, cross-bracing spacing 5-40 m, girder depth 1400-2000 mm, and span length 30-50 m. In all cases, simply-supported bridges with constant deck slab thickness and prismatic steel girders are considered. To study the contribution of one parameter (such as slab thickness) to the structural behavior of splayed girder bridges, all other parameters (such as splayedness angle, number of girders, girder stiffness, span length, etc.) were kept constant. In addition to the finite element analysis, AASHTO's LRFD recommended methods of analysis for regular bridges were carried out for all the considered splayed girder bridges. This included the flexural effect in the deck slab, as well as girder distribution values for shear and moment in interior and exterior girders.

7.2 Conclusion

Based on the obtained results and findings in this study, the following conclusions for splayed steel girder bridges are relevant.

7.2.1   Flexure in girders.

- The tributary width concept that is often used in practice is reliable for determining the dead load effect on the splayed interior and exterior girders. However, AASHTO's recommendation of equally sharing the superimposed dead load among the girders is not very accurate, since exterior girders receive higher loads from the parapet weight than interior girders.

- Increasing the splayedness ratio leads to reductions in GDF for flexure in both interior and exterior girders. The relationship between the GDF and splayedness ratio almost linear.

- The splayedness (angle) ratio and girder spacing ratio cannot be used as stand-alone indices in a splayed girder bridge without supporting them with the girder spacing. Therefore, in order to judge the magnitude of the GDF of a splayed girder bridge, a splayedness parameter plus one girder spacing at a specific location within the bridge must be specified.

- The effect of the slab thickness on the flexure GDF for splayed girder bridges is moderate on the interior girders and negligible on the exterior girders. Also, girder stiffness has little effect on the GDF for both interior and exterior girders. However, an increase in the number of girders beyond 5 can lead to some

reduction in the GDF of the exterior girder, due to the possibility of rigid body rotation over the increased width of the bridge and large eccentric truck loading, but not the interior.

- There is a significant effect on the interior girders for adding cross-bracing to splayed girder bridges, which is similar to the presence of the cross-bracing effect in regular bridges. Where the flexure GDF for interior girders dropped by more than 8% for adding cross-bracings at 5 m spacing, it increased the exterior girder GDF by only 2%. The location of cross-bracing spacing in reference to the longitudinal truck axle positions is important, as axles directly above a cross-bracing are more equally distributed among the girders compared to axles located between cross-bracings.

- The AASHTO LRFD GDF for flexure gave reasonable results compared to the FE models, where for the interior girders the difference was between 2%-13% on the conservative side. The high values of the flexure GDF computed following the AASHTO LRFD specifications compared with the FE results were due to the presence of cross-bracing, which is not considered in the AASHTO formulas. The GDF for exterior girders results obtained from the AASHTO LRFD formulas were also very reliable, where the difference was between -4% and 13.6%. The results representing slight unconservatism were recorded in bridges with extreme parameter values that exceeded the LRFD limits.

7.2.2 Shear.

- The tributary width concept is a good way for finding the dead load effect on splayed interior and exterior girders. However, superimposed dead load among the girders is not shared equally among the girders, as allowed by AASHTO, since exterior girders collect higher loads from the parapet weight than interior girders.

- Increasing the splayedness ratio leads negligibly affect the GDF for shear in both interior and exterior girders. The increase in the smaller-to-larger girder spacing ratio (while keeping the splayedness ratio constant) causes a significant increase in the GDF for shear in both the interior and exterior girders. As in the case of flexure, both the splayedness angle and the girder spacing ratios cannot

155

be used as stand-alone indices in a splayed girder bridge without the magnitude of the (smaller or larger) girder spacing.

- As in the case of flexure, the effect of slab thickness on the shear GDF for splayed girder bridges is moderate on the interior girders and negligible on the exterior girders. Also, girder stiffness, number of girders (above 5) and girder depth have little effect on the GDF for both interior and exterior girders.

- Adding cross-bracing to splayed girder bridges reduces the GDF for shear in the interior girders, particularly if the cross-bracing spacing is small (less than 10m). The effect of using cross-bracing in splayed girder bridges on the exterior girders GDF is small, even when they are placed at small spacing.

- The use of the lever rule to predict shear in interior or exterior splayed girders gave reliable results compared to the FE models. On the other hand, the AASHTO GDF for shear could not predict the live load effect reasonably; in some cases they were higher and in other cases lower than the FE results.

7.2.3 Deck slab.

- For positive moment case, despite that the maximum girder spacing is at the wide end of a splayed girder bridge, the maximum stress at the bottom layer of the deck slab might develop at the midspan. This is because, the girders deflect within the span of the bridge, which changes supporting condition especially at the mid span of the bridge.

- For negative moment case, decreasing the girder spacing due to splayedness of a bridge, reduces the maximum stress values at the top layer of the deck slab. However because of the girder deflection, a significant drop in the stress value is noticed at the midspan.

- The equivalent strip method suggested by AASHTO for deck slab analysis, gave reasonable results compared to the FE analysis in positive moment, negative moment or overhang regions at different sections along the span of the bridge.

- Moving toward the narrow end of the bridge, the stress values due to dead load drop, because of the decrease of load and spacing between the girders due to the bridge splayedness.

- Analyzing a one meter strip of a splayed girder bridge subjected to dead load, give conservative results compared to the FE findings at the same strip location

especially at the midspan for positive regions because of the deflection of girders.

7.3 Recommendations

Based on the results of the finite element analysis, AASHTO's LRFD GDF expressions, the lever rule, and the equivalent strip method, the following recommendations can be drawn:

- The tributary width concept is reliable for determining the dead load on the splayed interior and exterior girders. The parapet weight when placed on the hardened concrete deck tends to load the exterior girders much more than the interior girders.

- The girder distribution factors for flexure in the AASHTO LRFD specifications can be reasonably used for splayed girder bridges if the specific girder spacing at the location of each axle of the truck in the longitudinal direction is considered.

- The lever rule can provide a good estimate of the live load distribution among splayed girders when subjected to shear.

- The equivalent strip method can be a reasonable predictor of the critical positive and negative bending moments in the deck slab interior regions and in the overhang when subjected to dead and live load, provided that more than one strip is taken at some discrete locations along the bridge centerline.

7.4 Suggestion for Future Research

The scope of the study covered composite I-steel girders, simply-supported spans, dead load effect, and live load effect. Future studies on the subject may address the following topics:

- Prestressed concrete bridges.
- Box girder bridges
- Continuous span bridges.
- Dynamic loading.
- Lateral wind loading.
- Nonlinear behavior at ultimate

References

[1] Google Maps, 'Google Maps', 2015. [Online]. Available: http://www.google.com/maps/. [Accessed: 13- Apr- 2015].

[2] T. Bush, "Ten Mile Road Interchange SPUI Bridge Ideal Fit over I-84 in Idaho," HDR Engineering Inc, Idaho, 2011.

[3] *ANSYS®Academic Research,* Release 14.0.

[4] AASHTO, *LRFD Bridge Design Specification.* SI, 6th ed., Washington, DC: American Association of State Highway and Transportation Officials, 2012.

[5] R. M. Barker and J. A. Puckett, *Design of highway bridges: An LRFD approach,* 3rd ed. Hoboken, New Jersey: John Wiley & Sons, 2013.

[6] J. Ambrose, *Building Structures,* Hoboken, New Jersey: John Wiley & Sons, 1993.

[7] BCSA, Tata Steel and SCI, "steelconstruction.info," 2012. [Online]. Available: http://www.steelconstruction.info/File:A34_Wolvercote_Viaduct.JPG. [Accessed: 15- Apr- 2015].

[8] AASHTO, *Standard Specifications for Highway Bridges*, 16th ed., Washington, DC: American Association of State Highway and Transportation Officials, 1996.

[9] T. Zokaie, R. A. Imbsen and T. A. Osterkamp, "Distribution of wheel loads on highway bridges," Transportation Research Board, Washington, D.C, 1991.

[10] T. Zokaie, "AASHTO-LRFD live load distribution specifications," *Journal of Bridge Engineering,* vol. 5, no. 2, pp. 131-138, 2000.

[11] E. Junsik and A. S. Nowak, "Live load distribution for steel girder bridges," *Journal of Bridge Engineering,* vol. 6, no. 6, pp. 489-497, 2001.

[12] H. M. Westergaard, "Computation of stresses in bridge slabs due to wheel loads," *Public Roads,* vol. 11, no. 1, pp. 1-23, 1930.

[13] J. G. Buckler, F. W. Barton, J. P. Gomez, P. J. Massarelli and J. W. McKeel, "Effect of girder spacing on bridge deck response," Virginia Transportation Research Council, Charlottesville, VA, Final Rep., VTRC 01-R6, 2000.

[14] P. J. Barr and M. N. Amin, "Shear live-load distribution factors for I-girder bridges," *Journal of Bridge Engineering,* vol. 11, no. 2, pp. 197-204, 2006.

[15] S. W. Tabsh and K. Sahajwani, "Approximate analysis of irregular slab-on-girder bridges," *Journal of Bridge Engineering,* vol. 2, no. 1, pp. 11-17, February 1997.

[16] T. S. Song and H. Y. Chai, "Live-load distribution factors for concrete box-girder bridges," *Journal of Bridge Engineering,* vol. 8, no. 5, pp. 273-280, 2003.

[17] J. A. Puckett, D. Mertz, X. S. Huo, M. C. Jablin, M. D. Peavy and M. D. Patrick, "Simplified live load distribution factor equations," Transportation Research Board, Washington, D.C, NCHRP Rep. 592, 2007.

[18] AASHTO, "AASHTOWare Bridge Design," American Association of State Highway and Transportation Officials (AASHTO), Washington, D.C.

[19] Kansas. D. O. T. (KDOT), *LRFD Bridge Design*, Topeka, KS: Kansas Department of Transportation, 2009.

[20] Utah. D. O. T. (UDOT), *Bridge Management Manual*, Chapter 4, Salt Lake City, UT: Utah Department of Transportation, 2014.

[21] Washington and Texas DOT, "PGSuper Sofrware," BridgeSight Inc., 2009.

[22] M. A. Grubb, J. A. Corven, K. E. Wilson, J. W. Bouscher and L. E. Volle, *Load and Resistance Factor Design (LRFD) For Highway Superstructures*, Washington, D.C.: U.S. Department of Transportation, Federal Highway Administration, National Highway Institute, 2007.

[23] A. Hernnikoff, "Solution of problems of elasticity by the framework method," *Journal of Applied Mechanics,* vol. 8, no. 4, pp. 169-175, 1941.

[24] R. Courant, "Variational methods for the solution of problems of equilibrium and vibrations," *Bull. Amer. Math. Soc,* vol. 49, no. 1, pp. 1-23, 1943.

[25] J. M. Turner, W. R. Clough, C. H. Martin and J. L. Topp, "Stiffness and deflection analysis of complex structures," *Journal of the Aeronautical Sciences (Institute of the Aeronautical Sciences),* vol. 23, no. 9, pp. 805-824, 1956.

[26] W. R. Clough, "The Finite element method in plane stress analysis," in *2nd Conference on Electronic Computation*, Pitssburgh, 1960.

[27] D. Logan, *A First Course In The Finite Element Method*, 5th ed., Stamford CT: Cengage Learning, 2011.

[28] K. J. Bathe, *Finite Element Procedures*, New Jersey, Prentice-Hall, 1996.

[29] O. C. Zienkiewicz, R. L. Taylor and . J. Z. Zhu , *The Finite Element Method*, 7th ed., Kidlington, Oxford, UK: Butterworth-Heinemann, 2013.

[30] H. Falk and C. W. Beardsley, "Finite element pachages for personal computers," *Mechanical Engineering,* pp. vol. 107, no. 1, 54-71, Jan 1985.

[31] T. H. Chan and J. H. Chan, "The use of eccentric beam elements in the analysis of slab-on-girder bridges," *Structural Engineering and Mechanics,* vol. 8, no. 1, pp. 85-102, 1999.

[32] P. J. Barr, M. O. Eberhard and J. F. Stanton, "Live-load distribution factors in prestressed concrete girder bridges," *Journal of Bridge Engineering,* vol. 6, no. 5, pp. 298-306, 2001.

[33] J. C. Hays, L. M. Sessions and A. J. Berry, "Further studies on lateral load distribution using a finite element method," *Transportation Research Record,* vol. No. 1072, pp. 6-14, 1986.

[34] C. E. Ventura, A. J. Felber and S. F. Stiemer, "Determination of the dynamic characteristics of the Colquitz River Bridge by full-scale testing," *Canadian Journal of Civil Engineering,* vol. 23, no. 2, pp. 536-548, 1996.

[35] Y. Chen, "Distribution of vehicular loads on bridge girders by the FEA using ADINA: modeling, simulation, and comparison," *Computers & structures 72.1 (1999): 127-139.,* vol. 72, no. 1, pp. 127-139, 1999.

[36] S. W. Tabsh and M. Tabatabai, "Live load distribution in girder bridges subject to oversized trucks," *Journal of Bridge Engineering,* vol. 6, no. 1, pp. 9-16, 2001.

[37] A. G. Bishara, M. C. Liu and N. D. El-Ali, "Wheel load distribution on simply supported skew I-beam composite bridges," *Journal of Structural Engineering,* vol. 119, no. 2, pp. 399-419, 1993.

[38] M. A. Machado, E. D. Sotelino and J. Liu, "Modeling technique for honeycomb FRP deck bridges via finite elements," *Journal of Structural Engineering,* vol. 134, no. 4, pp. 572-580, 2008.

[39] M. E. Mabsout, K. M. Tarhini, G. R. Frederick and C. Tayae, "Finite element analysis of steel girder highway bridges," *Journal of Bridge Engineering,* vol. 2, no. 3, pp. 83-87, 1997.

[40] H. Wu, "Influence of live-load deflections on superstructure performance of slab on steel stringer bridges," PhD dissertation, Dept. Civil Eng., West Virginia University, Morgantown, WV, 2003.

[41] C. D. Eamon and A. S. Nowak, "Effects of edge-stiffening elements and diaphragms on bridge resistance and load distribution," *Journal of Bridge Engineering,* vol. 7, no. 5, pp. 258-266, 2002.

[42] W. Chung and E. D. Sotelino, "Three-dimensional finite element modeling of composite girder bridges," *Engineering Structures,* vol. 28, no. 1, pp. 63-71, 2006.

[43] K. I. Fang, J. A. Worley , H. N. Burns and E. R. Klingner, "Behavior of Ontario-type bridge deck on steel girders," PhD dissertation, Dept. Civil Eng., University of Texas at Austin, Austin, TX, 1985.

[44] P. Schonwetter, "Field testing and load rating of a steel-girder highway bridge", MS thesis, Dept. Civil Eng., University of Texas at Austin, Austin, TX, 1999.

[45] M. Ghosn, F. Moses and J. Gobieski, "Evaluation of steel bridges using in-service testing," *Transportation Research Record.* 1072, pp. 71-78, 1986.

[46] C. S. Cai, "Discussion on AASHTO LRFD load distribution factors for slab-on-girder bridges," *Practice periodical on structural design and construction,* vol. 10, no. 3, pp. 171-176, 2005.

Vita

Faress Hraib was born in Damascus, Syria. He studied and graduated from Al-Motafawiqeen School in 2006. He Studied in Damascus University in Damascus, Syria, from which he graduated in 2012 and obtained a Bachelor of Science degree in Civil Engineering.

Mr. Hraib moved to the United Arab Emirates in 2013 where he joined the Master's program in Civil Engineering at the American University of Sharjah. His research interests include finite element modeling, bridge engineering, and composite structures.